



Numerical modelling of multiple
borehole heat exchanger array for
sustainable utilisation of shallow
geothermal energy

Dissertation

Zur Erlangung des akademischen Grades

Doktoringenieur (Dr.-Ing.)

vorgelegt

der Fakultät Umweltwissenschaften

der Technischen Universität Dresden

von

M.Sc. Shuang Chen

geb. am 19.06.1988 in Sichuan, VR China

Gutachter:

Prof. Dr.-Ing. habil. Olaf Kolditz

Prof. Dr.-Ing. habil. Thomas Herlitzius

Prof. Dr.-Ing. Hartmut Hollände

Eingereicht am: 30.05.2021

Tag der Verteidigung: 19.07.2022

ÜBEREINSTIMMUNGSERKLÄRUNG

Die Übereinstimmung dieses Exemplars mit dem Original der Dissertation zum Thema:

*'Numerical modeling of multiple borehole heat exchanger array
for sustainable utilisation of shallow geothermal energy'*

wird hiermit bestätigt.

Hannover, 12.08.2022

.....
Ort, Datum

Shuang Chen

.....
Unterschrift (Vorname Name)

ABSTRACT

Nowadays, borehole heat exchanger (BHE) based ground source heat pump (GSHP) system is widely applied for shallow geothermal energy exploitation. However, the thermal load on a single BHE is usually limited due to its restricted length. Due to the high thermal demand from a commercial building or large residential projects, installing a large BHE array as the energy supplier is becoming more and more favorable in the GSHP industry. During the operation of the BHE array, the heat transfer process in the subsurface, in the BHEs, and the hydro-thermal processes within the entire pipe network are strongly coupled with each other. Among the coupling effects, the thermal interference among the BHEs is expected to have significant influences on the long-term performance of the system. In this work, a comprehensive numerical model was developed, in which the shallow subsurface, the multiple BHEs and the pipe network are all included and simulated in one coupled model. In the modeling software, special attention is paid to quantify the long-term thermal load shifting behavior among each individual BHE during the operation of a multiple BHE array. The thermal and hydraulic parts in the model are verified against analytical solution and existing modelling software respectively. Moreover, the model is validated based on the monitoring data from a real building project in Leicester, UK. With the newly developed modeling feature, detailed thermal load shifting behavior in a BHE array can be predicted and quantified. A linear correlation is found between the working fluid temperature increment and the amount of the accumulated heat injected into the subsurface. Based on the numerical results, measures for optimisation of the operation strategy for the BHE array system are suggested. Discussions on application specified factors e.g. thermal recharge, adjacent distance among BHEs, and their implications on the sustainability of large BHE array, are also given in this dissertation.

ZUSAMMENFASSUNG

Heutzutage wird das auf Erdwärmesonde basierende Erdwärmepumpensystem häufig für die Nutzung oberflächennaher Geothermie eingesetzt. Üblicherweise ist die Heizleistung einer einzelnen Erdwärmesonde durch seine beschränkte Länge begrenzt. Daher zur Erfüllung des hohen thermischen Bedarfs eines Geschäftsgebäudes oder großer Wohnungsprojekte wird die Installation einer großen Anlage mit mehreren Erdwärmesonden immer mehr beliebt in die Industrie. Während des Betriebs einer Anlage mit mehreren Erdwärmesonden sind die Wärmeübertragungsprozesse im Untergrund, in allen Erdwärmesonden, und die hydro-thermischen Prozesse innerhalb des gesamten Rohrnetzes miteinander stark gekoppelt. Unter diesen Kopplungseffekte ist die thermische Interferenz zwischen der Erdwärmesonden einen signifikanten Einfluss auf die langfristige Leistung des Systems zu erwarten. In dieser Arbeit wurde ein umfassendes numerisches Modell inklusive des Untergrundes, Erdwärmesonden und das Rohrnetz entwickelt. Mit dem Modell können die obengenannte Koppelungsprozesse zwischen unterschiedlichen Komponente gemeinsame simuliert. In der Modellierung wird besonderes Augenmerk auf die Quantifizierung der Verschiebung der Heizleistung zwischen jeder einzelnen Erdwärmesonde während des langfristigen Betriebs des Systems gelegt. Die thermischen und hydraulischen Teile des Modelles wurden anhand der analytische Lösung und der vorhandenen Modellierungssoftware verifiziert. Darüber hinaus wurde das gesamte Modell auf Basis der Messdaten eines realen Geothermieprojekts in Leicester, Großbritannien validiert. Mit der neu entwickelten Modell kann das ausführliche Verhalten der Überlagerung von thermischer Last in einer großen Anlage mit mehreren Erdwärmesonden vorhergesagt und quantifiziert werden. In der Studie wurde eine lineare Korrelation zwischen dem Temperaturinkrement des Arbeitsfluides und der Menge der in den Untergrund eingespeisten Wärme entdeckt. Basierend auf den numerischen Ergebnissen werden Maßnahmen zur Optimierung der Betriebsstrategie für ein mehr-Erdwärmesonden-System vorgeschlagen. Außerdem sind die Auswirkungen einiger für die Anwendung spezifizierte Faktoren (z.B. die thermische Aufladung für das System aus der Untergrunde Oberfläche, und der Abstand zwischen den benachbarten Erdwärmesonden) auf die Nachhaltigkeit eines mehr-Erdwärmesonden-Systems in dieser Dissertation diskutiert.

ACKNOWLEDGEMENTS

First of all, I would like give my heartfelt thanks to my supervisor Prof. Olaf Kolditz (Faculty of Environmental Sciences, Dresden University of Technology and Department of Environmental Informatics, Helmholtz-Centre for Environmental Research Leipzig - UFZ). Next, I'd like to express my deepest gratitude to Dr. Habing Shao, who leads group 'Geothermal Systems Analysis' in UFZ for his continuous highly qualified guidance of my work. Without his patient advising and constant supporting on my work, I would never get a chance to be where I am. Furthermore, I'd like to thank the reviewers for reviewing this dissertation. I want to acknowledge the funding of my work within in the project 'ANGUS II' under grant number 03ET6122B funded by the German Federal Ministry of Economic Affairs and Energy (BMWi). In addition, special thanks go out to project 'ESyQuart', which is also funded by BMWi under the grant number 03EGB0016C and lead by Prof. Anke Bucher (Faculty of Mechanical and Energy Engineering, Leipzig University of Applied Sciences - HTWK) and project collaborator Dr. Uwe-Jens Görke (UFZ)).

Many thanks to Francesco Witte (Flensburg University of Applied Sciences) for the pleasant collaboration and discussions on the TESP pipe network model in my research work. Special thanks to our team college Jakob Randow and Katrin Lubashevsky for the collaboration on the EASyQuart project. I would also like to thank my ENVINF colleagues for their professional support on various topics like programming, numerics and informatics. In this context, I'd especially like to mention Dr. Wenqing Wang, Dr. Lars Bilke, Dr. Dmitri Naumov, Dr. Karsten Rink and our previous colleagues Dr. Christoph Lehmann and Dr. Philipp Hein. Also I would like to thank to Sindy Bleiholder for her friendly secretary support for my work in UFZ.

I express my special appreciation to my UFZ colleagues and friends Dr. Renchao Lu, Chaofan Chen and Boyang Meng for the countless discussions, fruitful suggestions and not to forget the every gathering time during my PhD study these years. I would also like to thank to my friend Cui Zhen for her help about the Python programming at the very beginning of my PhD career.

Last but not least, I would like to thank my family. Without the solid supports from my parents for my PhD study these years, I would never get any of my current achievements. And finally, For my best love to the most important one of my life, Xuerui.

For Xuerui and my parents.

CONTENTS

1	INTRODUCTION	1
1.1	Motivation and Background	1
1.2	State-of-the-Art	2
1.3	Objectives and Scope of this dissertation	4
1.4	Outline of this dissertation	6
2	THEORY	7
2.1	Subsurface BHE model.	7
2.1.1	Physical processes	7
2.1.1.1	Heat transport	8
2.1.1.2	Groundwater flow	9
2.1.2	Analytical approaches	10
2.1.2.1	Soil temperature change in the BHE array subsurface	10
2.1.2.2	BHE array sizing tools.	11
2.1.3	Numerical model.	13
2.1.3.1	Dual-continuum model	14
2.1.3.2	Finite element realisation	15
2.1.3.3	Setting of boundary conditions	18
2.1.3.4	Schur complement method	20
2.2	Pipeline network model	21
2.2.1	Conservation laws within the pipeline network. . .	21
2.2.2	Solution algorithm	22
2.2.3	Pipeline network model in TESPpy.	23
2.3	Integrated BHE model with pipeline network	24
3	IMPLEMENTATION OF THE MODEL	26
3.1	Model preparation	26
3.2	Coupling OpenGeoSys and TESPpy.	28
3.3	PipeNetwork feature in OGS	30
4	VERIFICATION AND VALIDATION	31
4.1	Verification of the model.	31
4.1.1	Simulated Hydraulic Feature of the pipeline network 31	
4.1.2	Distribution and evolution of the soil temperature .	35
4.1.3	System thermal balance in the coupled model . . .	35
4.2	Validation of the model	36

5	APPLICATIONS	37
5.1	Heat shifting phenomenon in the large BHE array system	38
5.2	Sustainability of a multiple shallow BHE array system.	40
5.3	Discussion and outlook	42
6	CONCLUSIONS AND OUTLOOK	45
A	APPENDIX A	57
B	APPENDIX B	58
B.1	Paper 1	58
B.2	Paper 2	74
C	APPENDIX C	88
C.1	Python scripts	88

NOMENCLATURE

Roman letters

c	specific heat capacity	$[\text{J kg}^{-1} \text{K}^{-1}]$
D	diameter of the pipe	$[\text{m}]$
E_1	exponential integral function	
F_h	proportion of the operation time	$[\%]$
H	thermal sink/source term	$[\text{W m}^{-3}]$
h_f	hydraulic head	$[\text{m}]$
\mathbf{H}	Column matrix of source terms	
h	enthalpy of circulating fluid in Eq. (44)	$[\text{J Kg}^{-1}]$
\mathbf{I}	unit(identity) matrix	
\mathbf{j}	heat flux	$[\text{W}]$
J	jacobian matrix	
K	hydraulic conductivity	$[\text{m s}^{-1}]$
k_s	roughness coefficient of the pipe	$[\text{m}]$
L	length of BHE	$[\text{m}]$
\dot{m}	mass flow rate	$[\text{kg s}^{-1}]$
P	power of the component	$[\text{W}]$
p	hydraulic pressure of circulating fluid	$[\text{Pa}]$
Q	amount of heat	$[\text{J}]$
q	heat transfer rate	$[\text{W}]$
\dot{Q}	heat exchange rate of the BHE	$[\text{W}]$
\dot{Q}	amount of the heat flux in Eq. (1)	$[\text{W}]$
Q_L	hydraulic sink/source term	$[\text{m}]$
q_{lh}	designed thermal load at the building site	$[\text{W}]$
q_n	heat flux between soil, grout and pipe	$[\text{W m}^{-2}]$
R	thermal resistance	$[\text{m K W}^{-1}]$

r	distance	[m]
Re	Reynolds number	[-]
\mathbb{R}	Real Euclidean Space	[°C]
S	adjacent distance among BHEs	[m]
S_s	storage coefficient	[-]
T	temperature	[°C]
t	time	[s]
T_p	temperature penalty	[°C]
U	internal energy of a certain volume	[J]
\mathbf{v}	fluid velocity	[m s ⁻¹]
V	volume	[m ³]
v	flow velocity in pipelines	[m s ⁻¹]
\mathbf{u}	Darcy velocity of ground water flow	[m s ⁻¹]
\dot{V}	volumetric flow rate	[m ³ s ⁻¹]
W_h	system power input at design heating load	[W]

Greek Letters

α	thermal diffusion coefficient	[W m ⁻¹ K ⁻¹]
ϵ	error tolerance	[-]
Γ	domain boundary	[-]
λ	thermal conductivity	[W m ⁻¹ K ⁻¹]
Λ	hydrodynamic thermal dispersion tensor	[W m ⁻¹ K ⁻¹]
Ω	domain	[-]
ϕ	heat transfer coefficient	[W m ⁻² K ⁻¹]
π	mathematical constant Pi	[-]
ρ	density	[kg m ⁻³]
ϵ	porosity of the porous medium	[-]
ζ	friction factor of the pipe	[-]

Operators

Δ	difference operator
----------	---------------------

∇	spatial gradient operator
$\nabla \cdot$	spatial divergence operator
\otimes	tensor product

Subscripts

<i>a</i>	annual time
adv	advection
<i>b</i>	BHE borehole
<i>c</i>	cooling
<i>diff</i>	diffusion
disp	dispersion
<i>f</i>	fluid
<i>g</i>	grout
<i>i</i>	pipe-in or internal
<i>in</i>	inflow
L	transversal direction
<i>m</i>	monthly time
<i>o</i>	pipe-out or outer
<i>ov</i>	overall
<i>out</i>	outflow
<i>pe</i>	pipe
<i>sp</i>	short time thermal pulse
<i>st</i>	short time
T	longitudinal direction
<i>wo</i>	heat pump outlet
<i>wt</i>	heat pump inlet

Superscripts

B	BHE part
<i>eff</i>	effective
f	fluid

<i>in</i>	water inflow
<i>out</i>	water outflow
S	soil part
<i>s</i>	solid phase

ACRONYMS

1U	Single U-shape pipe
2D	Two-dimensional space
3D	Three-dimensional space
ANSYS	ANalysis SYStem
ASHRAE	American Society of Heating, Refrigerating and Air-Conditioning Engineers
BC	Boundary condition
BHE	Borehole heat exchanger
BTES	Borehole thermal energy store
COP	Coefficient of performance
DBHE	Deep borehole heat exchanger
DCA	Dual-continuum approach
DOF	Degree of freedom
DST	The Duct Storage model
EER	Energy efficiency ratio
FDM	Finite Difference Method
FEFLOW	Finite element subsurface flow simulation system
FEM	Finite Element Method
FLS	Finite line source
FVM	Finite Volume Method
GFEM	Galerkin Finite Element Method
GSHP	Ground source heat pump
ILS	Infinite line source
LHS	Left hand side
NWWA	National Water Well Association
OGS	OpenGeoSys

ORC	Organic Rankine Cycle
PLF	Part-load factor
PSTL	Proportion of the shifted thermal load
RHS	Right hand side
SHER	Specific heat exchange rate
SVD	Singular Value Decomposition
TESPy	Thermal Engineering Systems in Python
TCRM	Thermal capacity-resistor model
THMC	Thermo-hydro-mechanical-chemical
TRNSYS	TRaNsient SYstems Simulation
VDI	Verein Deutscher Ingenieure

INTRODUCTION

1.1 Motivation and Background

As a low-carbon technology of providing heating and cooling to buildings, utilizing geothermal energy through Ground Source Heat Pump (GSHP) system has received increasing interest in recent years [1, 2]. In densely populated urban areas, shallow geothermal exploitation is even favourable, because the accelerated heat fluxes from the warm basement often lead to elevated temperatures in the subsurface [3, 4]. Since the thermal extraction rate of a single BHE is limited, large GSHP system is usually required targeting the thermal demand of commercial buildings and small neighborhood. These large GSHP systems are typically constructed by connecting and linking hundreds of Borehole Heat Exchangers (BHE) through a pipe network [5].

Unlike the single BHE system, for the design of such multiple-BHE arrays, only limited guidance can be found in the current literature. For instance, in the Germany guideline *VDI4640* [6], detailed designing criterion is only given to arrays limited up to no more than five BHEs. It is suggested that, for systems with more than five BHEs or with a total thermal capacity larger than 30 kW, further numerical or analytical modelling studies should be conducted. Similar as the Germany guideline, most guidelines from other countries put a restriction on the minimum capacity or size of the multiple-BHE array, rather than providing a complete designing approach [7]. Among the methods all over the world, the most influential one for designing the large BHE array is the ASHRAE approach [8] from the United States. In ASHRAE method, the required total length of BHE is estimated through systematical consideration of a series of design parameters, including the building thermal load, the thermal resistance of the ground etc. However, since its calculation framework is based on the line-source model originated from a single BHE, this approach may not be suited for the designing of a multiple-BHE array. Details about ASHRAE method and its shortages are further introduced and discussed in the Section 1.2 and Section 2.1.1.2.

Compared to the single BHE system, the physical processes involved in a multiple-BHE array are more complicated, more affecting factors should be considered. On the one hand, due to its large size, the local environment conditions, such as soil properties, groundwater flow

and ground surface temperature are expected to have more distinct influence on the system behavior. On the other hand, in a multiple-BHE array system, thermal interference among each BHE occurs during the long-term operation cannot be ignored [9]. Moreover, currently in the industry different kinds of BHE array arrangement are applied in the GSHP projects [10, 11]. In these systems, the complex hydraulic and thermal processes within the entire pipe network can further affect the individual behavior of each BHE in the array. To sum up, there is still lack of full understanding of the system behavior, especially during the long-term operation of a multiple-BHE array. To reduce the potential system operation risks, further investigations on the coupled physical processes and the corresponding long-term system behaviour in a multiple-BHE array are required.

1.2 State-of-the-Art

In general, two major categories of modelling techniques are commonly applied to investigate the behavior of a BHE based GSHP system, i.e. the analytical- and numerical-based models. Due to the easy handling and high computational efficiency, analytical models are favourably adopted to investigate the temperature field in the subsurface or to determine the size of a BHE array or the length of each BHE. One of the well-known analytical approaches to investigate the subsurface soil temperature change, is the super-positioned infinite line source model proposed by Eskilson [12]. This model contains the concept of the well-known g-function, which represents a non-dimensional temperature response factor that relates the borehole wall temperature and an instantaneous thermal load on the BHE. Later, Based on the cylindrical heat source method, Bernier et al. [13] developed an mathematical technique by considering the thermal response effect from previous steps to the current temperature distribution. By adopting the Laplace transforms, Beier [14] developed an analytical model which enables to calculate the transient thermal behavior within a U-tube borehole. In his recent research work, the geothermal gradient is further successfully added into the BHE analytical model [15]. Koochi-Fayegh and Rosen [16] presented a semi-analytical model that couples a heat pump with the borehole, using the conductive heat transfer model to regulated the heat flux from the soil. By using the model, the effect of thermal interaction such as borehole distance on the performance of the heat pump was investigated. To optimise the seasonal heating and cooling strategy during the operation of a multiple-BHE array, Bayer et al. [17] developed a mathematical procedure also based on the super-position principle. For the analytical approaches which are adopted to size a BHE system, they focus on the heat transfer process between soil around the BHEs and the working fluid within the BHEs. Based on the pre-defined ground tempera-

ture, the working fluid temperature and the thermal resistance of the model, the specific heat exchange rate (SHER in W m^{-1}), which is a key parameter for the model, can be determined by dividing the thermal demand of the system by the total length of the BHE. According to this relationship, different BHE sizing models are set up. The earliest sizing model may be the concentric cylinder model developed by Carslaw and Jaeger [18]. Based on it, various improved models were developed, such as the world-wide mostly used ASHRAE method [8]. In its method, a more accurate thermal resistance model is developed by considering the time of the system operation effect. Furthermore, the thermal interaction effect in a multiple-BHE array is considered in its mathematical algorithm. And the required BHE length of the designed project is calculated by iteratively correcting the thermal penalty caused by the thermal interference among the BHEs. Details about its mathematical procedure is introduced in the Section 2.1.1.2. During the operation of a real GSHP project, the working fluid temperature within the system is found to be a key parameter to characterise the system working performance. To protect the heat pump and avoid ground freezing, usually, the temperature of working fluid at the inlet of the heat pump should not exceed 35°C , and remain above 0°C at the inlet of the BHE [19]. To fulfill these requirements, adopting the working fluid temperature as the target parameter in the calculation procedure is becoming favorable in many analytical solution. For example the method from the the National Water Well Association (NWWA) [20] suggest a calculation procedure to iteratively determine the length of the BHEs. Since the ground thermal response parameters vary with the borehole length, this results in a corresponding working fluid temperature through the analytical approach. The optimised BHE length can then be determined, when the calculated working fluid temperature is approaching the target temperature limit. A comprehensive review on the available BHE array designing procedures can be found by Ahmadfard and Bernier [19].

In recent years, numerical methods deserve more attentions in the investigation of the BHE-array behavior. Over the world, software based on different type of numerical approaches can be found. The Duct Storage (DST) model [21] is commonly used to design and analyse the underground energy storage system. It adopts the two-dimensional finite difference method (FDM) to calculate the global temperature change within a DST model. The model has been implemented in the software TRANSYS [22] and is known as Type 557. With this TRNSYS model, De Rosa et al. [23] developed a novel BHE model and investigated its short-term dynamic performance. By using the finite volume method (FVM) based software ANSYS Fluent [24], Koohi-Fayegh and Rosen [25] verified their developed BHE analytical model. Research works by using the Finite Element Method (FEM) based software can also be found. For example Saaly et al. [26] quantified the heat loss

in a geothermal energy pile system in Canada based on the software COMSOL Multiphysics [27]. Le Lous et al. [28] investigated the thermal performance of a deep borehole heat exchanger with the FEFLOW software [29]. And Hein et al. [30] simulated the soil temperature evolution induced by a configuration of four individual GSHP systems via the simulator OpenGeoSys (OGS) [31]. In the software FEFLOW and OGS, a developed dual-continuum approach (DCA) method are adopted, which enables the model to get a higher computational efficiency by comparing to the common FEM based software. Details about this method is introduced in the Section 2.1.3. Compared to the analytical methods, the numerical methods usually requires a large computing resources. However, they have shown their advantages to handle the heterogeneous subsurface conditions, as well as the capability of considering more complicated physical processes. For example, recent numerical studies have achieved success in simulating the BHE system along with the groundwater flow process [32, 33], geothermal gradient [34] or thermal recharge effect [35], which is considered to be difficult for the analytical models. Besides, compared to analytical approaches, the numerical models are more suitable for an overall energy analysis (e.g. the research work from Saaly et al. [26]), since the dynamic temperature distribution in the entire domain can be simulated.

1.3 Objectives and Scope of this dissertation

Although in recent works, certain success has been achieved in the quantification of the system behavior especially in single BHE system, the understanding of the multiple-BHE array still remains unclear. Firstly, thermal interactions among the BHEs [5, 36] are not comprehensively addressed in the above mentioned models. In most analytical and numerical models, the specific heat exchange rate on the BHE is defined as a Neumann boundary condition. Usually, in the simulation of a multiple-BHE array, the thermal load on each BHE is assumed to be identical and the surrounding soil temperature distribution is assumed to be always in an equilibrium state. These assumptions hold true in the ideal condition where no thermal interference exists among BHEs. However, over the long-term operation of a multiple-BHE array, the overlapping thermal plumes from each BHE can lead to low temperature zones in the centre of the array [9]. This thermal imbalance in the subsurface can further affect the load distribution on each individual BHE of the array. To ensure that the impacts of such thermal imbalance is minor and thus negligible, in the ASHRAE guidelines, usually a minimum borehole separation distance S is given for the designing of a multiple-BHE. However, this minimum borehole distance is only empirically determined and currently there are no theoretical and systematic analysis targeting to estimate it. Thus, no

unified value can be found for this minimum distance among the guidelines from different countries. For instance, in Switzerland, a minimum distance of 5 m is required (cf. Miglani et al. [37]). In the German VDI guideline, this value increased from 5 m to 6 m in its 2019 updated version [6, 38], which is consistent with the recommend value in United States [8]. In China, a distance between 3 m to 6 m is suggested [39]. Although the minimum borehole separation distance can reduce the effect of thermal imbalance to certain extent, the thermal interference among the BHEs can not be completely eliminated. Moreover, since the thermal interference increases with the operation time, the implication of the adjacent distance S to the long-term behavior of a multiple-BHE array is still unknown.

Secondly, the pipe network in the BHE array system are usually not considered. In most research works, the models are constructed only with individual BHEs and the surrounding subsurface. However, in a real large BHE array based GSHP system, the BHEs and other components, e.g. the water pump, check valve, heat pump are connected with each other through a complex pipe network. The thermal and hydraulic status within the entire network are determined by the thermal demand on the heat pump, as well as the circulation pump performance. Moreover, the aforementioned thermal interference is directly influenced by, and also feed back to the hydraulic status within the pipe network. In a multiple-BHE array, the amount of the heat flux on each individual BHE is determined by temperatures of both surrounding soil and the circulation fluid. Since the pipe network connects different BHEs, the flow transport within it could also contribute to the balance of the thermal load among different BHEs. Thus, it can be inferred that without an explicit consideration of hydraulic and thermal balance in the pipe network, the thermal interference phenomenon in the multiple-BHE array may not be accurately quantified. Furthermore, compared to a single BHE system, the effect of the thermal interference and pipe network in a multiple-BHE array results in an unequal and unstable circulation fluid temperature distribution on each individual BHE. As stated in the Section 1.2, the thermal load performance of a GSHP system is limited, since the working fluid temperature within the pipe system is required not to exceed a reasonable range. Therefore, it is interest to investigate the relationship between the circulation fluid temperature change and the system imbalanced thermal load, when the thermal interaction in a BHE array is considered.

Besides, the thermal recharge is less addressed in most of the analytical solutions. Due to the large field size, the long-term recharged heat amount from the ground surface [40] to the BHE array, and the resulted geothermal gradient [35] may not be neglected. When large multiple-BHE array system is operated, the long term system imbalanced thermal load results in the thermal anomalies in the BHE array

subsurface. A larger thermal gradient can be occurred in the centre of the array, which reinforces the thermal recharge effect from the ground surface and the bottom of the BHE array. Thus, it is necessary to analyse the deviations in the calculations of a multiple-BHE array with and without consideration of the thermal recharge.

Bearing the the above mentioned gaps in mind, this PhD work further extends the current numerical modeling framework in order to investigate the long-term behavior of the multiple-BHE array. In this work, a comprehensive numerical model is developed by quantifying the heat transport in the subsurface surrounding the BHEs, in the pipe network and the fluid transport explicitly in a coupled manner. The model is successfully implemented in the numerical simulator OpenGeoSys(OGS), an open-source, Finite Element based software for the simulation of coupled thermo-hydro-mechanical-chemical (THMC) processes. The developed numerical model is applied in a case study to investigate the detailed thermal load shifting behavior in a large BHE array. Based on this comprehensive model, the relationship between the working fluid temperature within the pipe network and the total amount of exploitable heat within a particular BHE array is investigated. Implications of different factors on the BHE array system behavior, such as thermal recharge effect and borehole adjacent distance are discussed. Based on the simulation and prognosis of a real-world geothermal project, specific suggestions are given on how to optimise the performance of a large BHE array system (cf. Section 5.3).

1.4 Outline of this dissertation

This dissertation is composed of six parts. In Chapter. (2), the theoretical background related to a multiple-BHE array based GSHP system is introduced. Chapter. (3) describes the technical details regarding the implementation of the developed model. In Chapter. (4), the model verification based on the analytical solution and model validation against the monitored data in a real large BHE array project are presented. In Chapter. (5), several model applications are described, and the key findings in these works are summarised. In the final Chapter. (6), the achievements in this PhD work are summarized. Besides, an outlook on the further research works is given. The related Publications are included at the end of the dissertation as Appendix. B.

THEORY

In this chapter, the theoretical background and the mathematical framework for the modelling of multiple-BHE array based GSHP system are introduced. The developed numerical model in this PhD study is composed of two parts: a subsurface BHE model and a pipeline network model. They are explicitly coupled with each other. The details of the approaches and constructions of these two models, and their coupling strategies are introduced in the following three subsections. In the first subsection, the physical processes in the subsurface, which have relevant influences on the operation of the BHE array, are presented first. Then, the mathematical model to describe those physical processes are introduced. After that, analytical solutions to the calculations of temperature change in subsurface soil caused by the operation of BHE, and different sizing tools for a BHE array are described. Next, the dual-continuum approach based BHE numerical model adopted in this work and its governing equations are provided. Its finite element realisation is introduced step-by-step. In the second subsection (Section 2.1.2), the working framework and the governing equations within a pipeline network model are introduced. Moreover, the algorithm to derive the thermal and hydraulic steady states of the entire network is proved. In the last subsection (Section 2.2.3), the schematised procedure of the comprehensive model is presented.

2.1 Subsurface BHE model

2.1.1 *Physical processes*

When BHE is utilised to extract or inject heat from or into the subsurface, the circulation fluid is pumped through the U-pipe within the BHE. The temperature difference between the circulation fluid and the surrounding soil leads to a heat exchange between them, thus changes the temperature distribution in the soil. Therefore, in the subsurface BHE model, the heat transport in the soil and heat flux between BHEs and the surrounding soil should be considered. Moreover, if the groundwater is present in the system, heat transport in the subsurface is additionally governed by the advection of the groundwater. In this case, the groundwater flow and the associated convective heat transport should also be simulated.

2.1.1.1 Heat transport

Heat transport is the transport of the thermal energy in or between the physical phases. Considering a certain volume within a context of geothermal energy system, the local thermodynamic equilibrium can be written as

$$\frac{dU}{dt} + \dot{Q} = H \quad (1)$$

Where, U is the internal energy of a certain volume. \dot{Q} denotes the amount of the heat flux and H is the thermal sink/source term within the volume. These terms are further described by the relevant thermal processes in the geothermal systems, which are heat conduction, heat advection, heat dispersion and heat storage.

Heat conduction, or diffusion, is the heat transfer driven by the molecular activity inside a medium without mass transport. Usually it can be described by the famous Fourier's law,

$$\mathbf{j}_{diff} = -\lambda^{eff} \nabla T \quad (2)$$

where \mathbf{j}_{diff} is the diffusive heat flux, ∇T is the spatial thermal gradient. λ^{eff} denotes the effective thermal conductivity of the porous medium, which can be calculated by,

$$\lambda^{eff} = \varepsilon \lambda^f + (1 - \varepsilon) \lambda^s \quad (3)$$

Where ε is the porosity of the porous media. λ^f and λ^s are the thermal conductivity of the fluid and solid phase in the porous media, respectively. During the operation of a GSHP system, the heat flux exchange between the circulation fluid in the BHE U-pipe and the surrounding soil is dominantly governed by heat conduction. If ground water flow is not present, heat conduction is the major process caused heat transfer in the subsurface.

Besides heat conduction, advection is another relevant process that contributes to the heat transfer. It describes the heat transport following the fluid advection. The advective heat flux can be calculated by

$$\mathbf{j}_{adv} = \rho^f c^f T \mathbf{u}. \quad (4)$$

where ρ^f and c^f are the density and specific heat capacity of the fluid. \mathbf{u} denotes the Darcy fluid velocity. In a real geothermal GSHP system, the heat transfer in the pipeline system is governed by the heat advection following the flow process of the refrigerant. Another heat advection process comes from the scenario, when groundwater is

available in the geothermal site. The heat advection due to the groundwater flow, will cause additional thermal recharge in the subsurface. It will be introduced in the next Section 2.1.2.

Within a porous medium, its structure results in a dispersive transport of heat. This hydro-dynamic dispersion process is so called the heat dispersion. The heat flux caused by the dispersion can be written as

$$\mathbf{j}_{disp} = -\rho^f c^f [\alpha_T \|\mathbf{u}\| \mathbf{I} + (\alpha_L - \alpha_T) \frac{\mathbf{u} \otimes \mathbf{u}}{\|\mathbf{u}\|}] \nabla T. \quad (5)$$

Where α_T and α_L denote the transversal and longitudinal dispersivity, respectively. \mathbf{I} is the identity matrix.

Heat storage describes the amount of thermal energy that can be stored in the porous media. In winter, the heat energy stored in the storage media can be extracted to meet the heating demand from the building. In summer, the excessive heat from the building can be injected into the subsurface. The equation to calculate the amount of stored heat Q in a medium with a volume of V reads

$$Q = (\rho c)^{eff} VT, \quad (6)$$

with effective volumetric heat capacity,

$$(\rho c)^{eff} = \varepsilon c^f \rho^f + (1 - \varepsilon) c^s \rho^s. \quad (7)$$

With consideration of all the above mentioned thermal processes, the heat transport equation in the subsurface can be derived by

$$(\rho c)_{eff} \frac{\partial T}{\partial t} + (\rho c)_f \mathbf{u} \cdot \nabla T - \nabla \cdot (\Lambda \cdot \nabla T) = H, \quad (8)$$

with the tensor of thermal hydrodynamic dispersion Λ given by

$$\Lambda = [\varepsilon \lambda^f + (1 - \varepsilon) \lambda^s] \mathbf{I} + \rho^f c^f [\alpha_T \|\mathbf{u}\| \mathbf{I} + (\alpha_L - \alpha_T) \frac{\mathbf{u} \otimes \mathbf{u}}{\|\mathbf{u}\|}]. \quad (9)$$

2.1.1.2 Groundwater flow

When groundwater flow exists in the underground, it brings in additional recharge to the subsurface, and enhances the heat extraction capacity of the BHE array. The governing equation of groundwater flow process is derived from the mass balance of liquid. In a saturated and confined aquifer, it is given by

$$S_s \frac{\partial h_f}{\partial t} = \nabla \cdot \mathbf{u} + Q_L, \quad (10)$$

where S_s is the storage coefficient, h_f is the hydraulic head, Q_L denotes the sink/source term. \mathbf{u} represents the Darcy flow velocity of groundwater. In the case of laminar flow, it can be calculated according to the Darcy's law

$$\mathbf{u} = -K\nabla h_f, \quad (11)$$

where K is the hydraulic conductivity.

When considering the advection of heat flux caused by ground water flow, the advection flow flux \mathbf{u} , which can be obtained by solving the ground water flow processes, should be further transferred into the advection term in the heat transport Eq. (8).

2.1.2 Analytical approaches

In this subsection, the line-source based analytical model for the calculation of the soil temperature change in the subsurface caused by BHE array is introduced. Moreover, different analytical approaches for sizing a BHE array system is summarised and separately described.

2.1.2.1 Soil temperature change in the BHE array subsurface

During the heating or cooling application of a single BHE system, the temperature change ΔT in an infinite homogeneous subsurface can be calculated using the infinite line-source analytical model,

$$\Delta T = \frac{q}{4\pi\lambda} E_1 \frac{r^2}{4\alpha t} \quad (12)$$

where q is the heat transfer rate in the line source. E_1 denotes the exponential integral function, which reads

$$E_1(z) = \int_1^\infty \frac{e^{-tz}}{t} dt. \quad (13)$$

r refers to the distance between the observation point and the line-source. α is the thermal diffusion coefficient. In this model, the BHE is simplified as a nodal source term. More details including its derivation, and some other similar models such as the finite line source model can be found in Stauffer et al. [41]. For multiple BHEs system, Eskilson [12] firstly proposed the super-position borehole model to estimate the soil temperature distribution, where the BHEs are considered as infinite line sources. Based on the superposition principle, the temporal temperature changes can be considered as the result of the superposition of a sequence heat exchange rate pulse at different time steps. Thus, the temperature change at an observation

point with a local coordinate of (i, j) under the influence of a set of $k = 1, \dots, n$ BHE array is given by,

$$\Delta T_{i,j}(t, q_{k=1, \dots, n}) = \sum_{k=1}^n \Delta T_{i,j,k}(t, q_k). \quad (14)$$

Based on the same superposition principle, Bayer et al. [17] proposed a more comprehensive analytical solution to the temporal temperature change at an arbitrary location (i, j) during the operation of a BHE array system. Its mathematical formulation reads

$$\Delta T_{i,j}(x, y, t, q_{k=1, \dots, n, l=1, \dots, m}) = \sum_{l=1}^m \sum_{k=1}^n \frac{q_{k,l}}{4\pi\lambda} \left(E_1 \left[\frac{(i-x_k)^2 + (j-y_k)^2}{4\alpha(t_m - t_{l-1})} \right] - E_1 \left[\frac{(i-x_k)^2 + (j-y_k)^2}{4\alpha(t_m - t_l)} \right] \right). \quad (15)$$

where $q_{k,l}$ denotes the sequence of heat transfer pulses on the k_{th} heat source term at $t = l$ time step. (x_k, y_k) are the location of the k_{th} BHE. Interested readers may also refer to Appendix C.1 for the python script, which reproduces this analytical solution following the concept of Bayer et al. [17].

2.1.2.2 BHE array sizing tools

Recently, various analytical approaches have been developed for the designing of the BHE array. A comprehensive review on these methods and their categories can be found in Ahmadfard and Bernier [19]. Historically, under the assumption that the heat conduction is the only process in the subsurface, Carslaw and Jaeger [18] firstly developed the concentric cylinder source method for the calculation of the heat transfer around a cylinder which is buried in the subsurface. This model was later promoted by Ingersoll and Zobel [42] to be an appropriate method for sizing the multi-BHE array. With consideration of the BHE as a cylinder source, the heat exchange rate \dot{Q} can be calculated by

$$\dot{Q} = \frac{L(T_s - T_f)}{R_{ov}}. \quad (16)$$

where L is the required BHE length. T_s and T_f are the undisturbed ground soil temperature and the temperature in the working fluid within the BHE U-pipe, respectively. R_{ov} is the overall thermal resistance of ground and borehole. With this equation, the required borehole length L to meet designed BHE thermal load can be estimated. According to the Bernier's classification [19], this method is counted as the first category of BHE sizing tools.

Based on Eq. (16), a second category namely two pulse method was developed. For instance, the approach adopted in the Chinese guideline GB50366 – 2019 [39] belongs to this category. In this method, the required BHE lengths under cooling and heating working mode are separately calculated and compared. With two different length values calculated, the greater one will be chosen as the required length for the BHE array. In the two pulse method, the required BHE length of a GSHP system during the heating period can be estimated by,

$$L = \frac{q [R_f + R_{pe} + R_b + R_s \times F_h + R_{sp} \times (1 - F_h)]}{T_s - T_f} \left(\frac{\text{COP} - 1}{\text{COP}} \right). \quad (17)$$

And for cooling application,

$$L = \frac{q [R_f + R_{pe} + R_b + R_s \times F_h + R_{sp} \times (1 - F_h)]}{T_s - T_f} \left(\frac{\text{EER} + 1}{\text{EER}} \right). \quad (18)$$

where the thermal resistance of the entire system consists five parts - resistance of the working fluid R_f , the pipe R_{pe} , the borehole R_b , the ground R_s , and the resistance caused by the short time thermal pulse R_{sp} . Moreover, F_h is the proportion of the working period in terms of the whole working duration. COP and EER denote the system coefficient of performance and energy efficiency ratio, respectively. Be noticed that the thermal interaction among the BHEs in a multiple array is considered in R_s with a specific correction term.

The third category, also named as the three pulse method, requires the thermal load to be divided into three successive pulses, i.e. the peak load, the monthly average load, and the annual average load. The well-known ASHRAE method recommended by American Society of Heating, Refrigerating and Air-Conditioning Engineers [8] belongs to this category. In this method, the system required total BHE length under heating condition is calculated by

$$L = \frac{q_a R_a + (q_l \times \left(\frac{\text{COP} - 1}{\text{COP}} \right)) (R_b + \text{PLF}_m R_m + F_{sp} R_{st})}{T_s - \frac{T_{wt} + T_{wo}}{2} - T_p}. \quad (19)$$

For cooling application,

$$L = \frac{q_a R_a + (q_l \times \left(\frac{\text{COP}_c + 1}{\text{COP}_c} \right)) (R_b + \text{PLF}_m R_m + F_{sp} R_{st})}{T_s - \frac{T_{wt} + T_{wo}}{2} - T_p}, \quad (20)$$

Where q_a refers to the annual average heat transfer in the ground. q_l is the designed thermal load at the building site. COP_s is the cooling coefficient of performance for the heat pump. PLF_m denotes the part-load factor within a individual month. F_{sp} is the short-circuit heat loss factor. T_{wt} and T_{wo} represent the fluid temperature at the inlet and outlet of the heat pump, respectively. The most important

parameters in the equation are the thermal resistance factors R_a , R_m , R_{st} , that are caused by the three successive pulses respectively, and the temperate penalty parameter T_p . These three thermal resistance factors can be calculated by the well known G-function. Details about the formulation of the G-function is introduced in Ingersoll and Zobel [42]. During the operation of a multiple-BHE array, when the heating and cooling load is in equilibrium state, the q_a and T_p are equal to zero in the Eq. (19,20). Then, the total length of all BHEs are directly calculated based on the short-term peak load and the temperature difference between the ground and the system mean working fluid. If the heating and cooling load is imbalanced, a non-zero penalty temperature T_p (Eq. (21)) should be considered,

$$T_p = \frac{Q_{stored}}{\rho c S^2 L} \times f(N, C_{fHoriz}), \quad (21)$$

where S denotes the adjacent distance among the BHEs. $f(N, C_{fHoriz})$ is a constant correction factor according to the arrangement of the array. The Eq. (21) also depicts the relationship between the change of excessive soil temperature within the array area (T_p) and the imbalanced thermal amount of the system (Q_{stored}). In this method, the total BHE length is iteratively determined by successive correcting the value of T_p . The comprehensive procedure of this iteration is described in the ASHRAE guideline [8].

As stated in Section 1.3, thermal interaction among BHEs are non-ignored in a multiple-BHE array system. Although in some approaches such as the one in the ASHRAE or Chinese guideline, corrections have been added to consider the thermal interactions, the corrections are based on empirical relations and relative simple. Moreover, the heat extraction rate on each BHE is considered as identical, which is however not the case due to the thermal interference in the real BHE array. Beside the difficulties in the handling of the thermal interactions, another inherent shortage of the most analytical models is that they are not able to accurate model a BHEs system under a complex conditions. As alternative to the analytical approaches, numerical modelling offers the possibility to reproduce the BHEs performance, the thermal interactions among BHEs, and their influence on the subsurface under more complex conditions.

2.1.3 Numerical model

In this work, numerical modelling is adopted to investigate the system behavior of a multiple-BHE array in long-term operation. The numerical approach implemented in the OpenGeoSys (OGS) software is a Finite Element based modelling platform, which is developed specifically for the simulation of the coupled THMC processes in porous media (cf. Kolditz et al. [31]).

2.1.3.1 Dual-continuum model

The subsurface BHE model used in this work is based on the dual-continuum approach (DCA), which was originally proposed by Al-Khoury et al. [43, 44], and it was further developed and extended later by Diersch et al. [45, 46].

Figure 1 (a) illustrates the mesh of a simple subsurface BHE model based on the DCA. The prism elements represent the subsurface soil part, while the BHE is represented by the line elements and marked in grey color. The BHE line elements are set on the edge of the prism and share the same nodes with that soil element. In the DCA, the BHE part does not have a full spatial extension, which contains different components within a BHE. Instead, all BHE components such as BHE U-pipe and borehole grout are incorporated in one line element. To describe the heat transfer among different BHE components, an extended thermal capacity-resistor model (TCRM) proposed by Bauer et al. [47] is applied. The right sketch in Figure 1 (b) illustrates the TCRM model for the 1U-type BHE. The components with indices "i", "o", "g", and "s" represent the inlet pipe, outlet pipe, grout, and soil materials respectively. Within the cross-sectional areas ($A-A'$ in Figure 1), the heat transfer between the soil and grout parts, the grout #1 and grout #2, the grout #1 and inflow fluid, the grout #2 and outflow fluid are separately calculated. Besides, the heat storage in each grout parts is considered. In this model, thermal resistances between each two components are denoted by different R . Since the BHE element is sharing the same mesh node with the surrounding soil element, the borehole wall temperature in the BHE model is consistent with the soil temperature at the node. By applying the TCRM model, the fluid circulation process inside the borehole U-pipe, together with the associated heat transport through the grout to the soil, are able to be simulated by governing equations on 1D vertical line elements. The heat exchange between the borehole and the surrounding soil is regulated by the heat flux calculation that depends on the temperature difference and the heat transfer coefficient between the two compartments. The DCA model allows 3D simulations of groundwater flow facilitated heat transport in the heterogeneous subsurface, while achieving a considerable reduction in the number of mesh elements. This allows great speed-up of the large BHE array model simulation, while high-level computational accuracy is still achieved.

According to Diersch et al. [45], the governing equations for the heat transport within soil subsurface reads,

$$\frac{\partial}{\partial t} \left\{ \left[\varepsilon \rho^f c^f + (1 - \varepsilon) \rho^s c^s \right] T_s \right\} + \nabla \cdot \left(\rho^f c^f \mathbf{u} T_s \right) - \nabla \cdot (\Lambda \cdot \nabla T_s) = H_s. \quad (22)$$

Where ε is the porosity of the soil. \mathbf{u} is the Darcy velocity of ground water flow. And Λ denotes the thermal dispersion coefficient in the subsurface. H_s refers to the heat source and sink term.

In grout zone #1 and #2,

$$\begin{aligned} \frac{\partial}{\partial t} (\varepsilon_g \rho^g c^g T_{g1}) - \nabla \cdot (\varepsilon_g \lambda^g \nabla T_{g1}) &= H_{g1} \quad \text{in } \Omega_{g1} \\ \frac{\partial}{\partial t} (\varepsilon_g \rho^g c^g T_{g2}) - \nabla \cdot (\varepsilon_g \lambda^g \nabla T_{g2}) &= H_{g2} \quad \text{in } \Omega_{g2} \end{aligned}$$

with

$$\begin{aligned} q_{nT_{g1}} &= -\Phi_{gs}^{1U} (T_s - T_{g1}) - \Phi_{fig}^{1U} (T_{i1} - T_{g1}) - \Phi_{gg}^{1U} (T_{g2} - T_{g1}) \quad \text{in } \Gamma_{g1} \\ q_{nT_{g2}} &= -\Phi_{gs}^{1U} (T_s - T_{g2}) - \Phi_{fig}^{1U} (T_{o1} - T_{g2}) - \Phi_{gg}^{1U} (T_{g1} - T_{g2}) \quad \text{in } \Gamma_{g2}. \end{aligned} \quad (23)$$

Where ε_g is the porosity of the grout. Ω and Γ denote the domain and the boundary of each grout part, respectively. q_n refers to the heat flux on the boundaries. ϕ is the heat transfer coefficient between each components.

For fluid within the inlet and outlet pipe,

$$\begin{aligned} \frac{\partial}{\partial t} (\rho^r c^r T_{i1}) + \nabla \cdot (\rho^r c^r \mathbf{v} T_{i1}) - \nabla \cdot (\Lambda^r \cdot \nabla T_{i1}) &= H_{i1} \quad \text{in } \Omega_{i1} \\ \frac{\partial}{\partial t} (\rho^r c^r T_{o1}) + \nabla \cdot (\rho^r c^r \mathbf{v} T_{o1}) - \nabla \cdot (\Lambda^r \cdot \nabla T_{o1}) &= H_{o1} \quad \text{in } \Omega_{o1} \end{aligned}$$

with

$$\begin{aligned} q_{nT_{i1}} &= -\Phi_{fig}^{1U} (T_{g1} - T_{i1}) \quad \text{in } \Gamma_{i1} \\ q_{nT_{o1}} &= -\Phi_{fig}^{1U} (T_{g2} - T_{o1}) \quad \text{in } \Gamma_{o1}, \end{aligned} \quad (24)$$

Where \mathbf{v} denote the velocity of circulating fluid inside the pipe. Λ denotes the thermal dispersion coefficient of the circulation fluid.

2.1.3.2 Finite element realisation

In the OpenGeoSys software, the governing equations for heat transport in soil (Eq. (22)), in grout zone (Eq. (23)), and in the fluid flow within the pipes (Eq. (24)) are solved using finite element method (FEM). When steady state of groundwater flow is assumed, the advection term in Eq. (10) can be applied. Besides, constant advective velocity \mathbf{u} is adopted in Eq. (22), indicating a fixed circulation flow rate in the BHE. For the finite element formulation, the weak form should be obtained by introducing a weighting function (W_j^e) in the strong form of the problem, which is derived by integration of the governing equations over the entire domain. The standard Bubnov-Galerkin-method (cf. Zienkiewicz et al. [48]) is applied for the spatial discretisation, where the shape function is adopted also as weighting function (i.e. $N_j^e = W_j^e$). As a consequence, a set of algebraic equations

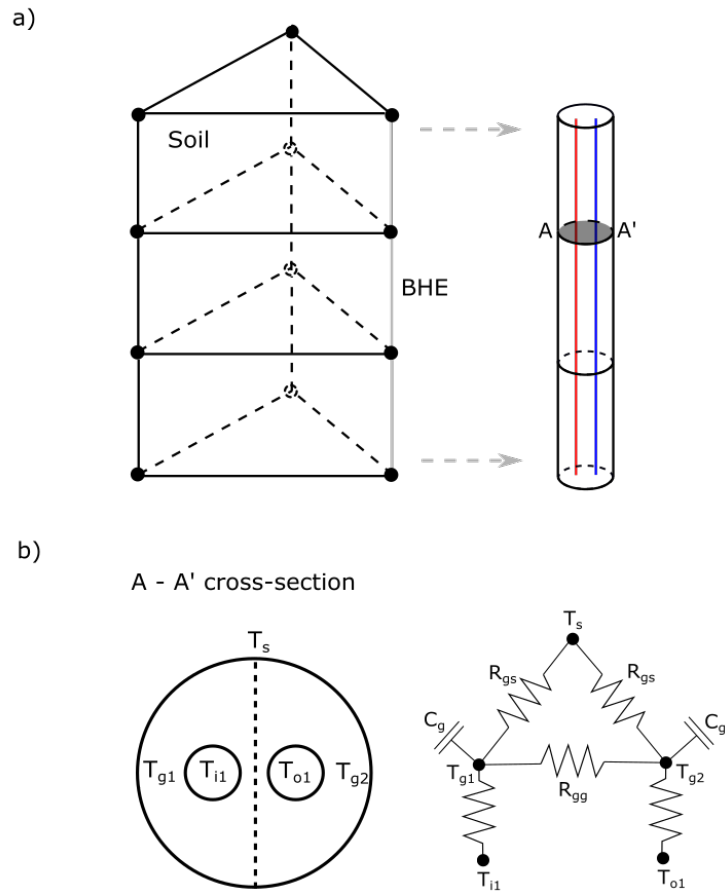


Figure 1: (a): Subsurface BHE numerical model for the dual-continuum approach. Mesh with prism soil element and the line element for the BHE. (b): Schematic sketch of a 1U-type BHE for the dual-continuum approach and its TCRM model (reproduced after Diersch et al. [45])

for the unknowns (soil temperature (T_s), BHE inflow temperature (T_{i1}), outflow temperature (T_{o1}), grout temperature (T_{g1}, T_{g2})) are obtained and given in the following general form,

$$\hat{\mathbf{M}}^S \cdot \hat{\mathbf{T}}^S - (\hat{\mathbf{L}}^S - \hat{\mathbf{R}}^B) \cdot \hat{\mathbf{T}}^S - \hat{\mathbf{R}}^{SB} \cdot \hat{\mathbf{T}}^B = \mathbf{H}^S, \quad (25)$$

$$\hat{\mathbf{M}}^B \cdot \hat{\mathbf{T}}^B - \hat{\mathbf{L}}^B \cdot \hat{\mathbf{T}}^B - \hat{\mathbf{R}}^{BS} \cdot \hat{\mathbf{T}}^S = \mathbf{0}, \quad (26)$$

where the indices **B** and **S** represent the BHE and soil part, respectively. Thus, $\mathbf{T}_B = (\mathbf{T}_{i1}, \mathbf{T}_{o1}, \mathbf{T}_{g1}, \mathbf{T}_{g2})$. Further, the Matrix and vectors in this equation can be extended expressed as

$$\hat{\mathbf{M}}_k = \sum^e \int^{\Omega_k^e} [(\rho c)_h N_i N_j] d\Omega^e \text{ for } k = i1, o1, g1, g2, \quad (27)$$

$$\hat{\mathbf{L}}_k = \sum^e \int^{\Omega_k^e} [N_i (\rho c)_h \nabla N_j + \nabla N_i \cdot (\lambda_h \cdot \nabla N_j)] d\Omega^e \text{ for } k = i1, o1, \quad (28)$$

$$\hat{\mathbf{L}}_k = \sum^e \int^{\Omega_k^e} [\nabla N_i \cdot (\lambda_g \cdot \nabla N_j)] d\Omega^e \text{ for } k = g1, g2, \quad (29)$$

$$\hat{\mathbf{R}}^{BS} = \sum^e \int^{\Gamma_k^e} \Phi N_i N_j d\Gamma^e \text{ for } k = i1, o1, g1, g2. \quad (30)$$

Applying the numerical integration – GAUSS-Quadrature method, the final integral system is transformed into a weighted sum of the function values at specified integration points.

For the entire domain, the local element matrix present above have to be assembled into a global matrix system,

$$\begin{pmatrix} \mathbf{M}^S & \mathbf{0} \\ \mathbf{0} & \mathbf{M}^B \end{pmatrix} \cdot \begin{pmatrix} \hat{\mathbf{T}}^S \\ \hat{\mathbf{T}}^B \end{pmatrix} - \begin{pmatrix} \mathbf{L}^* & \mathbf{R}^{SB} \\ \mathbf{R}^{BS} & \mathbf{L}^B \end{pmatrix} \cdot \begin{pmatrix} \mathbf{T}^S \\ \mathbf{T}^B \end{pmatrix} = \begin{pmatrix} \mathbf{H}^S \\ \mathbf{0} \end{pmatrix} \quad (31)$$

where $\mathbf{L}^* = \mathbf{L}^S - \mathbf{R}^B$, $\mathbf{R}^{SB} = \mathbf{R}^{BS}$, and \mathbf{H}^S denotes the source/sink term.

For the time discretisation, fully implicit scheme – backward Euler method is applied. And the global matrix system then becomes

$$\begin{pmatrix} \mathbf{A}^S & \mathbf{R}^{SB} \\ \mathbf{R}^{BS} & \mathbf{A}^B \end{pmatrix} \cdot \begin{pmatrix} \mathbf{T}^S \\ \mathbf{T}^B \end{pmatrix}_{n+1} = \begin{pmatrix} \mathbf{B}^S \\ \mathbf{B}^B \end{pmatrix}_{n+1,n}, \quad (32)$$

with

$$\begin{aligned}
\mathbf{A}^S &= \frac{1}{\Delta t_n} \mathbf{M}^S - \mathbf{L}^*, \\
\mathbf{B}^S &= \frac{1}{\Delta t_n} \mathbf{M}^S \cdot \mathbf{T}_n^S + \mathbf{W}_{n+1}^S, \\
\mathbf{A}^B &= \frac{1}{\Delta t_n} \mathbf{M}^B - \mathbf{L}^B, \\
\mathbf{B}^B &= \frac{1}{\Delta t_n} \mathbf{M}^B \cdot \mathbf{T}_n^B.
\end{aligned}
\tag{33}$$

where n and $n + 1$ denote the previous and current time step, and $\Delta t_n = t_{n+1} - t_n$ represents the current time step size. To be noticed, all the four heat exchange terms \mathbf{A}^S , \mathbf{R}^{BS} , \mathbf{R}^{SB} , \mathbf{A}^B in the Eq. (33) are independent on the unknowns \mathbf{T}_B and \mathbf{T}_s . It means the present global system matrix is possible to be a linear problem.

2.1.3.3 Setting of boundary conditions

Since the circulation fluid temperature within the BHE U-pipe could change over time, as one of the boundary conditions the inlet fluid temperature imposed on the top node of the BHE line element should be updated at each time step. Besides, at the bottom node of the BHE line element, the inlet temperature should be consistent with the temperature from the outlet pipe. Such boundary conditions are imposed in the global algebraic system according to the following procedure,

- i Assuming we know the boundary value on one of the node in the global matrix (Eq. (34)), record the index of boundary node, say "i".
- ii The right hand side (RHS) vector \mathbf{b} is subtracted with the multiplication product of fixed boundary node value with the i-th column of left hand side (LHS) matrix.
- iii Record the i-th row and column entry value in the LHS matrix as a TMP parameter.
- iv Make the i-th row and i-th column values in the LHS matrix to be all zeros.
- v Overwrite the i-th value in RHS vector using the TMP parameter times the fixed boundary value.
- vi Overwrite the i-th row and column entry value in LHS matrix as the TMP parameter.

$$\begin{bmatrix} a_{11} & a_{12} & a_{13} & \dots & a_{1n} \\ a_{21} & a_{22} & a_{23} & \dots & a_{2n} \\ \dots & \dots & \dots & \dots & \dots \\ a_{i1} & a_{i2} & a_{i3} & \dots & a_{in} \\ \dots & \dots & \dots & \dots & \dots \\ a_{n1} & a_{n2} & a_{n3} & \dots & a_{nn} \end{bmatrix} \begin{bmatrix} x_1 \\ x_2 \\ \dots \\ x_i \\ \dots \\ x_n \end{bmatrix} = \begin{bmatrix} b_1 \\ b_2 \\ \dots \\ b_i \\ \dots \\ b_n \end{bmatrix} \quad (34)$$

Different boundary conditions can be applied on the BHE top node to consider different operation strategies for the BHE array. For instance, during the operation, if the inlet of the BHE is fixed with constant or time dependent temperature, the imposed boundary conditions x_i at the BHE top node is independent of other primary variables. Thus, in this case, the coupled heat transport problem remains to be linear. In contrast, if a constant or a time dependent power is fixed by the BHE, which means the BHE operation is under a power boundary condition, depending on the required power the inflow temperature is correlated with the outflow temperature in each time step. Mathematically, the correlation between the inflow T_{in} and outflow temperature T_{out} should satisfy the Eq. (35).

$$\dot{Q} = (\rho c)_f \dot{V} (T_{in} - T_{out}), \quad (35)$$

where \dot{Q} is the required thermal load on the BHE. \dot{V} is the volumetric flow rate within the BHE U-pipe. In this case, since the primary variable - the BHE inlet fluid is dependent on another primary variable - the BHE outlet fluid, the global matrix becomes non-linear. In this case, the Picard or Newton iteration schemes have to be applied.

As aforementioned, on the BHE bottom node the fluid temperature from the inlet pipe should equal to the fluid temperature from the outlet pipe, which imposes an additional constrain on the linear equation system. In the currently released OGS version (OGS6.3.3), in the module *HeatTransportBHE* process, an additional boundary condition is defined on the outlet temperature at the bottom node of BHE, whose value is assigned with the calculated temperature of the inlet pipe at the same location from the last iteration. In this case, the problem remains non-linear, thus Picard iteration is applied, which leads to a increase of the computational cost.

Alternatively, to handle this correlation between the inlet and outlet fluid temperature on the bottom point we introduced an add additional condition in the global equation matrix. To be specific, suppose that there is an additional condition to the linear equation system $\mathbf{Ax} = \mathbf{b}$, which is $x_i = x_j$ (with $i, j \in \{1, \dots, n\}$ and $i \neq j$). The condition is equivalence to the equation $x_i - x_j = 0$. Then an extra row vector $\vec{a} = (0, \dots, 1, \dots, -1, \dots, 0) \in \mathbb{R}^{1 \times n}$ can be added into the bottom of \mathbf{A} matrix, where 1 is at the i -th position and -1 is at the j -th position. In real operation, this 1 and -1 can be factorized to e.g. 1000 and -1000 ,

based on the magnitude of the values in the same column of the $\vec{\mathbf{A}}$ matrix. After this numerical manipulation, the previous \mathbf{A} matrix is changed to $\vec{\mathbf{A}}$, with

$$\vec{\mathbf{A}} = \begin{pmatrix} \vec{\mathbf{A}} \\ \vec{a} \end{pmatrix} \in \mathbb{R}^{(n+1) \times n}. \quad (36)$$

The RHS vector \mathbf{b} needs to be changed accordingly, with

$$\vec{\mathbf{b}} = \begin{pmatrix} \mathbf{b} \\ 0 \end{pmatrix} \in \mathbb{R}^{(n+1)}. \quad (37)$$

When multiple conditions are given, we can generalise them as several linear equations $f(x) = 0$. By rewriting the new equations in a matrix form e.g. $\vec{\mathbf{A}}\mathbf{x} = \vec{\mathbf{b}}$, a new global equations system can be constructed by adding the new matrix into the given matrix \mathbf{A} , which is

$$\begin{pmatrix} \mathbf{A} \\ \vec{\mathbf{A}} \end{pmatrix} \mathbf{x} = \begin{pmatrix} \mathbf{b} \\ \vec{\mathbf{b}} \end{pmatrix}. \quad (38)$$

Note that the extended linear equation system is now $\vec{\mathbf{A}}\mathbf{x} = \vec{\mathbf{b}}$, where the rank of $\vec{\mathbf{A}}$ is larger than it of \mathbf{x} . For solving this under-determined linear equation system, the Singular Value Decomposition (SVD) approach can be adopted.

2.1.3.4 Schur complement method

Usually, all the soil and BHE primary variables can be monolithic solved in the global equation system (Eq. (32)). However, there is still a way to reduce the size of the global system and make the computational procedure more effective. The mathematical conversion is so called the Schur complement method, which is described in details in section 13.5.2.2 of Diersch [29].

Taking the second row in the matrix system (Eq. (32)), the equation yields

$$\mathbf{T}_{n+1}^{\mathbf{B}} = (\mathbf{A}^{\mathbf{B}})^{-1} \cdot (\mathbf{B}_{n+1,n}^{\mathbf{B}} - \mathbf{R}^{\mathbf{BS}} \cdot \mathbf{T}_{n+1}^{\mathbf{S}}). \quad (39)$$

Then, for the first row in matrix system (Eq. (32)), the BHE temperature vector $\mathbf{T}_{n+1}^{\mathbf{B}}$ within the equation can be eliminated by using the Eq. (39). Finally, the global matrix system can be reduced to the form as follows.

$$(\mathbf{A}^{\mathbf{B}} - \mathbf{A}^{\mathbf{BS}}) \cdot \mathbf{T}_{n+1}^{\mathbf{S}} = \mathbf{B}_{n+1,n}^{\mathbf{S}} - \mathbf{B}_{n+1,n}^{\mathbf{BS}} \quad (40)$$

with

$$\begin{aligned}\mathbf{A}^{\text{BS}} &= \mathbf{R}^{\text{SB}} \cdot ((\mathbf{A}^{\text{B}})^{-1} \cdot \mathbf{R}^{\text{BS}}) \\ \mathbf{B}_{n+1,n}^{\text{BS}} &= \mathbf{R}^{\text{SB}} \cdot ((\mathbf{A}^{\text{B}})^{-1} \cdot \mathbf{B}_{n+1,n}^{\text{BS}}).\end{aligned}\quad (41)$$

In the Eq. (40), the modified matrix $\mathbf{A}^{\text{B}} - \mathbf{A}^{\text{BS}}$ is known as the Schur complement [49]. Usually, this modified matrix can be locally computed. The reason is the computational cost of inverting the matrix $((\mathbf{A}^{\text{B}})^{-1})$ is negligible in comparison to the solution of global equation (Eq. (32)). Compared to the solution of global matrix system (Eq. (32)) in a monolithic manner, the Schur complement method has obvious advantages. Firstly, the size of the new global matrix system (Eq. (40)) is reduced, as all the BHE part in the matrix is eliminated. And when the soil temperature vector \mathbf{T}_{S} is obtained, the BHE temperature vector can be directly recomputed from Eq. (39). Secondly, after the Schur complement, the global matrix becomes very regular, since there is only soil part in it. Based on it, the parallelization scheme can be easily applied on the global matrix system (Eq. (40)), which may effectively accelerate the computation when the simulation of a large BHE model is needed.

2.2 Pipeline network model

In a multiple-BHE based GSHP system, the BHEs are connected with each other through pipeline network. In the heating mode, the circulated fluid in the pipe network is firstly pumped into the network with an elevated hydraulic head. Then the fluid is divided into different sub-branches and flows into each BHE U-pipe with the designed array arrangement. After completing the heat exchange in each BHE, the fluid from each sub-branch is merged together and flows back to the heat pump, where the heat is extracted to the building side. Finally, the fluid flowing out of the heat exchanger enters the circulation pump again and completes this closed circulation.

2.2.1 Conservation laws within the pipeline network

In this work, we assume the fluid in the entire pipeline network is in steady state. According to the mass conservation law, the total amount of fluid entering a single ($\dot{m}_{in,j}$) component must be equal to the same amount leaving ($\dot{m}_{out,i}$) it (Eq. (42)).

$$\sum_j \dot{m}_{in,j} = \sum_i \dot{m}_{out,i}. \quad (42)$$

Due to the hydraulic resistance of the pipe, a drop in hydraulic head can be observed between the inlet and outlet of the pipe. To quantify

this head loss, the well known Darcy-Weisbach equation (cf. Böswirth and Bschorer [50]) is adopted

$$\begin{aligned} p_{in} - p_{out} &= \frac{\rho}{2} \cdot v^2 \cdot \frac{\zeta(Re, k_s, D) \cdot L}{D} \\ &= \frac{8 \cdot \dot{m}^2 \cdot L \cdot \zeta(Re, k_s, D)}{\rho \cdot \pi^2 \cdot D^5}, \end{aligned} \quad (43)$$

where the friction factor of the pipe ζ is a function of the Reynolds number Re , roughness coefficient of the pipe k_s , and the pipe's diameter D . The Reynolds number Re can be determined according to the pressure, the enthalpy, and the flow rate. Similar formulations as Eq. (43) also exist to quantify the head loss caused by the friction between the pipe and fluid, e.g. the Hazen-Williams equation and the Manning equation. Details about these empirical equations can be found in Houghtalen et al. [51].

To calculate the heat distribution within the pipeline network, energy balance (Eq. (44)) between the inflow and outflow of a single component is also adopted,

$$\dot{Q} + P = \sum_i \dot{m}_{out,i} \cdot h_{out,i} - \sum_j \dot{m}_{in,j} \cdot h_{in,j}. \quad (44)$$

In the above equation, the power P and the heat transfer \dot{Q} can be zero in certain cases where an adiabatic component does not have additional power or transfer heat.

2.2.2 Solution algorithm

Historically, different methods have been developed to solve the hydraulic and energy balance of the pipe network. One of the well-known methods is the Hardy-Cross Method [52], which is the earliest systematic approach adopted for network analysis. In this method, the flow rate and hydraulic head balance in every closed-form pipe loop can be calculated. The Newton-Raphson method may be viewed as an extension of the Cross's closed loop method, where the Newton-Raphson derivation is incorporated. The optimisation method [53] is another commonly used approach, which uses mathematical optimization techniques to solve the non-linear equation problem in network analysis. Moreover, in [54] Todini and Pilati's gradient method was proposed, which is based on the hybrid node-loop approach method and may be regarded as a bridge between the optimisation method and the Newton-Raphson method. This gradient method is applied in the widely recognised software EPANET [55], which is used as the standard tool in US for the modelling of drinking water supply systems. In this work, the software Thermal Engineering Systems in

Python (TESPy) developed by Witte [56] was adopted to solve the thermal and hydraulic balance equations representing the pipe network. TESPy is specifically designed for the simulation of coupled thermal-hydraulic processes in the field of thermal engineering. TESPy allows the definition of the topological and properties of different components in a thermal system, including pipes, heat exchangers and different types of turbomachinery. TESPy uses the Newton-Raphson method to handle the non-linear systems behaviour. Due to the non-linearity from Eq. (42) to (44), the multi-dimension Newton-Raphson method is adopted, where all the system equations are summarized into a nonlinear equations system $f(x_i) = 0$.

In the first iteration, a set of arbitrary start values x_1, x_2, \dots, x_k for each unknown are assigned into the equation system. Then, the residuals of $f(x_i)$ are determined by applying these values. Meanwhile, by applying partial derivatives of the above equations over the primary variables, the jacobian matrix of the governing equations (Eq. (45)) can be obtained, which reads

$$J(x) = \begin{pmatrix} \frac{\partial f_1}{\partial x_1} & \frac{\partial f_1}{\partial x_2} & \dots & \frac{\partial f_1}{\partial x_k} \\ \frac{\partial f_2}{\partial x_1} & \frac{\partial f_2}{\partial x_2} & \dots & \frac{\partial f_2}{\partial x_k} \\ \vdots & \vdots & \ddots & \vdots \\ \frac{\partial f_n}{\partial x_1} & \frac{\partial f_n}{\partial x_2} & \dots & \frac{\partial f_n}{\partial x_k} \end{pmatrix} \quad (45)$$

In the next iteration, the increment of the primary variables Δx is calculated by multiplied the system residual with the inverted Jacobian matrix. The iteration process is repeated until the norm of the residual $\|f(x_i)\|$ is smaller than a pre-defined error tolerance ϵ . The the above Newton iteration procedure, the steady state hydraulic and thermal status of the system can be obtained.

$$\|f(x_i)\| \leq \epsilon \quad (46)$$

2.2.3 Pipeline network model in TESPy

In TESPy, the network model is constructed with component based architecture. The respective components can be connected in an arbitrary topological network model. The characteristics of the network system are specified with giving the topology and applying the specific parameters of the components in the network. Then, a set of coupled equations (Eqs. (42) to (44)) on each component and connection within the entire network are generated. Due to the highly non-linearity of the coupled global system equations, the above mentioned Newton-Raphson algorithm is adopted. Moreover, the simulated processes in the network are highly coupled. For instance, the temperature change

of the circulation fluid can lead to the change of the fluid density and viscosity, which could further affect the pressure and enthalpy. To handle these coupling phenomenon, the CoolProp library (Bell et al. [57]) is internally called and adopted in TESPpy to capture the temperature variation induced change of fluid properties. In TESPpy, the mass flow, fluid pressure and enthalpy at every connection point of the network are chosen as the primary variables and solved in the thermal and hydraulic steady-state. Then the temperature, which is treated as a secondary primary variable, is calculated in CoolProp library based on the calculated pressure and enthalpy. More details about TESPpy inclusive its benchmarks and tutorials, can be found in the TESPpy online documentation [58].

2.3 Integrated BHE model with pipeline network

In order to quantify the thermal load on each individual BHE in the array as introduced in Section 1.3, temperature distribution in soil and the hydro-thermal interference in the network must be calculated in a coupled manner. For this purpose, a comprehensive numerical model is developed in this work, in which the shallow subsurface, multiple BHEs, and pipe network are simulated with the interactions explicitly considered. In this model, the heat transport process in the subsurface and BHEs is modelled by OGS, while the hydro-thermal process within the pipe network is solved by TESPpy. Figure 2 illustrates the coupling mechanism between OGS and TESPpy, along with the solution strategy. In the first iteration, within one time step t_i , the subsurface soil and BHE heat transport model is firstly solved in OGS, using the inflow temperature T_{in} and the volumetric flow rate \dot{V} from the previous time step as the Dirichlet boundary conditions. The solved outflow temperature T_{out} on each BHE is then transferred to TESPpy through a data exchange interface. With T_{out} and the current hydraulic and thermal state serving as boundary conditions, TESPpy will calculate the thermal and hydraulic balance of the pipeline network. This gives a set of numerical solution of the inflow temperature T_{in} and the flow rate \dot{V} of each BHE. The computed result will then be transferred back to OGS for the next iteration. The iterations between OGS and TESPpy are considered to be converged, when the relative error tolerance ϵ between the current and the previous iteration is smaller than a pre-set value. When the above mentioned convergence criterion is fulfilled, the thermal, hydraulic, and energy balance in both the OGS subsurface model and TESPpy pipeline network model will be guaranteed.

One thing to be noticed is that the heat transport in OGS model is transient, while the fluid and heat flow in the pipe network is treated as in steady state. Thus, the model may not be valid for the short-term scenarios (seconds to minutes). However, when the time step is set to be large (days to weeks), the assumption of steady-state flow and

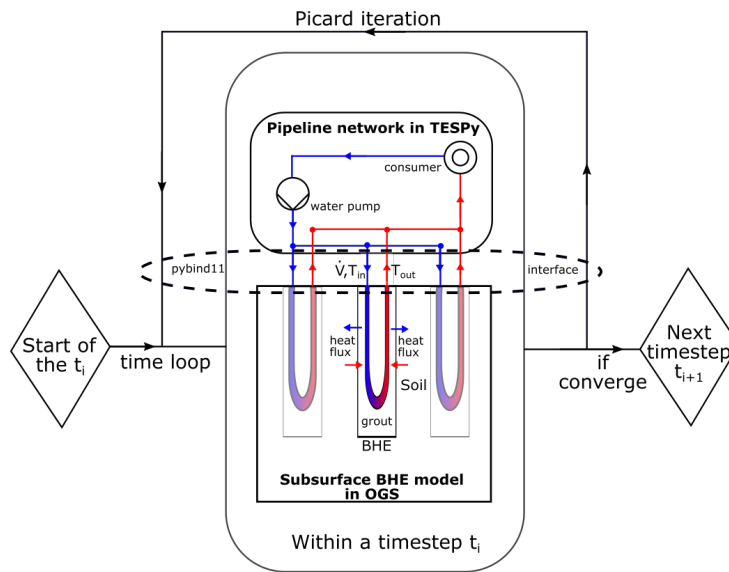


Figure 2: Schematised procedure of the coupling subsurface BHE model in OpenGeoSys with pipeline network model in TESPpy software.

heat transfer in the pipe network can be well preserved. Therefore, the coupled OGS-TESPpy model is dominantly applied for the investigation of the long-term behaviour of a BHE array, for example over decades of operation.

IMPLEMENTATION OF THE MODEL

In this chapter, the implementation scheme of the BHE array model coupled with the pipeline network, and the usage of this model based on a simple example are described. This BHE array model is implemented based on the existing *HeatTransportBHE* module in OGS6 and specified with the name *PipeNetwork*. The example to demonstrate the application of the new feature is a three-BHE benchmark. Its description can be found in the OGS online documentations [59, 60].

3.1 Model preparation

OpenGeoSys

Before running the simulation, a subsurface model containing the required number of BHEs should be constructed in OGS. Details about the workflow for the model construction can be found in the PhD dissertation of Hein [61] and the lecture notes of Shao et al. [62]. In the benchmark example illustrated in Figure 3, three 1U type BHEs are constructed, with prism elements for the soil part and line elements for the BHEs. These BHE line elements are located in the centre of the model with an adjacent distance of 6 m from each other. For the simulations, the model parameters for both BHEs and subsurface soil (e.g. thermal conductivity, storage, etc.) should be assigned. Moreover, the corresponding initial soil temperature and corresponding boundary conditions should be given.

TESPy

The connections of the BHEs in an array are defined in TESPpy within a pipeline network. As shown in Figure 4, these three BHEs are connected parallelly. Other relevant components in the network, e.g. the water pump, the heat pump, the splitter manifold and the merge to collect the flow, are all added into the network. A full list of available components can be found in the TESPpy components module [58].

Generally, in the TESPpy model, the fluid can be set to emerge from a source or being drained in a sink term. Moreover, as illustrated in Figure 4, the fluid can be circulated in a loop. For all components in the network their characteristics of the system should be specified. In the present example, a pump curve for the water pump rate, the physical

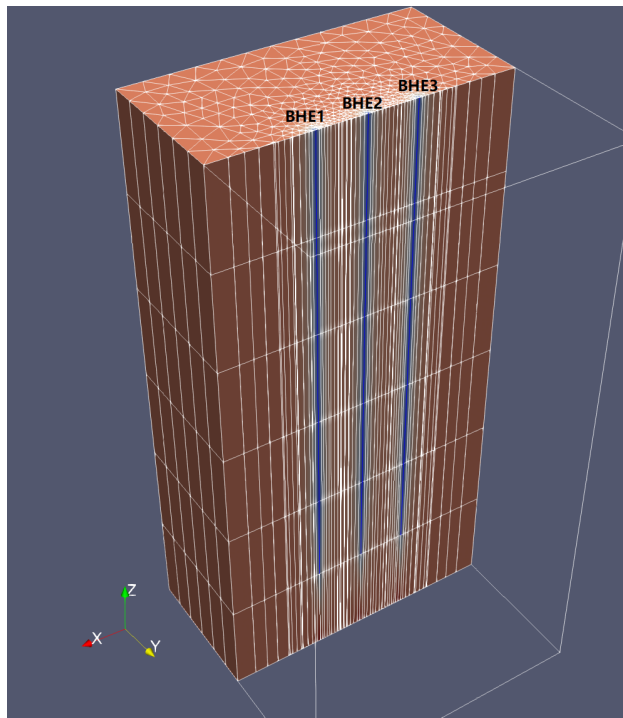


Figure 3: Model domain of the three BHE subsurface model

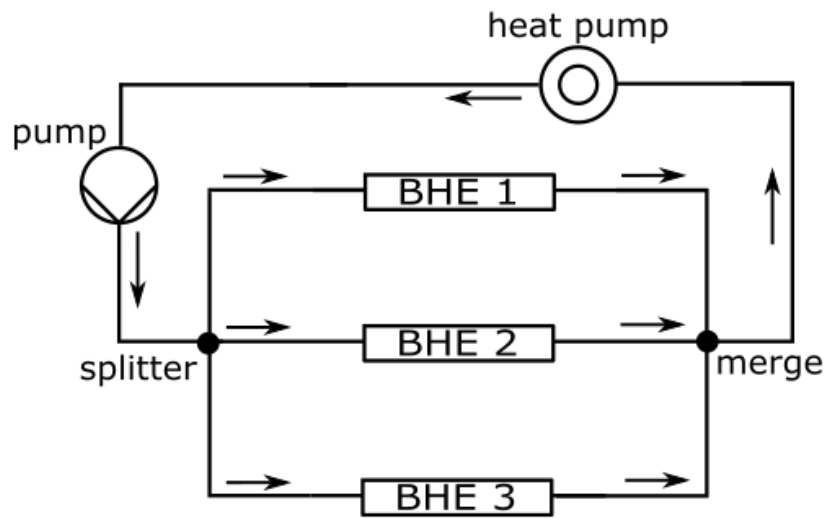


Figure 4: Topological Pipeline network model in TESPpy

properties (e.g. length, diameter, roughness) of the BHE pipes, and the imposed thermal load on the heat pump are assigned. In the present model, heat pump is assumed not to consume any electricity and deliver additional heat to the system. However, users may also choose to define a comprehensive heat pump model in TESPYPY, by which the COP is dependent on the fluid temperature. Before calculation, several system boundary conditions are required to be specified on the connections. For instance, the inflow rate and pressure are given in this case on the entry points of the pump. And all BHEs are specified with an outflow temperature. Only after the configuration and characterisation of these components and the connections, the steady state of the network system can be solved. To be noticed is that these boundary conditions value in the TESPYPY model is time dependent and will be updated according to the computational results from OGS in each time step.

3.2 Coupling OpenGeoSys and TESPYPY

In order to couple OGS and TESPYPY, an OGS-TESPYPY interface was developed between the OGS subsurface model and the TESPYPY network model using Python. The interface is designed for the data exchange between OGS and TESPYPY, within each iterations through the simulation. In the interface, the following three functions were defined, enabling the users to specify self-defined time-dependent boundary conditions.

- *network_status*: This function allows the user to switch on or off the network in TESPYPY in any time step.
- *consumer_demand*: With this function, the user can specify a time dependent thermal load on the heat pump component.
- *dyn_frate*: This function enables the user to define a specified time-dependent flow rate at the inlet of the pipeline network.

According to the user-specified information in the functions above, the coupled model will adjust its thermal and hydraulic boundary conditions in each time step.

In the OGS-TESPYPY python interface, the main solver for calling the TESPYPY pipe network calculation is given in the class *BC(OpenGeoSys.BHENetwork)*. In this class, two functions *initializeDataContainer* and *tespySolver* are defined. The first one will initialise the data exchange container and all the pipe network based BHE parameters in the OGS *HeatTransportBHE* process. The second one, which is the *tespySolver* function, contains the main TESPYPY calculation process for the pipe network. During the simulation, this function will be called in each calculation iteration to update the circulation fluid variables as introduced in Section 2.3.

The above mentioned python interface is embedded in the OGS source code via the *pybind11* library. *pybind11* is a lightweight header-only library that exposes C++ types in Python, with the main purpose to create Python bindings in existing C++ code [63]. It has been embedded in OGS6 Lehmann [64] and enables the definition of boundary conditions of the model via an external Python script. Figure 5 depicts the framework of data exchange that is implemented in the *PipeNetwork* feature in OGS. Through the *pybind11* library, the functions defined in the OGS-TESPy interface *BC* class can seamlessly be called as an external script in the OGS *HeatTransportBHE* process.

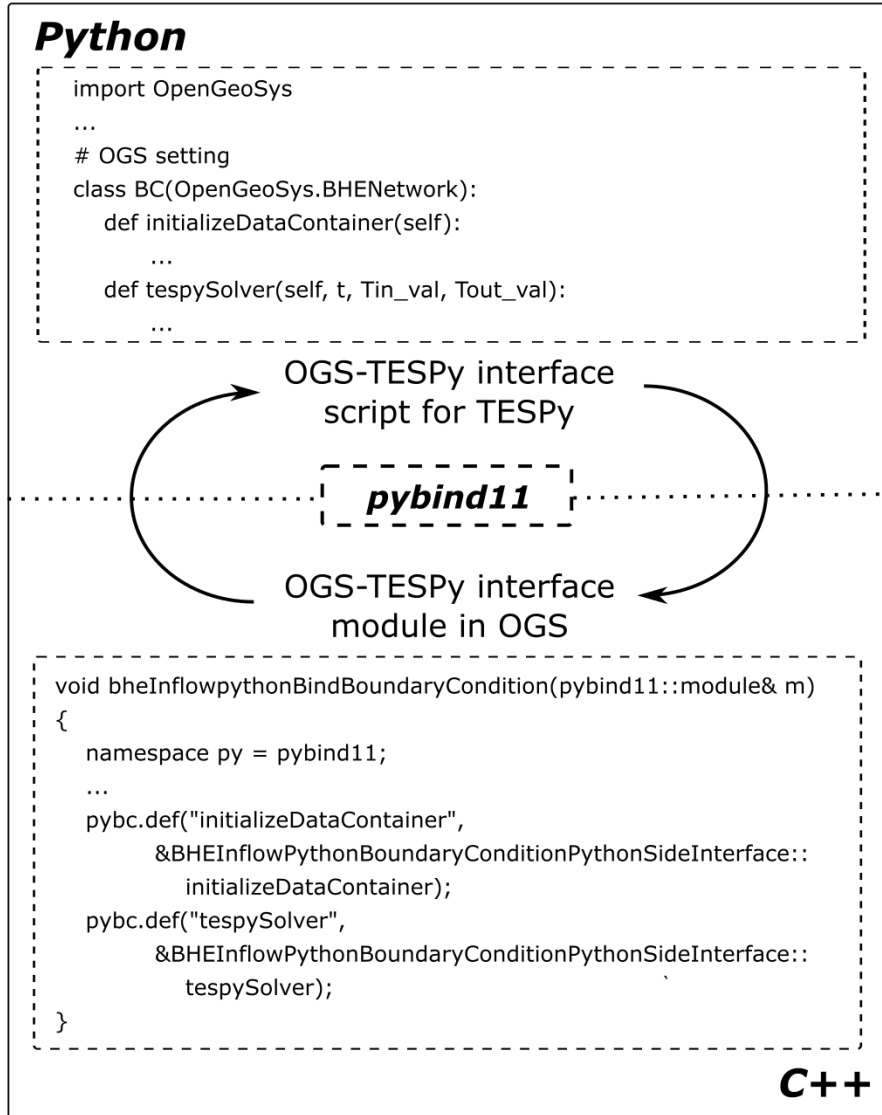


Figure 5: Interface codes through *pybind11* to couple the OGS subsurface model with TESPYPY network model

3.3 PipeNetwork feature in OGS

The source code of the *PipeNetwork* feature in OGS are composed of three parts. The first part is the initialisation process, which is embedded in the *CreateHeatTransportBHEprocess.cpp*. Here the *PipeNetwork* feature is activated in the modelling project, the OGS-TESPy interface binding will be created by *pybind11* library as depicted in Figure 5. Then the pipeline network in TESPpy will be initialised via the function *initializeDataContainer*.

The second part is the python boundary condition module for BHE, which contains the base functions for the *PipeNetwork* feature and the OGS-TESPy interface class. Their individual functions are described as the following.

- *BHEInflowPythonBoundaryConditionPythonSideInterface*: It is the base class for *PipeNetwork* feature. It contains the definition of the functions applied in the OGS-TESPy interface.
- *BHEInflowPythonBoundaryConditionModule*: It is the derived class of the above base class, which contains the OGS-TESPy interface for calling the the external python script.
- *BHEInflowPythonBoundaryCondition*: It is a derived class of the *BoundaryCondition* in the OGS. When the *PipeNetwork* feature is activated, the assignment of the boundary condition for the *HeatTransportBHE* process is executed in this class during each iteration of the simulation.

The third part is the source code for calling the external pipe network calculation within the *HeatTransportBHE* process, which is written in the function of the *postIterationConcreteProcess* located in the *HeatTransportBHEProcess.cpp* file. Here, the circulation fluid outflow temperature from the OGS current iteration will be transferred to TESPpy. Then the updated T_{in} and the flow rate calculated by TESPpy solver will be returned to OGS and stored in a pre-defined data container vector called *dataframenetwork*. In every OGS iteration, the boundary conditions of the BHE model will be updated by imposing the value which stored in the data container.

VERIFICATION AND VALIDATION

The developed model has been verified against the corresponding analytical solutions as well as experimental data. In this work, the verification was conducted based on the decoupled simulations in OGS and in TESP_y, and was composed of three parts. In the first part, the simulated hydraulic results from the constructed pipe network model in TESP_y is verified against the computed results of the same model by the software EPANET [55]. In the second part, the simulated soil temperature using the subsurface BHE array model in OGS without consideration of the pipeline network, was compared with the Bayer's super-position based analytical solution (cf. Eq. (15)). The system thermal balance of the comprehensive coupled model is also checked to guarantee the correct implementation. The processes and results of the model verification of the last two parts have been included in Chen et al. [65]. The model validation is based on the simulation of a real project with multiple-BHE array – the Leicester project in United Kingdom. More information about this validation work is presented in Chen et al. [66].

4.1 Verification of the model

4.1.1 *Simulated Hydraulic Feature of the pipeline network*

To verify the hydraulic calculation by TESP_y, a simple pipeline network with three BHEs was constructed. The simulated hydraulic results by TESP_y have been compared to the corresponding results computed by EPANET. The topology of the network, and the connected components are illustrated in Figure 6. In this network, the pressure at the inlet was firstly raised by a pump. The lifted pressure in the water pump is flow rate dependent and their relationship is described by a 2nd-order polynomial pump characteristic curve (see Figure 7). Through definition of network topology, the flow was divided into two branches. Because the number of BHEs are different in each branch, it will lead to a deviation in the loss of hydraulic head, which will further produces different flow rate in each branch before the merging point. After mixing of flow from the two branches, the total extracted heat from

the BHE array is consumed by an end-user, for instance through the radiators in the buildings.

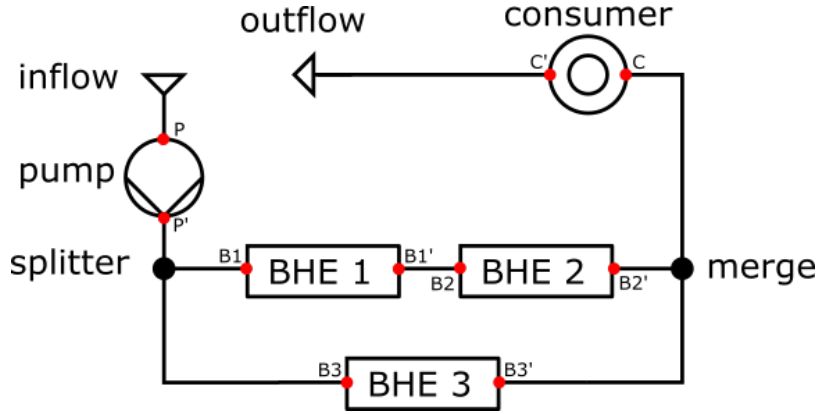


Figure 6: Topology of the pipe network

At the inlet of the network, a constant hydraulic pressure of 2 bar is imposed as the boundary condition. The hydraulic loss caused by the friction on the pipeline surfaces is calculated based on the Hazen-Williams Eq. (47)(cf. Houghtalen et al. [51], section 3.8),

$$h_f = \frac{10.67\dot{V}^{1.852}L}{R^{1.852}D^{4.8704}}, \quad (47)$$

where h_f is the head loss in meters. \dot{V} denotes the volumetric flow rate. L , R , D are the length, resistance coefficient and diameter of the pipe, respectively. The relevant model parameters are summarised in Table 1. All three BHEs are assumed to have the same geometries and material properties (Table 1). The welded and seamless steel is selected as the pipeline material, which has a resistance coefficient of 100 [67]. Since EPANET can not calculate the heat transfer process, the same fluid temperature is set at both the inlet and outlet of the network. Moreover, to avoid the thermal consumption, the heat extraction rate at all BHEs is set to be zero, not only on each BHE but also at the building side.

Table 1: Parameters adopted in the hydraulic and thermal simulation by TESP

Parameter	Symbol	Value	Unit
Inflow water pressure	h_f^{in}	2	bar
Outflow water pressure	h_f^{out}	2	bar
Length of the BHE	L	100	m
Resistance coefficient of the BHE	R	100	—
Diameter of the BHE	D	0.02733	m
Inflow temperature	T_{in}	10	°C
Outflow temperature	T_{out}	10	°C

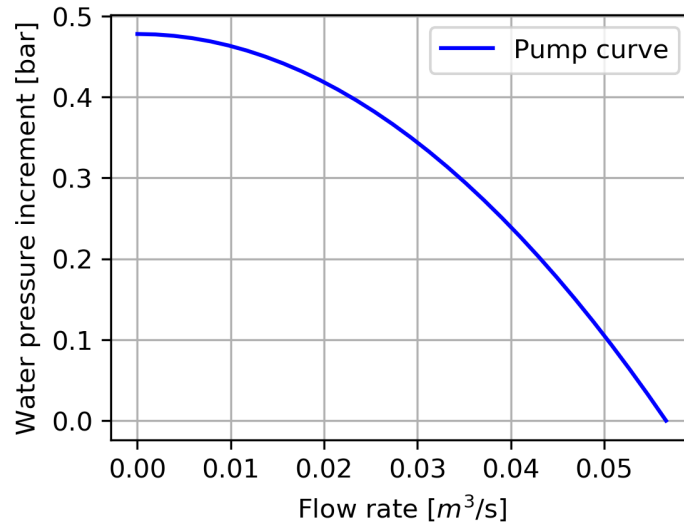


Figure 7: Graphical depiction of the pump characteristic curve

Result

For the comparison between two software, several observation points are selected, the location of which are marked with red dots in Figure 6. Since EPANET cannot calculate the temperature distribution, only the simulated flow rates and water pressure are compared. As mentioned above, the amount of thermal consumption was intentionally set to zero in the network, hence the temperature of the circulating water should remain constant. The change in hydraulic pressure in different parts of the network are mainly caused by the friction loss. Since the two branches are connected at the same splitter and merge points, the hydraulic head difference in these two branches remain the same. However, due to the different length of pipeline, the flow rates should be different. The value of the simulated water pressure at each observation points, along with the corresponding flow rate, are summarised in Table A1 and Table A2 in Appendix A. As the flow in the upper branch passes through BHE#1 and BHE#2 (200 m), which is longer than the lower branch with only BHE#3 (100 m) in it, a lower flow rate of 0.144 kg s^{-1} is being simulated for the upper branch, compared to a higher flow rate of 0.210 kg s^{-1} in the lower one. The comparison of the computed flow rate and water pressure computed in TESPpy and EPANET with the regression line are depicted in Figure 8. The hydraulic calculation from TESPpy show a good agreement against that from the software EPANET. The calculated R-square values are higher than 99% in both cases, indicating that both results are nearly identical.

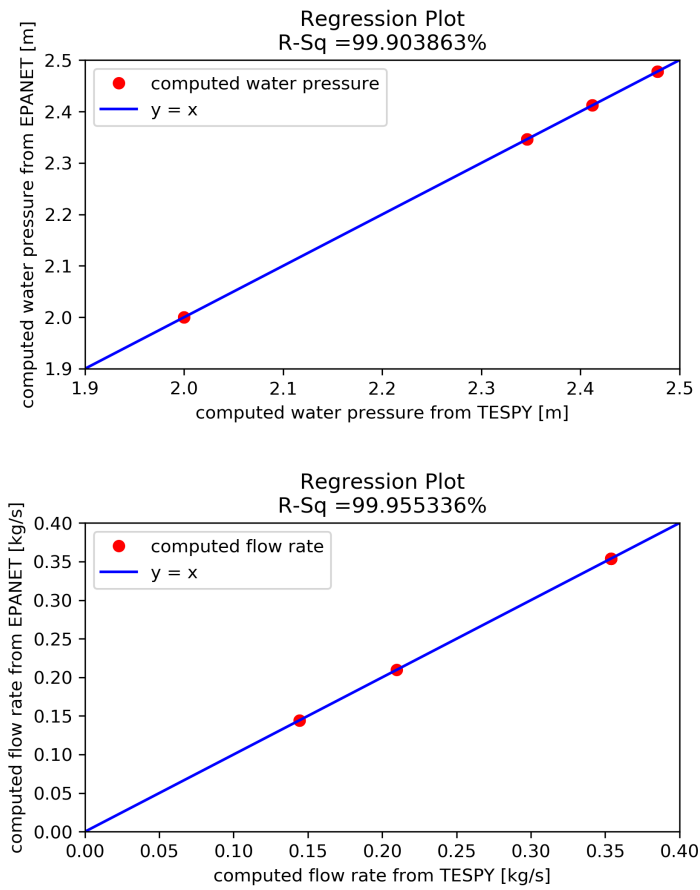


Figure 8: Upper: Water pressure at each observation point; Lower: Flow rates at each observation point

4.1.2 *Distribution and evolution of the soil temperature*

For the verification of BHE subsurface model in OGS, a 2D model containing 25 BHEs was set up. The model domain has a size of 300×300 m, with no-flux boundaries on the peripheries of the domain. The 25 BHEs are located in the centre of the domain. They are arranged in a 5×5 array with a constant distance of 6 m from each other. In the model, the BHEs are simplified as heat source terms, which corresponds to the infinite line source adopted in the analytical solution of Eskilson [12]. In the simulation, an annual heat extraction rate curve is specified on each BHE. A total of 10 years' long operation of the BHE array was simulated. The simulation results have been verified against the results calculated using the Bayer's super-position analytical solution (see Eq. 15). Details about the verification are introduced in the Section 3.1 of Appendix B.1. Interested readers may also refer to Appendix C.1 for the python script that reproduces Bayer's super-position based analytical solution.

The simulated temperature distribution in the subsurface after 10 years' operation, and the temperature evolution at several selected observation points are compared with the corresponding analytical solution (cf. Figure 2 in B.1). The L2 norm of the difference between each compared data set turned out to be 1.3×10^{-4} and 1.6×10^{-4} . This indicates that the heat transport in the subsurface of an multiple-BHE array is correctly simulated by the OGS software.

4.1.3 *System thermal balance in the coupled model*

In order to verify that the model is thermally balanced, a comprehensive 3D numerical model was constructed, including 25 BHEs, the surrounding subsurface, and a coupled pipeline network. The arrangement of the BHE array is the same as that in Section 4.1.2. In addition, a pipe network has been set up, in which all 25 BHEs are connected in a parallel manner. In the simulation, an annual thermal load curve (Figure 7 in Appendix B.1) is imposed on the heat pump, reflecting varying thermal load over different seasons. The thermal load imposed on the heat pump is assumed to be only supplied by these 25 BHEs. The heat extraction rate on each BHE is automatically calculated according to the temperature distribution in the soil and pipeline network. In reality, due to the connection among the BHEs through pipeline network, the system itself has an intrinsic feature of re-balancing the thermal load among different BHEs. With the consideration of the pipeline network and the thermal interactions among BHEs, this thermal re-balancing feature can be captured by the model.

The simulation results (Figure 3 in Appendix B.1) show that the heat extraction rate on each BHE is different and it deviates from

the calculated average value of the system. This deviation reflects the thermal interference in the BHE array. Despite of the unequally distributed thermal load, according to the energy balance, the total system thermal load should be equal to the summation of the calculated heat extraction rates on all BHEs. Based on this relationship derived from energy balance, the model was verified. The superposition of the computed heat extraction rate on all BHEs has a nearly 1:1 correlations with the imposed total thermal load with a R-squared of 99.89%. As the thermal balance is fulfilled in the modeling, it can be confirmed that the coupling of heat transport between OGS and TESP_y is correctly implemented.

4.2 Validation of the model

To validate the model, the operation of a real large BHE array project located in Leicester, UK (hereafter as Leicester Project) [68] was simulated by the newly implemented OGS-TESP_y code. The BHE array was designed for both heating and cooling of the building. For energy utilisation, 56 BHEs are installed in the subsurface, each of which has a depth of 100 m and a diameter of 125 mm. For the project operation, the thermal load from the building site, heat pump operation, and inflow and outflow temperature of the ground loop were monitored for over 3 years with minute-wise data reading. The detailed monitoring data was published by Naicker et al., which can be accessed from the Research Data Archive at the University of Leeds [69].

Applying our coupled OGS-TESP_y model, two years' operation of the BHE array was simulated. The model configuration was set corresponds to the arrangement of the BHE array in the project. The simulated outflow temperature and the amount of exchanged heat in the whole system have been compared with the measured data. A fairly good agreement was achieved between the predicted and monitored outflow temperature. The computed modest year-by-year increase in the outflow temperature during the first and second year is consistence with the observed and well explained phenomenon in [68]. The calculated temporary evolution of heat amount show a consistent tendency with the measured evolution, which corresponds well to the evolution of the outflow temperature. Quantitatively, only a slight difference (3.2%) is obtained in the simulated amount of heat accumulated, in comparison to the measured value.

APPLICATIONS

PREFACE

The OGS-TESPy model developed in this work has been applied to analyse the system behavior of the multiple-BHE array in two studies. Special attention is paid to the investigation of the thermal interaction among the BHEs. In the first study, the model is applied for the quantification of the heat shifting phenomenon among the BHEs, during the long-term operation of such array. In the second study, a series of numerical experiments were carried out based on the data published in the Leicester Project [68], targeting to investigate the response of circulation fluid temperature to different load of imbalanced heat. Details of these two studies are published in two peer-reviewed journal papers [65, 66]. In this chapter, only a short description of the studies and summary of the main findings are presented. Besides, except for the application on the shallow BHE array project, the developed OGS-TESPy model is recently successfully applied in an Deep Borehole heat exchanger(DBHE) array project in Xi'an, China , targeting to investigate the thermal interaction behaviour among each DBHE [70].

5.1 Heat shifting phenomenon in the large BHE array system

OBJECTIVE

During the long-term operation of a multiple-BHE array based GSHP system, the influence of the thermal interaction among BHEs become significant in the subsurface. As a consequence, the thermal extraction rate on different BHEs is found to be different, depending on its location in the array. Targeting to analyse the complex hydro-thermal processes that lead to the thermal interference phenomenon in an multiple-BHE array, the comprehensive numerical model OGS-TESPy was adopted. In the numerical analysis, three different BHE array models are constructed, which contain 1, 9 (3×3) and 25 (5×5) BHEs, respectively. In all three models, the heat transport around the BHEs and inside the pipe network are quantified in a coupled manner. A series of heating-only numerical experiments have been performed to quantitatively investigate the amount of shifted thermal extraction rate in these large BHE arrays. All scenarios have been simulated for 10 years. Besides, based on the comparison of the numerical results with the analytical solution, the accuracy of super-positioned based infinite line source approach is also discussed, for its applicability in predicting the long-term behavior of the multiple-BHE array.

OUTCOME

Over the duration of system operation, the initial identical thermal extraction rate on each BHE changes successively and becomes unequal from each other. To describe the change of heat extraction rate on each BHE during the long-term operation quantitatively, the proportion of the shifted thermal load PSTL is calculated,

$$\text{PSTL} = \Delta\dot{Q}_i / \dot{Q}_{mean}, \quad (48)$$

where $\Delta\dot{Q}_i = \dot{Q}_i - \dot{Q}_{mean}$ denotes the amount of shifted heat extraction rate on i_{th} BHE from the average heat extraction rate \dot{Q}_{mean} . In the 3×3 and 5×5 models, the calculated PSTL by the centre BHE decreases at least 7% and 12% after 10 years of operation, while the rate on the BHE located at the edge of array increases about 3% and 13% respectively. It indicates that over the long-term operation, the thermal load is gradually shifted from the centre BHEs towards those located at the outer boundary of the array. Due to the seasonal variations, the maximum PSTL of 40% and 105% is found in September, when the lowest system heating demand is imposed. On the contrary, in the peak thermal demanding month (January), the shifted percentage is determined to be minimum. Moreover, when comparing the results calculated in the 5×5 model to those obtained by the 3×3 model, this shifting phenomenon becomes significant in the array with larger

number of BHEs. The minimum calculated PSTL on the centre BHE is below -100%, which indicates that the subsurface is recharged by the BHE even during the heating period, and the system thermal load is mainly supplied by the BHEs at the periphery of the field. It suggests that the BHEs located at the outer part are more important to maintain the system working status during the operation.

Additionally, the super-position method as described in Section 2.1.2.1 (Eq. (15)) is adopted to calculate the soil temperature change in the subsurface of the same 5×5 BHE array as that in the numerical simulation. A maximum soil temperature difference of 2.5°C after 10 years of operation was obtained between the analytical and numerical solutions. In the analytical approach, as the subsurface recharge process is not considered, the reduction of soil temperature could be overestimated. Be noticed that, a relatively low specific heat extraction rate (maximum 12.5 W m^{-1}) is imposed on each BHE in this study. If a higher thermal load is applied on the BHE array, a higher deviation from the real temperature distribution in soil can be estimated by the analytical approach. Moreover, to analyse the influence of the thermal shifting on the soil temperature, another numerical case without consideration of the thermal load shifting was performed. A relatively limited temperature difference ($T < 0.5^\circ\text{C}$) was found between the case with or without considering thermal shifting. Compared to the effects from the recharge from the subsurface, the temperature variation in soil caused by heat shifting is rather negligible. The numerical results also indicate that the thermal plume induced by the BHEs system extends successively with increasing operation time. After 10 years of operation, the affected subsurface area extends to about 40 m away from the array outer boundary.

REFERENCE

S. Chen, F. Witte, O. Kolditz, H. Shao (2020). *Shifted thermal extraction rates in large Borehole Heat Exchanger array – A numerical experiment. Applied Thermal Engineering*, 167, 114750.
DOI: 10.1016/j.applthermaleng.2019.114750.
(cf. Chen et al. [65], Appendix B.1)

5.2 Sustainability of a multiple shallow BHE array system

OBJECTIVE

In most BHE array projects, it is usual that the amount of extracted thermal energy during the annual heating season can not be fully balanced by the thermal recharge in the cooling phase. This imbalanced seasonal thermal load may cause the accumulation of low or high temperature zones near the centre of the array, which would further lead to a gradually ascending or descending working fluid temperature over the operation time. In real world applications, as the working fluid temperature is treated as one of the most important parameters to estimate the working status of a GSHP system, analysis of the temperature change in the circulation fluid in response to the amount of imbalanced thermal load would be of great interest to the engineers working on the design of the BHE array. In this work, several numerical experiments were carried out based on the simulation of a real BHE array project in Leicester, UK. The main purpose of these experiments is to investigate the system behavior under different settings of the imbalanced thermal load. Furthermore, the potential implications are discussed on the impact of BHE adjacent distance S to the sustainability of a GSHP system.

OUTCOME

According to the report of the Leicester project, the measured actual system peak thermal load is 73 kW, which only accounts for 20.3% of the designed peak value (360 kW). Thus, different scenarios with elevated thermal load, i.e. 100%, 197%, 296%, 395% and up to 493%, were imposed on the BHE array. Numerical simulations were performed for 20 years of operation. It is found that the highest outflow temperature simulated by the model is predicted in the scenario with the highest peak thermal load (493% of the real load). The maximum outflow temperature reaches 34.5 °C, which is already very close to the 35 °C threshold value (Section 1.2). This finding suggests that with the designed peak value the BHE array can be sustainably utilised for 20 years, but not much longer. Be noticed that the current project is cooling dominant and the COP of the heat pump is not considered in this case. Thus, the actual working fluid temperature would even raise higher as the one calculated by the numerical model. Moreover, a linear relationship was found between the rise in the outflow temperature and the amount of the accumulated heat that is injected into the subsurface. This linear relationship suggests that, when factors such as the adjacent distance S and the physical parameters of soil are determined, it is possible to develop a formula to estimate the change in working fluid temperature in response to the total accumulated

amount of the imbalanced heat over the years. In another word, once the linear relationship is identified, the total amount of exploitable heat within a particular BHE array subsurface can be inversely predicted with a giving threshold of the working fluid temperature.

To investigate the implication of the adjacent distance S to the long-term behavior of the system, additional numerical experiments with increased S values were carried out. The numerical results indicate that the specific heat stored in the array subsurface decreases from 20.0 kWh m^{-3} to 12.9 kWh m^{-3} , when S increases from 5 m to 7 m. Accordingly, the temperature of circulation fluid decreases from 34.5°C to 30.5°C . Such results suggest that the adjacent distance among BHEs are not only playing a role on the intensity of the thermal interference among the BHEs (cf. Chapter 35.1 in ASHRAE [8]), but it can also affect the long-term sustainability of a GSHP system.

REFERENCE

S. Chen, W. Cai, F. Witte, X. Wang, F. Wang, O. Kolditz, H. Shao (2020). Long-term thermal imbalance in large borehole heat exchangers array - A numerical study based on the Leicester project. Energy and Buildings, 231, 110518. DOI: 10.1016/j.enbuild.2020.110518.
(cf. Chen et al. [66], Appendix B.2)

5.3 Discussion and outlook

Optimise the operation strategy for a large BHE array system

In the above introduced applications, detailed thermal load shifting phenomenon are clearly observed on BHE arrays during the long-term operation. Such unequal seasonal shifting behaviour give us new opportunities in the future to optimise the operation strategy for such BHE array system. Specific suggestions are given as follows.

Firstly, it is recommended to maintain an annual thermal load balance for large BHE arrays, i.e. the designed amount of injected thermal energy during a cooling season should equal to the same amount extracted during heating. A balanced thermal load strategy can guarantee a consistent thermal load behavior of all BHEs over decades of long-term operation.

However, a balanced thermal load strategy is not always realistic in most projects. In low latitude areas, most projects are cooling dominant, while in high latitude countries, heating-dominant projects are the majority. In this context, although the thermal imbalance in the subsurface can not be avoid, a lower thermal load imbalance among each BHEs can still be achieved when alternative heating and cooling are applied within every year. As shown in our Leicester project application (cf. Figure 5(c) in the section 3.5.2 in Chen et al. [66]), when a heating phase is applied in between the cooling seasons, the thermal recharge of the subsurface can partially mitigate the shifting phenomenon.

When the thermal load shifting happens, it should be noticed that the BHEs located at the edge of the array have larger heat exchange rates, while those at the centre have lower values. Therefore, The BHEs at the periphery are more important to maintain the working status of the system during the long-term operation. Optimisation strategy based on this phenomenon can be found by other researchers. For example, Bayer et al. [17] developed an operation strategy by disconnecting a given number of BHEs located at the centre of the array in a step-wise manner. Following their approach, the thermal anomalies in the BHE array subsurface can also be effectively mitigated.

Improvement of the computational efficiency of the large BHE array model

In recent years, due to the increased demand of the shallow geothermal energy, large BHE array projects containing hundreds to thousands of BHEs become more and more popular in the industry. The computational cost on the simulation of such large BHE array project with consideration of the interactions between the each BHE and their coupled complex pipeline network system could be extremely expensive. Thus, there is a need to improve the computational efficiency of

the current model. For this purpose, we firstly quantified the actual computational cost of each modeling part. Based on that different strategies to improve the computational efficiency are investigated.

The computational cost is quantified based on the simulation of the 56 BHE array project in Leicester (Section 5.2). In each iteration, the consumed time by the simulation of the pipeline network in TESP_y, solving the BHE model in OGS and data exchange in the interface between OGS and TESP_y is recorded. For instance, in one specified iteration, the calculation of the entire pipeline network model in TESP_y costs about 0.9 s. In the OGS BHEs model, the major time consumption is found by the matrix assembly and the solution using the linear solver, which take 2.9 s and 9.3 s, respectively. The data processing on the interface needs about 0.08 s. Within the entire simulation period, the iteration number varied by each time step from a minimum number of 2 to a maximum number of 30.

According to the analysis of the computational cost, there are two main parts recognised to be the most time consuming. One is the sequential iterations between the solutions in OGS and in TESP_y. Since the iteration is caused by the boundary condition settings on the OGS BHE model (Section 2.1.3.3), When power boundary condition is imposed on the BHE, the iterations between the calculations in OGS and in TESP_y are inevitable. However, there is possibility to accelerate the computational speed within one iteration in special case. At the TESP_y model side, if the boundary conditions within the pipeline network keep constant along the time, the linear relationship between the BHE inflow and outflow temperature can be characterised as a time independent factor. Its value can be obtained by once executing the TESP_y solver during the simulation's initialisation stage. Then the calculated factor number can be stored in a prepared data vector in OGS. Within each iteration, this stored number can be always reused to calculate the required BHE inflow temperature from the computed BHE outflow temperature in the OGS model. It means, for the entire simulation process, the calculation on the TESP_y software and data transferring between the TESP_y and OGS can be avoided.

The second time consuming part lies on the global linear solver, whose size is dependent on the total degree of freedom. With the increased number of soil and BHEs elements, the degree of freedom can increase to tens of millions, especially in large scale BHE models. As indicated in the aforementioned analysis of the Leicester project, the solution of the global matrix by the linear solver took the most time within each iteration. When more elements are added in the model mesh, the computational cost for solving the global matrix increases quadratically. The main approach to accelerate the linear solver may be the application of parallelization scheme for the coupled OGS-TESP_y model. This is actually the main focus of our current work. As described in the Section 2.1.3.4, when Schur complement method is

implemented in the OGS source code, the current OGS parallelization scheme can be easily applied on the global matrix system of a BHE model, which may greatly accelerate the computational speed.

One further possibility to improve the computational efficiency of such multiple BHE array model is to couple a semi-analytical method into the numerical model. In our preliminary work, a coupled semi-analytical numerical framework has been developed, in which the Bayer's super-position method (Eq. (15)) and the Beier's BHE analytical model [14] are applied to solve the thermal processes, while the coupled hydraulic process is solved by TESP. Similar to the comprehensive numerical modeling, this semi-analytical method is proved to be able to capture the thermal interference phenomenon during the operation of a multiple-BHE. Besides, compared to the pure numerical model, the computational efficiency has been much improved. However, due to the simplifications made in the semi-analytical framework, the ability in handling groundwater flow and heterogeneous subsurface layers may be compromised.

CONCLUSIONS AND OUTLOOK

The present work focuses on the investigation of the long-term behavior in the multiple-BHE array based shallow GSHP system. For this purpose, a comprehensive BHE array model containing a BHE subsurface model and a pipe network model were developed. The BHE subsurface model was implemented in the Finite Element code OpenGeoSys and explicitly coupled with the pipeline network model, which is constructed in the TESPpy simulator. In this comprehensive model, the hydraulic processes in the pipeline network and the resulted heat advection in the circulation fluid, the heat transport in the subsurface as well as the thermal interactions caused by the operation of BHEs are considered. This model has been verified step by step with the corresponding analytical solution and also validated against the experimental data. Through careful analysis, it has been verified that the detailed behavior of the thermal interaction among the BHEs during the system operation can be well quantified by the developed numerical model. Besides, this model was applied to simulate a real large BHE array in Leicester, UK, by which the long-term monitoring data-set is available. Based on the case studies and comparison of numerical results with the experimental observations, the predictive ability of the model is demonstrated and the long-term system sustainability are investigated.

Achievements

The main achievements of the present work are summarised as follows,

- Compared to the most BHE models known today, the developed numerical model in this work is capable not only to simulate the heat transport process within the BHE and in the subsurface, but also the thermal hydraulic process in the BHE array coupled pipeline network during the GSHP system operation.
- The flexible model settings allow the consideration of a GSHP system with arbitrary components and connections, and to easily handle a time-dependent thermal load and flow rate condition in an entire closed-loop system in cases of different system operation strategies. Further, this model can be extended through

coupling with external systems, such as temperature dependent heat pump system, Organic Rankine Cycle (ORC) power plant or solar power system.

- By applying the developed model, the shifting phenomenon of thermal load caused by the thermal interference among BHEs is captured and well quantified. Based on the spatially and seasonally varying shifting behavior, several optimisation strategies are proposed for the operation of such large BHE arrays.
- The comparison of numerical results with the commonly used analytical approach indicates that the application of the superpositioned based infinite line source analytical approach could over-estimate the long-term temperature changes in a BHE array, since the thermal recharge effect is not considered. The thermal interference can also lead to a different soil temperature distribution. Yet, this is rather negligible if compared to the one caused by the thermal recharge.
- Based on the Leicester project case study, the sustainability of a multiple-BHE array over long term is investigated. A perfect linear relationship is found between the working fluid temperature rise and the amount of accumulated imbalanced heat injected into the BHE array.
- The numerical experiments show that the adjacent distance among BHEs has an important role to determine the amount of imbalanced heat that can be sustained in a multiple-BHE array. The increased adjacent distance can not only be regarded as a measure to reduce thermal interference between individual boreholes, but also be a method to improve the system sustainability.

Outlook

Since the large BHE array based shallow GSHP system is widely utilised in densely populated urban areas, further researches on the sustainability of a BHE array based GSHP system within a limited spatial volume should be conducted. Specifically, first, the peak thermal demand and the annual thermal demand of the project should be carefully designed, targeting to maintain the system working fluid temperature within a reasonable range in long-term operation. Second, the thermal interaction among each BHE during the long-term system operation should be controlled, in order to keep a relatively balanced working condition on the entire BHE array. Third, the affected subsurface area during the geothermal energy exploitation should be controlled within the project's property lines. Regarding the above mentioned aspects, numerical analysis could play an essential role. Based on the numerical models, an optimisation method for

estimating the minimal required BHE length and the BHE adjacent distance could be developed. Besides, the linear relationship between the working fluid temperature rise and the accumulated imbalanced thermal amount of the system can be further developed to a simplified formula, with potential application to estimate the total amount of exploitable heat within a particular subsurface volume.

LIST OF FIGURES

Figure 1	(a): Subsurface BHE numerical model for the dual-continuum approach. Mesh with prism soil element and the line element for the BHE. (b): Schematic sketch of a 1U-type BHE for the dual-continuum approach and its TCRM model (reproduced after Diersch et al. [45])	16
Figure 2	Schematised procedure of the coupling subsurface BHE model in OpenGeoSys with pipeline network model in TESPpy software.	25
Figure 3	Model domain of the three BHE subsurface model	27
Figure 4	Topological Pipeline network model in TESPpy	27
Figure 5	Interface codes through <i>pybind11</i> to couple the OGS subsurface model with TESPpy network model	29
Figure 6	Topology of the pipe network	32
Figure 7	Graphical depiction of the pump characteristic curve	33
Figure 8	Upper: Water pressure at each observation point; Lower: Flow rates at each observation point .	34

LIST OF TABLES

Table 1	Parameters adopted in the hydraulic and thermal simulation by TESP _y	32
Table A1	Computed hydraulic results of the water pressure at each observation points from TESP _y and EPANET	57
Table A2	Computed hydraulic results of the flow rate at each objects in the network from TESP _y and EPANET	57

BIBLIOGRAPHY

- [1] OECD/IEA. Heating without global warming. International Energy Agency. France, 2014.
- [2] IRENA. Geothermal Power: Technology Brief. International Renewable Energy Agency. ISBN: 9789292600365. Abu Dhabi, 2017.
- [3] K. Zhu, P. Blum, G. Ferguson, K.-d. Balke, and P. Bayer. The geothermal potential of urban heat islands. In: *Environmental Research Letters* 5 (2010), 6pp. DOI: 10.1088/1748-9326/5/4/044002.
- [4] J. A. Rivera, P. Blum, and P. Bayer. Increased ground temperatures in urban areas: Estimation of the technical geothermal potential. In: *Renewable Energy* 103(C) (2016), pp. 388–400. ISSN: 0960-1481. DOI: 10.1016/j.renene.2016.11.005.
- [5] T. Kurevija, D. Vulin, and V. Krapec. Effect of borehole array geometry and thermal interferences on geothermal heat pump system. In: *Energy Conversion and Management* 60 (2012), pp. 134–142. ISSN: 01968904. DOI: 10.1016/j.enconman.2012.02.012.
- [6] The Association of German Engineers(Verein Deutscher Ingenieure). Thermal use of the underground - Ground source heat pump systems; VDI 4640, Part 2. Beuth Verlag GmbH, Berlin. 2019.
- [7] S. Haehnlein, P. Bayer, and P. Blum. International legal status of the use of shallow geothermal energy. In: *Renewable and Sustainable Energy Reviews* 14.9 (2010), pp. 2611–2625. ISSN: 1364-0321. DOI: 10.1016/j.rser.2010.07.069.
- [8] ASHRAE. 2019 ASHRAE Handbook - Heating, Ventilating, and Air-Conditioning Applications (SI Edition). Atlanta, GA: American Society of Heating, Refrigerating and Air-Conditioning Engineers, 2019. ISBN: 9781947192133.
- [9] P. Bayer, G. Attard, P. Blum, and K. Menberg. The geothermal potential of cities. In: *Renewable and Sustainable Energy Reviews* 106.February (2019), pp. 17–30. ISSN: 1364-0321. DOI: 10.1016/j.rser.2019.02.019.
- [10] H. M. Haq and E. Hiltunen. An inquiry of ground heat storage: Analysis of experimental measurements and optimization of system’s performance. In: *Applied Thermal Engineering* 148.October 2018 (2019), pp. 10–21. ISSN: 13594311. DOI: 10.1016/j.applthermaleng.2018.11.029.

- [11] K. W. Tordrup, S. E. Poulsen, and H. Bjørn. An improved method for upscaling borehole thermal energy storage using inverse finite element modelling. In: *Renewable Energy* 105 (2017), pp. 13–21. ISSN: 18790682. DOI: 10.1016/j.renene.2016.12.011.
- [12] P. Eskilson. Thermal Analysis of Heat Extraction Boreholes. PhD thesis. University of Lund, Sweden, 1987.
- [13] M. A. Bernier, P. Pinel, R. Labib, and R. Paillot. A Multiple Load Aggregation Algorithm for Annual Hourly Simulations of GCHP Systems. In: *HVAC&R Research* 10.4 (2004), pp. 471–487. DOI: 10.1080/10789669.2004.10391115.
- [14] R. A. Beier. Transient heat transfer in a U-tube borehole heat exchanger. In: *Applied Thermal Engineering* 62.1 (2014), pp. 256–266. ISSN: 13594311. DOI: 10.1016/j.applthermaleng.2013.09.014.
- [15] R. A. Beier. Thermal response tests on deep borehole heat exchangers with geothermal gradient. In: *Applied Thermal Engineering* 178.March (2020), p. 115447. ISSN: 13594311. DOI: 10.1016/j.applthermaleng.2020.115447.
- [16] S. Koochi-Fayegh and M. A. Rosen. An analytical approach to evaluating the effect of thermal interaction of geothermal heat exchangers on ground heat pump efficiency. In: *Energy Conversion and Management* 78 (2014), pp. 184–192. ISSN: 01968904. DOI: 10.1016/j.enconman.2013.09.064.
- [17] P. Bayer, M. de Paly, and M. Beck. Strategic optimization of borehole heat exchanger field for seasonal geothermal heating and cooling. In: *Applied Energy* 136 (2014), pp. 445–453. ISSN: 03062619. DOI: 10.1016/j.apenergy.2014.09.029.
- [18] H. Carslaw and J. Jaeger. Heat conduction in solids. Clarendon Press, Oxford. 1947.
- [19] M. Ahmadfard and M. Bernier. A review of vertical ground heat exchanger sizing tools including an inter-model comparison. In: *Renewable and Sustainable Energy Reviews* 110.April (2019), pp. 247–265. ISSN: 18790690. DOI: 10.1016/j.rser.2019.04.045.
- [20] D. P. Hart and R. Couvillion. Earth-coupled Heat Transfer: Offers Engineers and Other Practitioners of Applied Physics the Information to Solve Heat Transfer Problems as They Apply to Earth-coupling. National water well association, 1986.
- [21] G. Hellström. Ground heat storage : thermal analyses of duct storage systems. PhD thesis. Lunds University, Sweden, 1991.
- [22] S. Klein and U. of Wisconsin–Madison. Solar Energy Laboratory. TRNSYS, a Transient Simulation Program. EES report. The Laboratory, 1975.

- [23] M. De Rosa, F. Ruiz-Calvo, J. M. Corberán, C. Montagud, and L. A. Tagliafico. A novel TRNSYS type for short-term borehole heat exchanger simulation: B2G model. In: *Energy Conversion and Management* 100 (2015), pp. 347–357. ISSN: 01968904. DOI: 10.1016/j.enconman.2015.05.021.
- [24] ANSYS. ANSYS FLUENT theory guide. Canonsburg, PA, Release 15.0. 2013.
- [25] S. Koochi-Fayegh and M. A. Rosen. Examination of thermal interaction of multiple vertical ground heat exchangers. In: *Applied Energy* 97 (2012), pp. 962–969. ISSN: 0306-2619. DOI: 10.1016/j.apenergy.2012.02.018.
- [26] M. Saaly, P. Maghoul, M. Kavgic, and D. Polyzois. Performance analysis of a proposed geothermal pile system for heating and cooling energy demand for a building in cold regions. In: *Sustainable Cities and Society* 45. August 2018 (2019), pp. 669–682. ISSN: 2210-6707. DOI: 10.1016/j.scs.2018.12.014.
- [27] COMSOL. Introduction to COMSOL Multiphysics. 2018. URL: <https://www.comsol.de/documentation>.
- [28] M. Le Lous, F. Larroque, A. Dupuy, and A. Moignard. Thermal performance of a deep borehole heat exchanger: Insights from a synthetic coupled heat and flow model. In: *Geothermics* 57 (2015), pp. 157–172.
- [29] H.-J. G. Diersch. *Feflow*. Springer-Verlag Berlin Heidelberg, 2014, p. 996. ISBN: 978-3-642-38738-8. DOI: 10.1007/978-3-642-38739-5.
- [30] P. Hein, K. Zhu, A. Bucher, O. Kolditz, Z. Pang, and H. Shao. Quantification of exploitable shallow geothermal energy by using Borehole Heat Exchanger coupled Ground Source Heat Pump systems. In: *Energy Conversion and Management* 127 (2016), pp. 80–89. ISSN: 01968904. DOI: 10.1016/j.enconman.2016.08.097.
- [31] O. Kolditz, S. Bauer, L. Bilke, and et al. OpenGeoSys: an open-source initiative for numerical simulation of thermo-hydro-mechanical/chemical (THM/C) processes in porous media. In: *Environmental Earth Sciences* 67 (2012), pp. 589–599. ISSN: 1866-6280. DOI: 10.1007/s12665-012-1546-x.
- [32] A. Nguyen, P. Pasquier, and D. Marcotte. Geothermics Borehole thermal energy storage systems under the influence of groundwater flow and time-varying surface temperature. In: *Geothermics* 66 (2017), pp. 110–118. ISSN: 0375-6505. DOI: 10.1016/j.geothermics.2016.11.002.

- [33] B. Meng, T. Vienken, O. Kolditz, and H. Shao. Evaluating the thermal impacts and sustainability of intensive shallow geothermal utilization on a neighborhood scale: Lessons learned from a case study. In: *Energy Conversion and Management* 199, August (2019), p. 111913. ISSN: 01968904. DOI: 10.1016/j.enconman.2019.111913.
- [34] C. Chen, H. Shao, D. Naumov, Y. Kong, K. Tu, and O. Kolditz. Numerical investigation on the performance, sustainability, and efficiency of the deep borehole heat exchanger system for building heating. In: *Geothermal Energy* 7.1 (2019), p. 18. ISSN: 2195-9706. DOI: 10.1186/s40517-019-0133-8.
- [35] P. Hein, O. Kolditz, U. J. Görke, A. Bucher, and H. Shao. A numerical study on the sustainability and efficiency of borehole heat exchanger coupled ground source heat pump systems. In: *Applied Thermal Engineering* 100 (2016), pp. 421–433. ISSN: 13594311. DOI: 10.1016/j.applthermaleng.2016.02.039.
- [36] A. Gultekin, M. Aydin, and A. Sisman. Thermal performance analysis of multiple borehole heat exchangers. In: *Energy Conversion and Management* 122 (2016), pp. 544–551. ISSN: 01968904. DOI: 10.1016/j.enconman.2016.05.086.
- [37] S. Miglani, K. Orehoung, and J. Carmeliet. A methodology to calculate long-term shallow geothermal energy potential for an urban neighbourhood. In: *Energy & Buildings* 159 (2017), pp. 462–473. ISSN: 0378-7788. DOI: 10.1016/j.enbuild.2017.10.100.
- [38] The Association of German Engineers (Verein Deutscher Ingenieure). *Thermische Nutzung des Untergrunds Erdgekoppelte Wärmepumpenanlagen; VDI 4640, Blatt 2*. Beuth Verlag GmbH, Berlin. 2001.
- [39] GB50366. Technical code for ground-source heat pump system. Ministry of Housing and Urban-Rural Development, PR China. 2009.
- [40] J. Xi, Y. Li, M. Liu, and R. Z. Wang. Study on the thermal effect of the ground heat exchanger of GSHP in the eastern China area. In: *Energy* 141 (2017), pp. 56–65. DOI: 10.1016/j.energy.2017.09.060.
- [41] F. Stauffer, P. Bayer, P. Blum, N. Giraldo, and W. Kinzelbach. *Thermal Use of Shallow Groundwater*. 2013, p. 290. ISBN: 978-1-4665-6019-2. DOI: 10.1201/b16239.
- [42] L. Ingersoll and A. Zobel. *Heat conduction with engineering and geological application*, 2nd ed. McGraw-Hill, New York. 1954.

- [43] R. Al-Khoury, P. G. Bonnier, and R. B. Brinkgreve. Efficient finite element formulation for geothermal heating systems. Part I: Steady state. In: *International Journal for Numerical Methods in Engineering* 63.7 (2005), pp. 988–1013. ISSN: 00295981. DOI: 10.1002/nme.1313.
- [44] R. Al-Khoury and P. G. Bonnier. Efficient finite element formulation for geothermal heating systems. Part II: Transient. In: *International Journal for Numerical Methods in Engineering* 67.5 (2006), pp. 725–745. ISSN: 00295981. DOI: 10.1002/nme.1662.
- [45] H.-J. Diersch, D. Bauer, W. Heidemann, W. Rühaak, and P. Schätzl. Finite element modeling of borehole heat exchanger systems: Part 1. Fundamentals. In: *Computers & Geosciences* 37.8 (2011), pp. 1122–1135. DOI: 10.1016/j.cageo.2010.08.003.
- [46] H.-J. Diersch, D. Bauer, W. Heidemann, W. Rühaak, and P. Schätzl. Finite element modeling of borehole heat exchanger systems: Part 2. Numerical simulation. In: *Computers & Geosciences* 37.8 (2011), pp. 1136–1147. DOI: 10.1016/j.cageo.2010.08.002.
- [47] D. Bauer. Thermal modelling of borehole heat exchangers and borehole thermal energy stores. PhD thesis. Institute of Thermodynamics and Thermal Engineering, University of Stuttgart, 2011. DOI: 10.18419/opus-1979.
- [48] O. C. Zienkiewicz, R. L. Taylor, J. Z. Zhu. *The Finite Element Method: Its Basis and Fundamentals*. Elsevier Ltd, Oxford, 2013. ISBN: 978-1856176330.
- [49] O. Axelsson. *Iterative solution methods*. Cambridge university press, 1996.
- [50] L. Böswirth and S. Bschorer. *Technische Strömungslehre*. Springer Fachmedien Wiesbaden, 2014. DOI: 10.1007/978-3-658-05668-1.
- [51] R. J. Houghtalen and A. Osman. *Fundamentals of hydraulic engineering systems*. New York: Prentice Hall, 2009. ISBN: 978-0-13-601638-0.
- [52] H. Cross. *Analysis of flow in networks of conduits or conductors*. University of Illinois at Urbana Champaign, College of Engineering. Engineering Experiment Station. 1936.
- [53] M. Collins, L. Cooper, R. Helgason, J. Kennington, and L. LeBlanc. Solving the Pipe Network Analysis Problem Using Optimization Techniques. In: *Management Science* 24.7 (1978), pp. 747–760. ISSN: 0025-1909. DOI: 10.1287/mnsc.24.7.747.
- [54] E. Todini and S. Pilati. A gradient method for the analysis of pipe networks. In: *International Conference on Computer Applications for Water Supply and Distribution*, Leicester Polytechnic, UK, 1987.

- [55] L. a. Rossman. EPANET 2: users manual. In: Cincinnati US Environmental Protection Agency National Risk Management Research Laboratory 38.September (2000), p. 200.
- [56] F. Witte and I. Tuschy. TESPpy: Thermal Engineering Systems in Python. In: Journal of Open Source Software 5.49 (2020), p. 2178. DOI: 10.21105/joss.02178.
- [57] I. H. Bell, J. Wronski, S. Quoilin, and V. Lemort. Pure and Pseudo-pure Fluid Thermophysical Property Evaluation and the Open-Source Thermophysical Property Library CoolProp. In: Industrial & Engineering Chemistry Research 53.6 (2014), pp. 2498–2508. DOI: 10.1021/ie4033999. eprint: <http://pubs.acs.org/doi/pdf/10.1021/ie4033999>.
- [58] F. Witte. TESPpy Documentation. <https://tespy.readthedocs.io/en/master>. 2020.
- [59] S. Chen and H. Shao. A 3-BHE Array Coupled With Pipe Network. 2020. URL: https://www.opengeosys.org/docs/benchmarks/heat-transport-bhe/3d_3bhes_array/.
- [60] S. Chen, H. Shao, and F. Witte. Heat_Transport_BHE PipeNetwork Feature. 2020. URL: https://www.opengeosys.org/docs/userguide/process-dependent-configuration/heat_transport_bhe_pipelinenetwork/.
- [61] P. Hein. On the efficient and sustainable utilisation of shallow geothermal energy by using borehole heat exchangers. PhD thesis. Dresden University of Technology, Germany, 2016.
- [62] H. Shao, P. Hein, A. Sachse, and O. Kolditz. Geenergy Modeling II: Shallow Geothermal Systems. Springer, 2016. DOI: 10.1007/978-3-319-45057-5.
- [63] W. Jakob, J. Rhineland, and D. Moldovan. pybind11 — Seamless operability between C++11 and Python. <https://github.com/pybind/pybind11>. 2016.
- [64] C. Lehmann. Manufactured Solution for Laplace’s Equation with Python. <https://www.opengeosys.org/docs/benchmarks/python-bc/laplace-equation/python-laplace-eq/>; <https://github.com/ufz/ogs/pull/2170>. 2020.
- [65] S. Chen, F. Witte, O. Kolditz, and H. Shao. Shifted thermal extraction rates in large Borehole Heat Exchanger array – A numerical experiment. In: Applied Thermal Engineering 167.July 2019 (2020), p. 114750. ISSN: 1359-4311. DOI: 10.1016/j.applthermaleng.2019.114750.
- [66] S. Chen, W. Cai, F. Witte, X. Wang, F. Wang, O. Kolditz, and H. Shao. Long-term thermal imbalance in large borehole heat exchangers array-A numerical study based on the Leicester project. In: Energy and Buildings 231.Jan 2021 (2020), p. 110518.

- [67] T. E. ToolBox. Hazen-Williams Coefficients. https://www.engineeringtoolbox.com/hazen-williams-coefficients-d_798.html. [Online; accessed 15-July-2018]. 2018.
- [68] S. S. Naicker and S. J. Rees. Long-term high frequency monitoring of a large borehole heat exchanger array. In: *Renewable Energy* 145 (2020), pp. 1528–1542. ISSN: 18790682. DOI: 10.1016/j.renene.2019.07.008.
- [69] S. S. Naicker and S. J. Rees. Geothermal heat pump system operational data: high frequency monitoring of a large university building. University of Leeds. 2017. DOI: 10.5518/255.
- [70] W. Cai, F. Wang, S. Chen, C. Chen, J. Liu, and J. Deng. Analysis of heat extraction performance and long-term sustainability for multiple deep borehole heat exchanger array : A project-based study. In: *Applied Energy* 289.116590 (2021). DOI: 10.1016/j.apenergy.2021.116590.

A

APPENDIX A

Table A1: Computed hydraulic results of the water pressure at each observation points from TESP_y and EPANET

Observation points	Water pressure in TESP _y in <i>bar</i>	Water pressure in EPANET in <i>bar</i>
P	2.000000	2.000000
P'	2.477722	2.477952
B ₁	2.477722	2.477952
B ₁ '	2.412035	2.412233
B ₂	2.412035	2.412233
B ₂ '	2.346347	2.346515
B ₃	2.477722	2.477952
B ₃ '	2.346347	2.346515
C	2.346347	2.346515
C'	2.000000	2.000000

Table A2: Computed hydraulic results of the flow rate at each objects in the network from TESP_y and EPANET

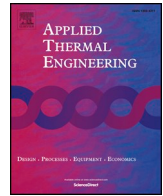
Objects in the network	Flow rate in TESP _y in kg s^{-1}	Flow rate in EPANET in kg s^{-1}
inflow	0.353871	0.353942
pump	0.353871	0.353942
splitter	0.353871	0.353942
BHE 1	0.144206	0.144227
BHE 2	0.144206	0.144227
BHE 3	0.209665	0.209715
merge	0.353871	0.353942
consumer	0.353871	0.353942
outflow	0.353871	0.353942

B

APPENDIX B

B.1 Paper 1

S. Chen, F. Witte, O. Kolditz, H. Shao (2020). Shifted thermal extraction rates in large Borehole Heat Exchanger array – A numerical experiment. Applied Thermal Engineering, 167 (July 2019), 114750. DOI: 10.1016/j.applthermaleng.2019.114750.



Shifted thermal extraction rates in large Borehole Heat Exchanger array – A numerical experiment

Shuang Chen^{a,b}, Francesco Witte^c, Olaf Kolditz^{a,b}, Haibing Shao^{a,d,*}

^a Helmholtz Centre for Environmental Research – UFZ, 04318 Leipzig, Germany

^b Dresden University of Technology, 01069 Dresden, Germany

^c Flensburg University of Applied Sciences, 24943 Flensburg, Germany

^d Freiberg University of Mining and Technology – TUBAF, 09599 Freiberg, Germany

HIGHLIGHTS

- A numerical model was developed to simulate an array of borehole heat exchangers.
- Heat extraction rate was shifted among BHEs over the long-term operation.
- Pipeline network has an intrinsic feature of re-balancing thermal load among BHEs.
- Thermal recharge limits the exploitable capacity of the shallow geothermal energy.

ARTICLE INFO

Keywords:

Shallow geothermal energy extraction
Ground Source Heat Pump (GSHP)
Borehole Heat Exchanger (BHE) array
Shifted heat extraction rate
OpenGeoSys (OGS)
Thermal Engineering Systems in Python (TESPy)

ABSTRACT

In large scale Ground Source Heat Pump (GSHP) systems, multiple Borehole Heat Exchangers (BHEs) are often connected with the pipe network array to extract shallow geothermal energy. In this study a comprehensive numerical model was developed. The heat transport within and around the BHEs and the pipe network is explicitly quantified in a coupled manner. The model allows a dynamic heat extraction calculation on the individual BHE that is determined by the hydro-thermal processes in the pipe network. The model is thus capable of capturing the long-term thermal interference among BHEs. The model was verified against analytical solution with respect to its hydraulic and thermal balances. Based on it, a series of numerical experiments have been performed to quantitatively investigate the amount of shifted thermal extraction rate in large BHEs array. It is found that, the heat extraction rate on the central BHEs was gradually shifted towards those located at the edge in the long-term operation. Over different seasons, the strongest shifting phenomenon was observed in the month with the lowest thermal load. The shift becomes significant with the increasing number of BHEs installed. The result of numerical study suggests that traditional super-positioned based infinite line source approach with a constant heat flux is not accurate enough for long-term prognosis since it does not fully consider the thermal recharge and the thermal interference effects.

1. Introduction

In the first decade of this century, the global installed geothermal heating and cooling applications have been increasing with a growing momentum [1,2]. Among the different technology options, utilising geothermal energy through Ground Source Heat Pump (GSHP) system has the most significant impact. It has the largest installed capacity worldwide (70.90%) and growing at a compound rate of 10.3% since 2010 [3]. A recent trend in the industry is to build large GSHP system targeting commercial buildings and small neighbourhood [4], where

dozens, in some cases hundreds of Borehole Heat Exchangers (BHEs), were connected with a pipe network to form a BHE array in order to supply the higher thermal load for large buildings. Especially in urban areas where the land is limited, this type of shallow geothermal exploitation is often favourable, because the accelerated heat fluxes between the warmed basement often leads to elevated temperatures in the urban subsurface [5–7].

For the design of such BHE arrays, various analytical and numerical models have been developed. Firstly, Eskilson [8] presented the super-position borehole model to estimate the soil temperature distribution

* Corresponding author.

E-mail address: haibing.shao@ufz.de (H. Shao).

<https://doi.org/10.1016/j.applthermaleng.2019.114750>

Received 29 July 2019; Received in revised form 25 November 2019; Accepted 29 November 2019

Available online 04 December 2019

1359-4311/ © 2019 Elsevier Ltd. All rights reserved.

Nomenclature*Roman letters*

a	proportion of the shifted thermal load over the mean load value (%)
c	specific heat capacity ($\text{J Kg}^{-1} \text{K}^{-1}$)
D	diameter of the pipe (m)
E_1	exponential integral function
H	thermal sink/source term (W m^{-3})
h	enthalpy of circulating fluid (J kg^{-1})
k_s	roughness coefficient of the pipe (m)
\dot{m}	flow rate of circulating fluid (kg s^{-1})
N_{dof}	number of degrees of freedom
P	power of the pipe network component (W)
p	hydraulic pressure of circulating fluid (Pa)
\dot{Q}	heat extraction rate of the BHE (W)
$q_{k,l}$	sequence of heat extraction pulses (W)
q_n	heat flux between soil, grout and pipe (W m^{-2})
Re	Reynolds number (–)
T	temperature ($^{\circ}\text{C}$)
t	time (s)
\mathbf{u}	velocity vector of circulating fluid (m s^{-1})
\mathbf{v}	Darcy velocity vector of groundwater flow (m s^{-1})
v	flow velocity in pipelines (m s^{-1})

Greek letters

α	soil thermal diffusion coefficient ($\text{W m}^{-1} \text{K}^{-1}$)
ϵ	numerical error (–)
η	viscosity of circulating fluid ($\text{kg m}^{-1} \text{s}^{-1}$)
Γ	domain boundary
Λ	hydrodynamic thermal dispersion tensor ($\text{W m}^{-1} \text{K}^{-1}$)
λ	thermal conductivity ($\text{W m}^{-1} \text{K}^{-1}$)
Ω	domain (–)

ϕ	heat transfer coefficient ($\text{W m}^{-2} \text{K}^{-1}$)
π	mathematical constant Pi (–)
ρ	density (kg m^{-3})
ϵ	volume fraction, porosity (–)
ζ	friction factor of the pipe in Eq. (5) (–)

Operators

Δ	difference operator
∇	spatial gradient operator
$\nabla \cdot$	spatial divergence operator

Subscripts

dof	degrees of freedom
f	fluid
g	grout
i	pipe-in or internal
o	pipe-out or outer

Superscripts

$1U$	single U-shape pipe
f	fluid
g	grout
r	circulating fluid (refrigerant)
s	solid or soil

Abbreviations

$1U$	single U-shape pipe
BHE	borehole heat exchanger
COP	coefficient of performance
$GSHP$	ground source heat pump

induced by infinite line source. This model contains the well known g-functions representing the non-dimensional thermal response deduced by an instantaneous thermal load. The method was further improved by Bernier et al. [9] by considering the past steps thermal response effect to the current temperature distribution. Using this super-position principle, several analytical solutions are further developed. Lamarche and Beauchamp [10] demonstrated a mathematical algorithm which is not dependent on the previous step thermal response. Koohi-Fayegh and Rosen [11] analyzed the two neighbouring boreholes and then further developed a more accurately analytical approach considered the thermal interference among BHEs that are connected in an array [12]. Qian and Wang [13] presented a model to investigate the relationship between the soil temperature distribution and the Coefficient of Performance (COP) of the heat pump. Based on the finite line source model, Rivera et al. [14] presented a semi-analytical approach which could estimate the transient temperature distribution in a three-dimensional domain. For the seasonal heating and cooling strategy in a multi-BHE array, Bayer et al. [15] developed a mathematical procedure also based on super-position principle to optimise the BHE field operation. Zhang et al. [16] summarised the most typical computational methods for ground dynamic thermal response.

On the other hand, numerical models targeting BHEs array design are making considerable advances in recent years, since they have the advantages in simulating the complex subsurface conditions that cannot be reliably calculated by analytical models. The well known Duct Storage model is widely applied in the design and analysis of underground energy storage system [17]. Morrone et al. [18] investigate the long term behaviour of an energy pile system with numerical simulator PILESIM2 [19]. Similar to the Duct Storage model, the PILESIM2

simulator aggregates all the heat exchanger piles into a store cylinder volume, by which the heat transfer between each BHE and the surrounding soil is not explicitly quantified. Lee and Lam [20] presented a three-dimensional model for a single cylindrical energy pipe. Koohi-Fayegh and Rosen [11] proposed a numerical model to investigate the thermal behaviour between two boreholes considering their possible thermal interference. Hein et al. [21] investigate the soil temperature evolution induced by a configuration of four individual GSHP systems. Saaly et al. [22] built a numerical 3D heat absorber panel model with the software COMSOL Multiphysics [23] to investigate the effect of heat loss in a building which was equipped with an geothermal energy pile system in Canada. Hénault et al. [24] simulated a hybrid ground-coupled heat pump system which could significantly reduce the electrical consumption of a building.

In the above mentioned analytical and numerical approaches, the heat extraction rate on each BHE is mostly defined as an imposed boundary condition and the surrounding soil temperature distribution is assumed to be in an equilibrium state to satisfy that. These assumptions hold true for a single BHE, but it may deviate from the reality when the thermal plumes from neighbouring BHEs are interfering with each other. In heating applications, the overlapping thermal plumes can lead to low temperature zones in the centre of the BHE array, indicating a thermal imbalance in the subsurface [4,7]. This imbalance may further lower the thermal extraction rate on the individual BHE, depending on where it is located. To quantify such interference, several analytical approaches have been developed. The well-known ASHRAE method [25] adopts the concept of temperature penalty to estimate the long-term ground temperature changes with explicit consideration of

soil thermal imbalances. Being aware of the different heat extraction rates, Gultekin et al. [26] further extended his analytical formulation, in which the individual extraction rate is dependent on the number of BHEs and the spacing between them. Witte [27] presented a simple diagram to assess the change of soil temperature in the vicinity of a BHE based on the distance to the next borehole and the thermal load imposed on it. You et al. [28] also proposed a coupled analytical approach, in which the heat extraction rate of each energy pile is coupled with the groundwater flow velocity, the depth of BHEs, as well as the spacing between them.

Despite of these developments, the modelling approaches mentioned above are limited in describing several important physical processes. Firstly, the thermal recharge is not considered in most of the analytical solutions. The seasonal surface temperature fluctuation at the ground surface and the vertical geothermal gradient contribute to the thermal recharge of shallow subsurface [29–31]. Without the quantification of thermal recharge, the long-term thermal imbalance in the subsurface cannot be accurately predicted and may lead to deviated results especially for the prognosis over 10 to 20 years. Secondly, most analytical approaches are based on the principle of super-position to calculate the change of dimensionless soil temperature. Over the long operation period, the groundwater flow velocity and the hydraulic condition around each BHE are always time-dependent. This makes it difficult to calculate the dimensionless soil temperature change. Thirdly, in most analytical and numerical approaches, the flow and heat transport in the pipe network are not considered. In a real GSHP system, the inflow and outflow temperatures on each individual BHE are time-dependent and closely coupled with the pipeline network. On the one hand, the heat flux on each BHE is determined by the temperature difference between the surrounding soil and the circulating fluid. On the other hand, the pipe network distributes and collects the fluid towards and from each BHE. The network itself has an intrinsic feature of balancing thermal extraction rates among different BHEs. Without the explicit consideration of hydraulic and thermal balance in the pipe network, the above mentioned coupling effect cannot be accurately quantified.

As the large BHE array is fairly new to the market, the current industrial standards and guidelines have not yet fully recognised coupled pipe network effect. Most of the guidelines just specifies a minimal distance between BHEs to mitigate the thermal interference. For example, Switzerland requires a minimum distance of 5 m is between the BHEs (cf. Miglani et al. [32]). In United Kingdom the value is 7 m [33]. The German guideline increased this value from 5 m to 6 m in its 2015 updated version [34,35]. And in China this distance is kept between 3 m to 6 m [36]. The 2015 version of the Germany guideline VDI4640 [35] partially recognised the varying heat extraction rates by introducing a penalty factor when the GSHP system contains less than five BHEs. For systems larger than that or bearing a capacity higher than 30 kW, numerical or analytical modelling studies become a mandatory requirement. After reviewing the state-of-art of current modelling approaches, one key scientific question emerges with regard to the system behaviour of large BHE arrays: How does the thermal extraction rate on individual BHE change in response to the thermal imbalance, which may occur due to insufficient thermal recharge in the long-term operation?

This study intends to answer the above question by introducing a comprehensive numerical model, with the shallow subsurface, the multiple BHEs and the pipe network explicitly quantified in a single numerical modelling framework. Section 2 explains the mathematical background of this numerical model. Section 3 verifies the model by comparing its result against analytical solution and by checking its thermal balance. In Section 4, a series of numerical experiments were designed to quantitatively investigate the amount of shifted thermal extraction rate in large BHE arrays. Interpretations and discussions were further given to reveal how the three compartments, i.e. the subsurface, the BHEs, and the pipe network, are interacting with each

other in response to supply heat or cool to the building. Additionally, the subsurface soil temperature distribution computed by the super-positioned infinite line source model were compared against the numerical model extended in this work, to see how much deviation it will be by assuming an imposed heat extraction rate on each BHE (Section 6.1). This manuscript finalises itself with specific suggestions to the design of large BHE arrays.

2. Method

In this section, the theoretical background and the mathematical framework are presented.

2.1. Subsurface BHE model

The BHE used in this paper contains a single U-shape pipe (1U type). The details about its finite element realisation has already been described in Diersch et al. [37]. The cylindrical borehole is equipped with a 1U pipe and filled with grout. In the heating season the refrigerant with a relative low temperature is pumped into the BHE inlet (denoted with $i1$). It is circulated through the 1U pipe and exits the BHE at the outlet (denoted with $o1$). Due to the temperature difference between the fluid, the grout and the surrounding soil, heat flux is established and transfers heat into the pipe and rises the temperature of the circulating fluid. The fluid then goes through the pipe network and its carrying heat is supplied to the heat pump. The heat was transferred through three different media, namely the soil, the grout, and the circulating fluid. Following Diersch et al. [37] the governing equations for the heat transport between soil and grout reads

$$\frac{\partial}{\partial t} \{ [\varepsilon \rho^f c^f + (1 - \varepsilon) \rho^s c^s] T_s \} + \nabla \cdot (\rho^f c^f \mathbf{v} T_s) - \nabla \cdot (\Lambda \cdot \nabla T_s) = H_s, \quad (1)$$

In grout zone #1 ($g1$, same in zone #2),

$$\begin{aligned} \frac{\partial}{\partial t} (\varepsilon_g \rho^g c^g T_{g1}) - \nabla \cdot (\varepsilon_g \lambda^g \nabla T_{g1}) &= H_{g1} \quad \text{in } \Omega_{g1} \\ \text{with} \\ q_{nT_{g1}} &= -\Phi_{gs}^{1U} (T_s - T_{g1}) - \Phi_{fg}^{1U} (T_i - T_{g1}) - \Phi_{gg}^{1U} (T_{g2} - T_{g1}) \quad \text{in } \Gamma_{g1}. \end{aligned} \quad (2)$$

For fluid within the pipe (e.g. the inlet side),

$$\begin{aligned} \frac{\partial}{\partial t} (\rho^f c^f T_{i1}) + \nabla \cdot (\rho^f c^f \mathbf{u} T_{i1}) - \nabla \cdot (\Lambda^f \cdot \nabla T_{i1}) &= H_{i1} \quad \text{in } \Omega_{i1} \\ \text{with} \\ q_{nT_{i1}} &= -\Phi_{fg}^{1U} (T_{g1} - T_{i1}) \quad \text{in } \Gamma_{i1}, \end{aligned} \quad (3)$$

where, ε is the porosity, Λ denotes the thermal dispersion, H denotes the heat sink and source term. For hydraulic parameters \mathbf{u} denotes the velocity of circulating fluid inside the pipe, and \mathbf{v} denotes the Darcy velocity of ground water flow. The governing Eqs. (1)–(3) can be simulated by the open-source scientific modelling software OpenGeoSys. The BHE feature in the OpenGeoSys has been verified against analytical and lab measurement data [30]. It has also been utilised to investigate the amount of extractable energy with both shallow [21] and deep borehole heat exchangers [31].

2.2. Pipeline network model

In order to investigate the effect of different pipe network layouts on the heat extraction rate of individual BHE in the array, the numerical model OpenGeoSys is coupled with the steady state power plant simulation software TESPpy developed by Witte [38]. The TESPpy software is capable of simulating coupled thermal-hydraulic status of the network, which is composed of pre-defined components including pipes, heat exchangers and different types of turbomachinery. In TESPpy, governing equations were constructed to achieve steady-state mass and pressure balances for all connected components. On the mass balance

side, the total amount of fluid entering into ($\dot{m}_{in,j}$) or flowing out ($\dot{m}_{out,i}$) of a component must be equal,

$$\sum_j \dot{m}_{in,j} = \sum_i \dot{m}_{out,i} \quad (4)$$

On the pressure side, the pressure drop in a specific pipe can be calculated by the Darcy-Weisbach equation (Eq. (5), Böswirth and Bschorer [39]). As flow velocity is not part of the variables in TESPpy, the equation implemented in TESPpy is deduced by calculating flow velocity v through the pipes dimensions, the fluids density and mass flow rate. The Reynolds number Re is a function of pressure, enthalpy and flow rate. The fluids density ρ depends on pressure and enthalpy,

$$P_{in} - P_{out} = \frac{\rho}{2} \cdot v^2 \cdot \frac{\lambda(Re, k_s, D) \cdot L}{D} = \frac{8 \cdot \dot{m}_{in}^2 \cdot L \cdot \lambda(Re, k_s, D)}{\rho \cdot \pi^2 \cdot D^5} \quad (5)$$

Furthermore, energy balance (Eq. (6)) was imposed with respect to enthalpy for every component. The power P or heat transfer \dot{Q} can be zero in certain cases where an adiabatic component does not transfer heat or a pipe does not transfer power,

$$\dot{Q} + P = \sum_i \dot{m}_{out,i} \cdot h_{out,i} - \sum_j \dot{m}_{in,j} \cdot h_{in,j} \quad (6)$$

From Eqs. (4)–(6), the coupled governing equations are highly nonlinear. For example, temperature changes of circulation fluid due to BHE operation will lead to the change of fluid density and viscosity, and they will further determine the pressure drop due to friction. To handle this, TESPpy accesses the CoolProp library [40] internally for the fluid property calculation.

The component based architecture of the software allows the creation of individual model by connecting the respective components to form a topological network. By doing so, the characteristics of a specific pipeline network are defined by its own topology as well as the parametrization of the network's components. With these input information available, TESPpy will automatically generate a set of nonlinear equations. The multi-dimensional Newton-Raphson algorithm is then adopted to solve the coupled equations for the primary variables mass

flow, fluid enthalpy, and pressure at every point of the network as these variables fully determine the state of the circulating fluid. Thus, the total number of primary variables is equal to three times the number of connections between the network's components. After specifying the thermal load of the building, no matter how complex the network is, TESPpy will be able to simulate the steady state temperature, pressure and mass flow rate throughout the pipe network. Interested readers may refer to the online documentation of TESPpy for the details of corresponding benchmarks and tutorials [38].

2.3. Coupling OpenGeoSys and TESPpy

According to Eq. (2) and Eq. (3), the thermal load of each BHE in a BHEs array is dependent on the soil temperature T_s around the BHE and the inflow fluid temperature T_{in} , which is directly determined by the configuration of the pipeline network. Therefore, to obtain the thermal load on each BHE in the model, the soil temperature distribution and the hydro-thermal interference in the network should be simulated. In this study, the numerical model OpenGeoSys (OGS) [41] has been coupled with the Thermal Engineering Systems in Python (TESPy) [38] to explicitly simulate both the BHE and pipe network. The coupling was achieved through a Python interface. The schematised procedure of the method is illustrated in Fig. 1. Within every time step and each iteration, the outflow temperature T_{out} from each BHE is simulated by OGS and transferred to TESPpy via the interface. The T_{out} and the current hydraulic state are then used as the boundary condition for the pipeline network simulation in TESPpy. TESPpy will calculate the current inflow temperature T_{in} of each BHE and their flow rate, which satisfies the overall thermal load of the building. These computed data will be transferred back to OGS for the next iteration. The convergence was achieved when the difference from the last two iteration results is smaller than a preset tolerance of 1×10^{-6} . To be noticed is that the heat flow in OGS model is transient but the fluid and heat flow in the pipe network is steady state, therefore the model should not be applied for the short-term (minutes to hours) scenario simulations. In this study, our intention is to investigate the long-term behaviour of the GSHP system, especially its response to over-exploration over a long time span. For this purpose, the time step size in our simulation was set to

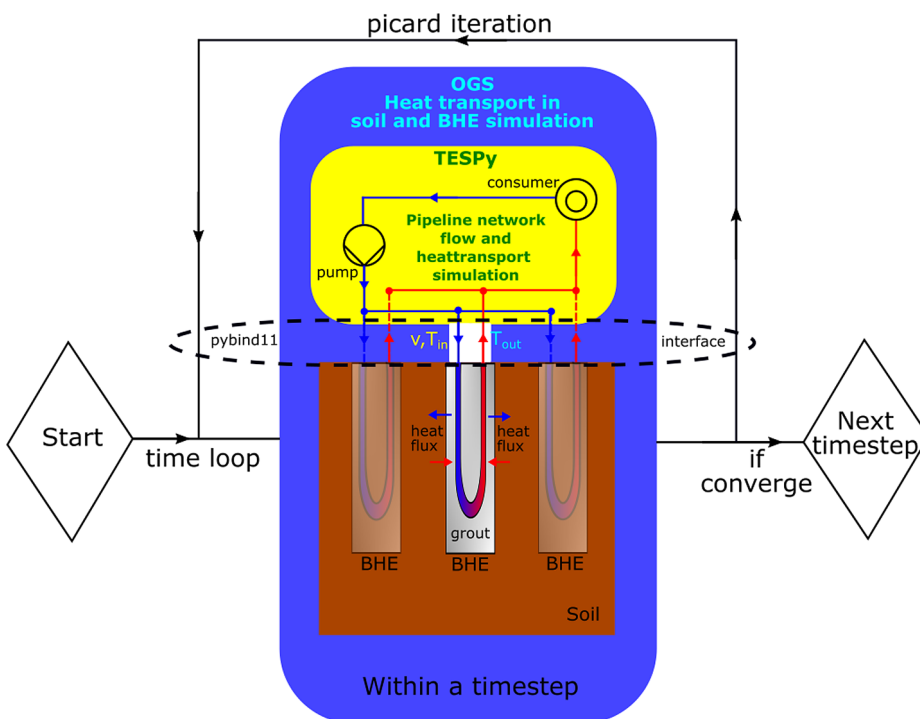


Fig. 1. Coupling scheme of the TESPpy (yellow) and OpenGeoSys (braun) software, the former simulates hydro-thermal processes in the pipe network and the latter models the subsurface heat transport around BHEs. (For interpretation of the references to color in this figure legend, the reader is referred to the web version of this article.)

3 h (10800 s). With this time step size, the steady-state flow and heat transfer in the pipe network are well preserved.

3. Model verification

As there is no analytical solution to our knowledge that is capable of predicting the temperatures in subsurface and in the pipe network simultaneously, the multi-BHE array model developed in this work will be verified in two separate steps. For the subsurface part, the simulated soil temperature evolution by OpenGeoSys was compared with the super-position analytical solution. For the pipe network part, the system thermal balance was examined to ensure the correctness of the model implementation.

3.1. Verification of the multi-BHE array model

For verification purpose, a 2D numerical model containing 25 BHEs was set up. The model domain has a geometry of 300×300 m. The peripheries of the domain were no-flux boundaries. The location of 25 BHEs is shown in Fig. 2. They are organised in a 5×5 array with a constant distance of 6 m from each other. On each of these BHEs, a heat sink term was imposed, which is equivalent to the infinite line source in the analytical solution by Eskilson [8]. A sequence of heat extraction rate is imposed identically on each BHE. This sequence is following the load curve applied in Section 4.2 and depicted in Fig. 7. Accounting a total length of BHE with 50 m, this translates to a specific heat extraction rate from a minimum of 0 W/m in the recovery months (May to August), up to 12.5 W/m in the peak month (January). A total of 10 years of BHE operation was simulated. For this setup, there exists the super-position analytical solution from Bayer et al. [15], which is capable of calculating the temporal temperature change at an arbitrary location (i, j) . The mathematical formulation of Bayer's analytical solution reads

$$\Delta T_{i,j}(x, y, t, q_{k=1, \dots, n, l=1, \dots, m}) = \sum_{l=1}^m \sum_{k=1}^n \frac{q_{k,l}}{4\pi\lambda} \left[E_1 \left[\frac{(i-x_k)^2 + (j-y_k)^2}{4\alpha(t_m - t_{l-1})} \right] - E_1 \left[\frac{(i-x_k)^2 + (j-y_k)^2}{4\alpha(t_m - t_l)} \right] \right], \quad (7)$$

where $q_{k,l}$ is a sequence of heat extraction pulses on the k_{th} heat source term at $t = l$ time step. (x_k, y_k) denotes the location of the k_{th} BHE. E_1 refers to the exponential integral function. λ is the thermal conductivity and α is the thermal diffusion coefficient.

For the verification, simulated soil temperature was compared along the observation profile $(A - A')$ as shown in Fig. 2. It is selected to be 0.05 m away from the diagonal of the domain. The reason of keeping this distance is to avoid the exact location of each sink term, where the analytical solution will produce an infinite value. The Fig. 2a depicts the numerical and analytical results along the observation profile after 10 years of operation, and Fig. 2b illustrates the evolution of numerical and analytical results at the nodes located 0.05 m aside from the selected BHEs over the 10 years. The long-term extraction of shallow geothermal resources causes a temperature draw-down especially in the middle section of the BHE array. The numerical results fits visually very well with the analytical solutions. To give a more quantitative measure of the deviation, the error ϵ was calculated according to the following equation,

$$\epsilon = \frac{\|T_{j,t} - \hat{T}_{j,t}\|_2}{N_{dof}}, \quad (8)$$

where N_{dof} denotes the number of degrees of freedom (600 in Fig. 2a case and 120 in the Fig. 2b), $T_{j,t}$ and $\hat{T}_{j,t}$ are the analytical and numerical solution of the soil temperature at the t timestep and at the j_{th} node on the observation profile respectively. A relative small value of $\epsilon = 1.3 \times 10^{-4}$ and 1.6×10^{-4} was achieved for the two figures

respectively, which proofed that the soil temperature distribution was correctly calculated by the numerical model OpenGeoSys.

3.2. Verification of the pipeline network model in TESPpy

To verify the heat transport feature predicted by TESPpy in the pipe network, a 25-BHE pipe network has been set up. The topological structure of the BHE system is illustrated in Fig. 6(c). All 25 BHEs are connected with each other in a double-layer parallel manner. The arrows in the figure indicates flow direction of the circulating fluid. Within the network, a pump was included to lift the hydraulic head and drive the fluid flow. The hydraulic balance within the entire network was verified against the results from the widely recognised software EPANET [42], which is the standard solution for the modelling of drinking water supply systems. The verification was completed by comparing the hydraulic head values at the connection points of the pipes. The EPANET and TESPpy simulated results are nearly identical. The standard deviation of the results from two software is only 2.18×10^{-5} and the computed difference is mainly due to the different convergence conditions in each software. Due to limited space in this manuscript, details of the hydraulic verification is not included here. Instead, we will focus on the thermal balance of the system. Detailed description of the fluid circulating process within the entire pipeline system could be found in Section 4.1.2.

In this case, a total of 10 years of BHE operation was simulated under different monthly heat demand strategy. An annual thermal demand curve was imposed on the heat pump, with the assumption that its thermal demand was supplied by the inter-connected 25 BHEs. The average heat extraction rate on each BHE differs over the months, but it can be obtained by normalising the total thermal demand over the number of BHEs (25 in this case). This calculated average heat extraction rate was illustrated as the black curve in Fig. 7. In each year the average heat extraction rate on each BHE varies from its peak (625 W)

in January down to the minimum load (78.125 W) in September. From May to August the load is set to zero, which is the recovery period. Based on the mathematical framework described in Section 2.2, the temperature and pressure distribution within the network could be computed by TESPpy in each time step. Based on the temperature difference at the inlet and outlet of each BHE and the flow rate \dot{m} within each pipe, OGS calculates the actual heat extraction rate on each BHE \dot{Q} according to

$$\dot{Q} = (\rho c)_f \dot{m} (T_{i1} - T_{o1}), \quad (9)$$

where $(\rho c)_f$ is the circulating fluid heat capacity.

From the results presented in Fig. 3, it can be observed that the heat extraction rate are unequal in different BHEs and they deviate from the calculated average value. This suggests that the thermal interference may already result in the shifting of extraction rate. In Fig. 3, the location of BHEs is marked with the index number as shown in Fig. 5. The six vertical columns with multiple colour dots indicate the varying total thermal load in different months. The simulated results showed that for BHEs at the centre of the array, it generally has an actual extraction rate lower than the average (below the black line). In the contrary, the BHEs at the outer part is sharing a higher thermal load (higher than black line). Considering the existence of thermal interference, it is physically reasonable that the actual heat extraction rates were deviating from the average value, but when looking into its annual trend, individual extraction rates are still largely controlled by the total system load. Since it is assumed that all supplied building heat comes from the BHEs, a

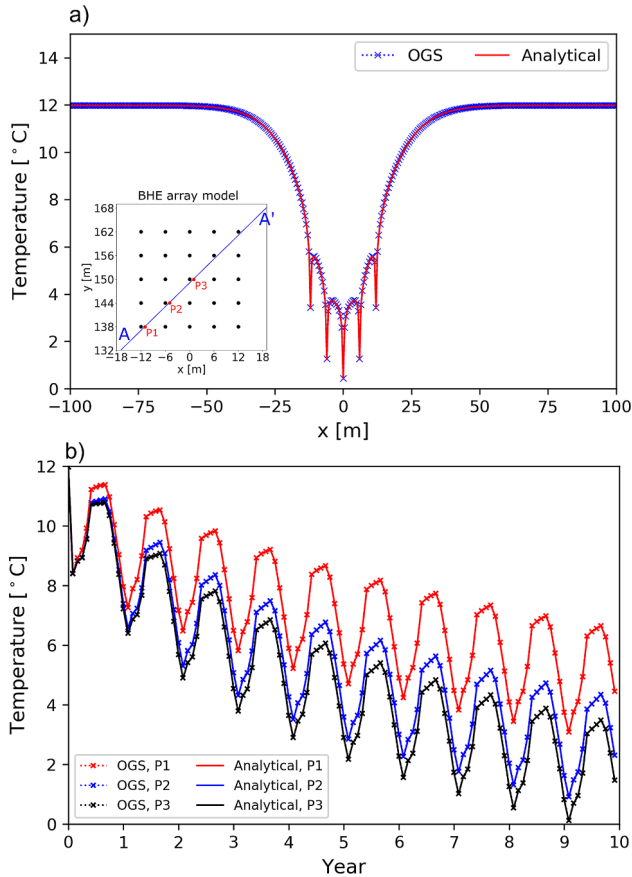


Fig. 2. (a) Numerically simulated and analytically calculated soil temperature distribution along the observation profile (A-A') after 10 years of BHE operation; (b) comparison of numerical and analytical result at locations 0.05 m aside from the BHEs over a 10-year-period.

virtual heat pump was added in the model, which does not consume any electricity or delivers additional heat to the building. Although the thermal load is not equally distributed, the total thermal load of the system should then be equal to the summation of actual heat extraction rates from all BHEs. We use this balance relationship to exam the correctness of the coupled model. Here the computed BHE heat extraction rate (after Eq. (9)) on each BHE were added up and the total value was compared against the imposed total thermal load (see Fig. 4). As shown in the Fig. 4, the comparison was nearly perfect with a R-squared value of 99.89%. The deviation attributes to the fact that the fluid density and viscosity were all assumed to be a constant in the OpenGeoSys code, while they were dynamically adjusted on the TESPpy side. Despite of this negligible difference, the comparison gives us strong confidence that the coupling of heat transport between the OpenGeoSys and TESPpy was correctly implemented.

4. Numerical experiments

In order to systematically investigate the shifting heat extraction rate as shown in the above section, three different BHE arrays were configured and simulated. Fig. 5 illustrates the domain representing the subsurface part, as well as the arrangements of the pipe networks. Fig. 6 further reveals how the pipes are connected in the three setups, namely the single BHE, the 3×3 , and the 5×5 cases. The detailed configuration of each model with their parameter and boundary condition settings are described subsequently.

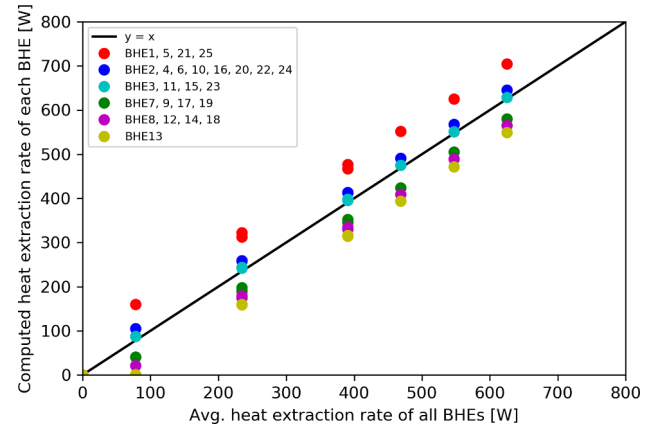


Fig. 3. Regression plot of the actual computed heat extraction rate on each BHE against the average heat extraction rate of all BHE in different heating months in the 10th year.

4.1. Model domain

4.1.1. Subsurface part

For the subsurface domain, a $300 \times 300 \times 160$ m mesh was constructed with prism and line elements. The total number of nodes and elements in the single BHE case was 3144 and 5530. For the 3×3 and 5×5 cases the numbers are 37248 and 68432 nodes, along with 70884 and 126197 elements respectively. The BHE arrays were installed always in the centre of the domain and composed of line elements in all scenarios. All BHEs have an identical length of 50 m, with its top located at a depth of 2 m. To satisfy the design requirement by the Germany VDI guideline [35], the distance between the adjacent BHEs is kept at a minimum of 6 m. Detailed parameters for soil, BHEs and circulating fluid applied in the model are listed in the Table 1.

It is well known that groundwater flow, by bringing in additional recharge to the subsurface, will enhance the heat extraction capacity of the BHE array. The OpenGeoSys code used for the numerical experiments is also capable of simulating the system operation along with the groundwater flow process (see e.g. Hein et al. [21]). However, groundwater flow regime is strongly location dependent, and it may not be present in every geothermal site. As a result, an assumption of no groundwater flow was applied for all modelling scenarios in this study. This allow us to focus on the impact of thermal interference between BHEs.

4.1.2. Pipe network

A closed-loop pipeline network system was constructed in TESPpy to couple with the OpenGeoSys model. Fig. 6(a) illustrates the basic configuration of the entire network with the single BHE case. After lifted by the pump, the circulating fluid will be divided into different branches by the splitter and then flow into each BHEs sub-arrays according to the pre-defined arrangement (see Fig. 6). In the 3×3 case, the system is divided into 3 sub-arrays, each of which are connected with 3 BHEs in a parallel way. In the TESPpy setup, both serial and parallel connections can be constructed. The pure parallel scheme was chosen in this work for two reasons. Firstly the parallel connection is most applied in a realistic projects. Secondly, identical inflow temperature can be guaranteed on all BHEs in the array during the simulation. In the 5×5 case, the number of sub-arrays and the connected BHEs are increased. The fluid leaving the BHE will firstly be mixed at the merging point and then being extracted for heat extraction through the heat pump. The length and the diameter of the BHE pipe in the TESPpy network are specified with the identical values as the properties used in the OGS model (see Table 1). Although the TESPpy program is capable of simulating both the hydraulic and heat loss in the connecting pipes and the BHE, we have configured the model in a way that the

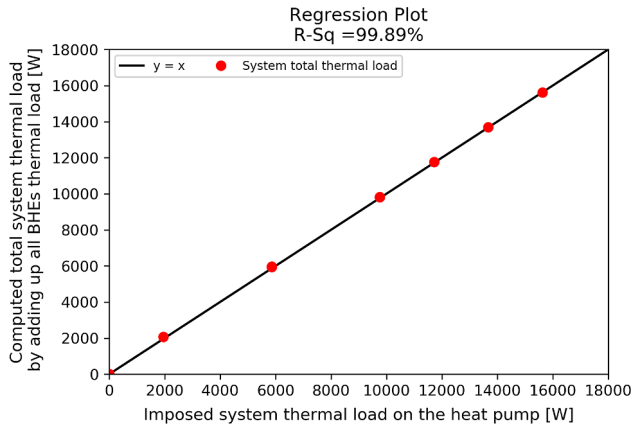


Fig. 4. Regression plot of the computed heat extraction rate on all BHE against the imposed thermal loading at the heat pump in different thermal loading months over the 10_{th} year.

hydraulic and heat loss along the connecting pipes are neglected. The reason behind this decision is to confine the heat loss only in the subsurface part and makes the thermal balance calculation in Section 3.2 possible. Only with such simplification, the super-imposed line source model is equivalent to the numerical one in reproducing the subsurface temperature distribution. If the hydraulic losses in the connecting pipes are added, an equal distribution of flow rates among the individual BHEs are no longer possible, as the lengths of connecting pipes on each BHE are clearly different.

4.2. Initial and boundary conditions

OpenGeoSys

Considering the existence of the geothermal gradient in the subsurface, the initial soil temperature in OpenGeoSys is specified with an increasing trend along the depth. In the region of Leipzig area, the geothermal gradient value $\left(\frac{\partial T}{\partial z}\right)_{geo}$ is known from the measurement to be 0.016 K m^{-1} (cf. Richter et al. [43]). Starting from the surface, the initial soil temperature was set according to the average annual ground surface temperature of $11.167 \text{ }^\circ\text{C}$, mimicking the Leipzig area. This value increases up to $13.727 \text{ }^\circ\text{C}$ at a depth of 160 m. As for the boundary conditions, an annual ground surface temperature curve is set, its variation is illustrated by the red line in Fig. 7. The temperature keeps constant within each month, its the lowest value is $2 \text{ }^\circ\text{C}$ in December and January, then gradually increases to a maximum of $21 \text{ }^\circ\text{C}$ in June and July. A fixed geothermal flux with 0.0384 Wm^{-2} is imposed at the bottom surface as the Neumann boundary condition of the model. This value is based on the calculation of thermal flux $q_{geo} = \lambda_s \left(\frac{\partial T}{\partial z}\right)_{geo}$.

TESPy

In the three simulation scenarios, a fixed circulation flow rate with 0.27 kg/s was assumed within each BHE. Due to the parallel layout, the total flow rate through the circulation pump can be determined by multiplying the above flow rate with the number of BHEs in the array. Therefore, the total flow rate in the array was calculated to be 2.43 kg/s and 6.75 kg/s for the two larger arrays respectively. The Darcy-Weisbach equation (Eq. (5)) was adopted to quantify the pressure loss due to friction in the pipeline. As for the total thermal load in each modelling cases, a seasonal dependent curve was specified (cf. Fig. 7). Every year, a peak thermal load was found to be in January, with a specific heat extraction rate of 12.5 W per meter length of BHE. For the single BHE case, this translates to 625 W of thermal load. In the 3×3 and 5×5 cases, the total thermal loads were proportionally increased to 5625 and 15625 W . In other months, due to elevated environmental temperature, the thermal load was decreased. The general trend of this load curve was following Hein et al. [30]. It should be noted that the

heat extracted from the BHEs serves as a heat supply of a heat pump. Thus, the actual heat supplied by a full system with a heat pump is much higher depending on the heat pump's COP. As the focus of this paper is on the BHE system instead of the heat pump, we choose this configuration in a way that the modelling result will not be influenced by the varying heat pump efficiency. Therefore, a virtual heat pump was added, by which all heat extracted from the subsurface will be transferred to the building side. No electricity was consumed by the heat pump. The advantages of this configuration is that the model can be verified with respect to its total thermal balance (as already shown in Section 3.2) and the shifting thermal extraction rates inside the BHE array can be clearly demonstrated. In reality, this is definitely not the case. TESPy can also be programmed to simulate heat pumps with its COP depending on the fluid temperature. We will demonstrate this feature in future publications.

All three cases were simulated for a period of 10 years. The time step size was controlled to be 10800 s (3 h). The simulation was carried out on a workstation equipped with 3.40 GHz CPU, 16 GB of memory. The model was configured to run in a serial mode without any parallelization scheme, i.e. only 1 CPU core was employed. The time needed for running the simulation depends strongly on the number of BHEs and the size of mesh correspondingly. For the single BHE case, the model simulation can be completed in 4.5 h. In the 3×3 and 5×5 cases, this increases to 74 and 144 h.

5. Results

In this section the simulated results from multiple scenarios defined in Section 4 are presented. The thermal interference, and hence the shifted thermal extraction rates on individual BHEs are analysed accordingly. The three BHE arrays are composed of 1, 9 (3×3) and 25 (5×5) BHEs. In each of the setup, BHEs located on some representative locations are selected and analysed. They are numbered as the BHE #1, #4 and #5 in the 3×3 case, and the BHE #1, #6, #7, #11, #12, and the #13 in the 5×5 case (see Fig. 5 for details).

5.1. Evolution of temperature

Fig. 8 depicts the soil temperature distribution in the 5×5 setup after 10 years. The left figure illustrates the 3D view of the temperature distribution near the centre of the BHEs array. A horizontal profile $Z - Z'$ at the depth of 27 m was depicted on the right. It can be observed that there exists a low temperature zone in the centre of the BHE array, indicating a thermal imbalance in the subsurface. To show this in a more quantitative way, Fig. 9 depicts the simulated evolution of soil temperature at 1 m distance from the selected BHEs at the same depth in the end of January every year, when the system is imposed with the peak heating load of that year. For comparison, the result of 1×1 BHE is also illustrated in both figures as the reference (black line). It can be observed that the soil temperature decreases gradually over time, due to the thermal interference between neighbouring BHEs. For the single BHE, the temperature reduction is the minimum, only about $0.6 \text{ }^\circ\text{C}$ after 10 years. After around 3 years, the soil temperature is already approaching a quasi-steady-state. Compared to the single BHE case, the temperature decrease in the 3×3 setup is much stronger. The temperatures at three different locations dropped by at least $2.6 \text{ }^\circ\text{C}$ after 10 years. The most intensive temperature decrease is found in the 5×5 case, where a reduction of at least $4 \text{ }^\circ\text{C}$ can be observed. Since the average heat extraction rate (625 W) on the individual BHE is identical, the 5×5 case has the maximum total system power (15625 W). In both the 3×3 and 5×5 cases, the soil temperature at the edge (BHE #1 in the 3×3 and 5×5 case) is general higher than that in the centre part of the array. When moving from the edge towards the centre, the temperature decrease also becomes larger. Since the soil at the centre is suffered by the most intensive accumulative effects from all sides, the soil temperature drop there is the most significant.

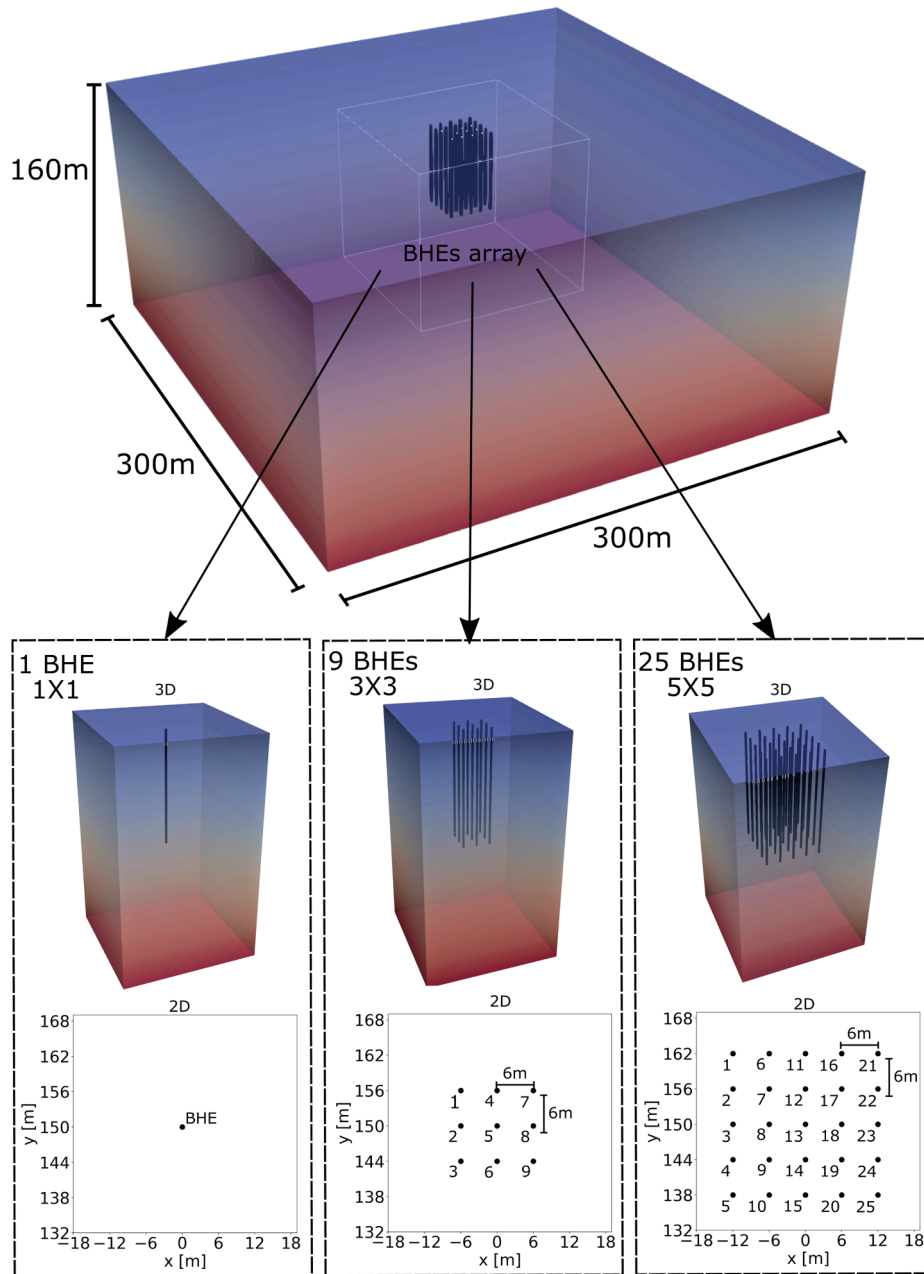


Fig. 5. Location of the BHEs in the subsurface model (3D views and horizontal cross-sections).

Similar trends can be observed in the evolution of BHE inflow and outflow temperature in the end of January, when the system is imposed with the peak heating load of each year, as illustrated in Fig. 10. The inflow and outflow refrigerant temperature in the single BHE case decreases slightly during the beginning 2 years and then stabilises at 3.8 and 4.3 °C respectively. Compared to that, the temperature drop in the multi-BHE array cases is considerably larger. In the 3 × 3 case, the inflow temperature is about 1.5 °C and the outflow remains at about 2.1 °C after 10 years. In the 5 × 5 case which more BHEs are coupled, a much lower inflow and outflow temperature were observed, with a minimum temperature of -0.2 °C and 0.4 °C respectively. Similar to the change of soil temperature as presented above, although the specific heat extraction rate remains the same in all cases (12.5 W/m). The inflow refrigerant was forced to decrease to a lower temperature when a larger BHE array is present. This is because, the increase in the number of BHEs connected in the system is also linearly related to the total amount of thermal load imposed. The insufficient recharge of heat

in the shallow subsurface can only be balanced with a decreasing temperature in the circulating refrigerant. As demonstrated in Fig. 9 and Fig. 10, the circulating temperature in the 3 × 3 and 5 × 5 cases are also different over time. It suggests that the ability of each BHE to extract heat from the subsurface is deteriorating once the extracted thermal energy is beyond the recharging capacity of the subsurface.

It needs to be noticed that although the soil, BHE inflow and outflow temperature is dropping over time, the inflow and outflow temperature on different BHEs in the same array are not deviating much away from each other at the same moment. For example, in 3 × 3, the maximal outflow temperature difference was observed between BHE #1 and BHE #5 with 0.06 °C after 10 years. Compared with it, the difference increases slightly up to value of 0.14 °C between BHE #1 and BHE #13 in in 5 × 5. The reason for the different evolution of the outflow temperature on each BHE within a multi-BHE array is due to the different soil distribution near each BHE in the array over the time, which is showed in the last Fig. 9. Since the inflow temperature of all BHEs in

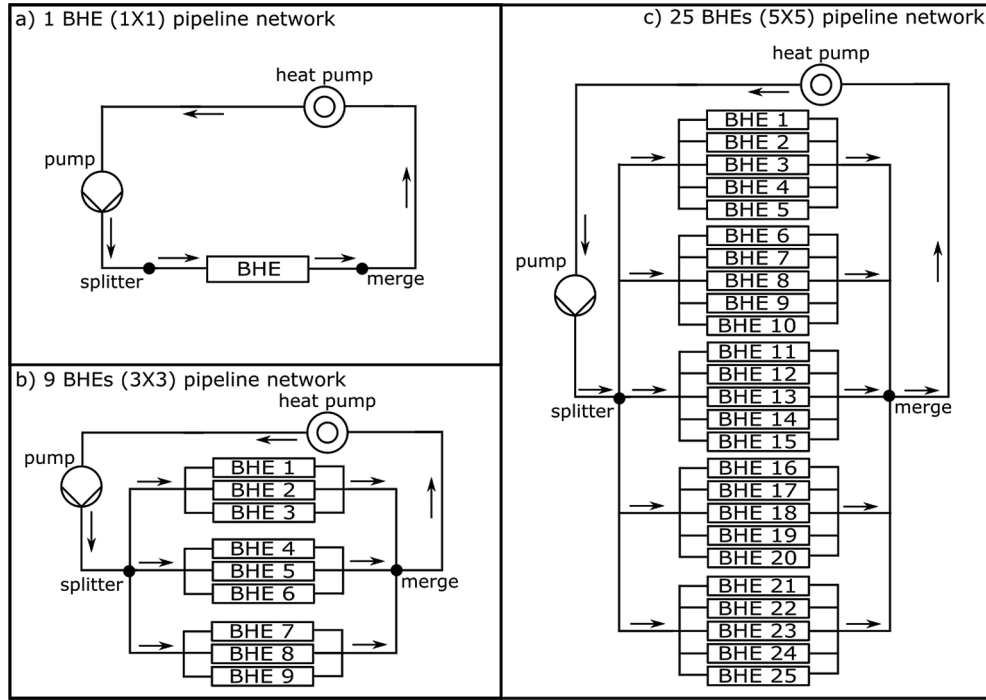


Fig. 6. Arrangement of BHE pipeline network in TESPy.

Table 1

Parameters of the Soil, the BHE, the circulating fluid and the pipeline network adopted in the model.

Parameter	Symbol	Value	Unit
Soil thermal conductivity	λ_s	2.4	$\text{W m}^{-1} \text{K}^{-1}$
soil density	ρ_s	1120	kg m^{-3}
Soil specific heat capacity	$(\rho c)_s$	2.0×10^6	$\text{J m}^{-3} \text{K}^{-1}$
Initial subsurface temperature	T_0	11.167	$^{\circ}\text{C}$
Length of the BHE	L	50	m
Diameter of the BHE	D	0.13	m
Diameter of the pipe in BHE	d_0	0.013665	m
Wall thickness of pipe	b_0	0.003035	m
Wall thermal conductivity	λ_0	0.39	$\text{W m}^{-1} \text{K}^{-1}$
Grout thermal conductivity	λ_g	0.806	$\text{W m}^{-1} \text{K}^{-1}$
Grout heat capacity	$(\rho c)_g$	3.8×10^6	$\text{J m}^{-3} \text{K}^{-1}$
Circulating fluid density	ρ_f	992.92	kg m^{-3}
Circulating fluid thermal conductivity	λ_f	0.62863	$\text{W m}^{-1} \text{K}^{-1}$
Circulating fluid heat capacity	$(\rho c)_f$	4.16×10^6	$\text{J m}^{-3} \text{K}^{-1}$
Circulating fluid viscosity	η	0.00067418	$\text{kg m}^{-1} \text{s}^{-1}$
Circulating fluid flow rate	u	0.00027	$\text{m}^3 \text{s}^{-1}$
Length of the pipe for BHE in network	l	100	m
Diameter of the pipe for BHE in network	d	0.013665	m
Roughness coefficient of the pipe	k_s	0.0001	m

each array arrangement keep identical due to the system parallel connected network, it indicates the ability for heat extraction on each BHE is different from the other during the system operation.

5.2. Shifting of thermal extraction rates

With the available data in Fig. 10, the actual average thermal extraction rate on each individual BHE \dot{Q} can be calculated with Eq. (9) and analysed for the 10-year-long simulated period. For each individual BHE, their actual individual heat extraction rate is compared to the system average value \dot{Q}_{mean} (cf. Fig. 7). Followed by this logic, the simulated data can be further treated. First, the amount of shifted

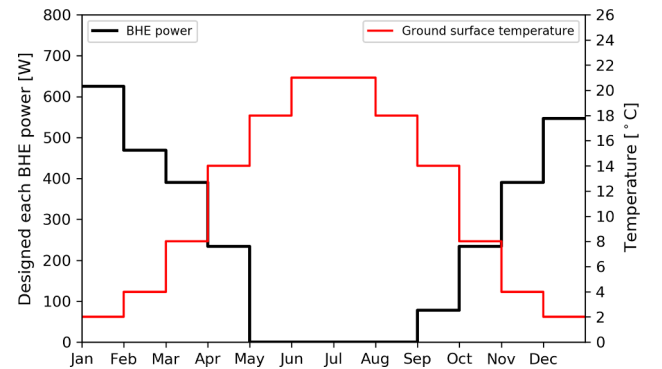


Fig. 7. Annual ground surface temperature curve and seasonal average heat extraction rate on each BHE.

thermal load $\Delta\dot{Q}$ was calculated for each BHE by subtracting the heat extraction rate \dot{Q} with the system average value \dot{Q}_{mean} . Then the shifted load is further normalised by the average value to show its proportion. The proportion of the shifted thermal load a is defined with the following Equation,

$$a = \Delta\dot{Q}/\dot{Q}_{mean}. \quad (10)$$

Firstly, the evolution of amount of shifted heat extraction rate $\Delta\dot{Q}$ was investigated. The Evolution of this “shifted load” is illustrated in Fig. 11. A few interesting phenomenon can be observed:

- In both array setups, the performance of the heat extraction rate on each BHE can be classified into two categories: BHEs located at the outer part of the array are experiencing a heat extraction rate increase (e.g. BHE #1 in 3×3 ; BHE #1, BHE #6, BHE #11 in 5×5), while the BHEs located at the inner part of array are experiencing a value reduction (BHE #4, BHE #5 in 3×3 ; BHE #7, BHE #12, BHE #13 in 5×5). For BHEs located at the edge and in the centre of the array, the maximal increase and reduction evolution are observed respectively. It indicates that the thermal load was systematically shifted away from the centre towards the outer part of the array

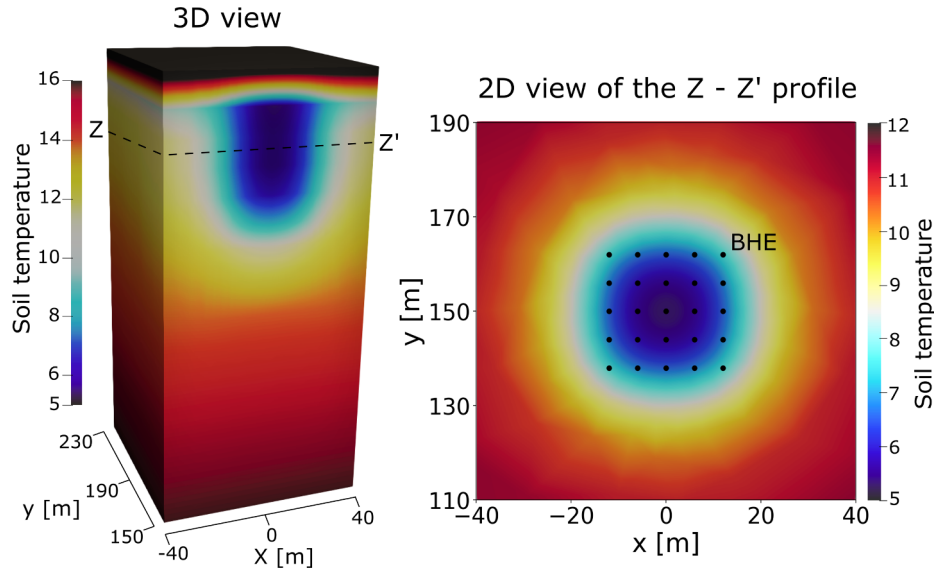


Fig. 8. Distribution of soil temperature in 5×5 setup after 10 years, 3D view of one the left and horizontal profile at the depth of 27 m on the right.

through the operation of the pipe network.

- In the 3×3 array, the maximum change of heat extraction rate of -48 W was observed in the BHE #5 located at the centre. Compared to it, the maximal value with 89 W was observed on BHE #1 at the edge in the 5×5 setup, which means the shifting effect is enhanced in the larger array setup.
- In the 3×3 setup, the shifted heat extraction rate changes intensively for all BHEs in the first 2 years, before a quasi-steady-state is reached. Whilst in the 5×5 case, reaching the quasi-steady-state will take more than 5 years. It indicates the system with a larger array setup needs more time to reach the balance.
- In the 3×3 case, the shifted heat extraction rate of all BHEs becomes smaller after the recovery period every year. For instance the shifted rate on BHE #5 located at the centre changes its value from -47 W to -30 W after the recovery period in the 10th year. In the 5×5 case, the change of shifted heat extraction due to the recovery becomes smaller compared to that in the 3×3 setup. The maximum shifted heat extraction rate due to recovery was observed on BHE #1

at the edge with only 6 W. The shifted rate on BHE #6 and BHE #13 becomes even larger after the recovery. This indicates the recovery of subsurface heat will mitigate the heat extraction rate shifting. Yet, its effect will gradually weaken with an increasing number of installed BHEs.

On the other hand, the shifting situation could be presented with respect to its proportion in comparison to the mean value (see Fig. 12). Over 10 years' period, the change of this proportion a follows the similar trend as the ΔQ in Fig. 11. Apart from this similarity, two phenomena were noticed. Compared to the trend of ΔQ , the proportion a varies much more intensively within every year. Besides, in the 5×5 case, the maximum proportion value exceeded 100% after 9 years. This means the BHE located at the centre was experiencing a negative thermal load during the heating season. It suggests that partially closing those BHEs located in the array centre for a certain period will be helpful to increase the efficiency of the entire system. Also, as shown in Fig. 12, the range of shifted heat extraction rates are elevated from 3 to

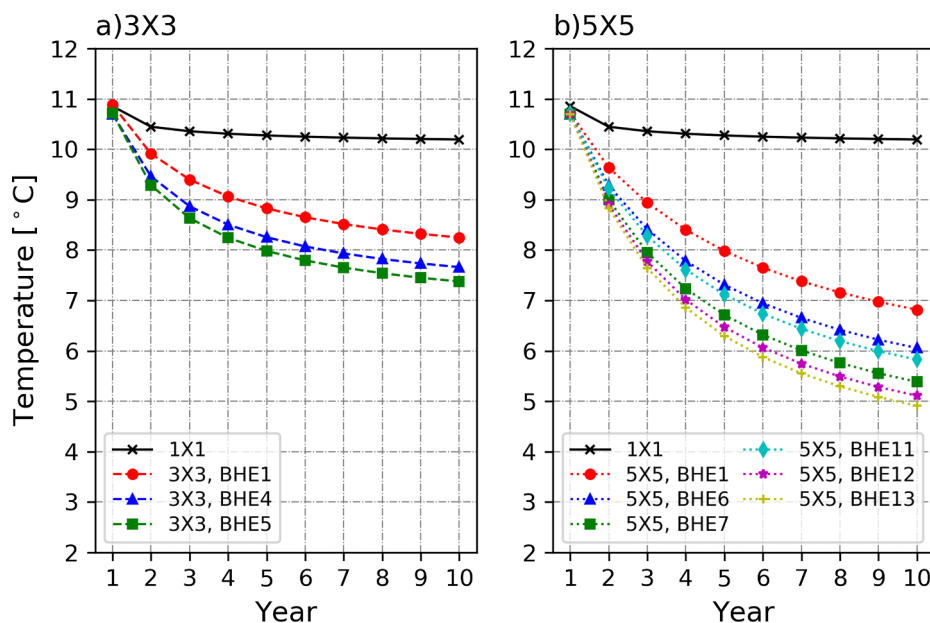


Fig. 9. Evolution of soil temperature over 10 years at 1 m distance from the selected representative BHEs at a depth of 27 m in the end of January.

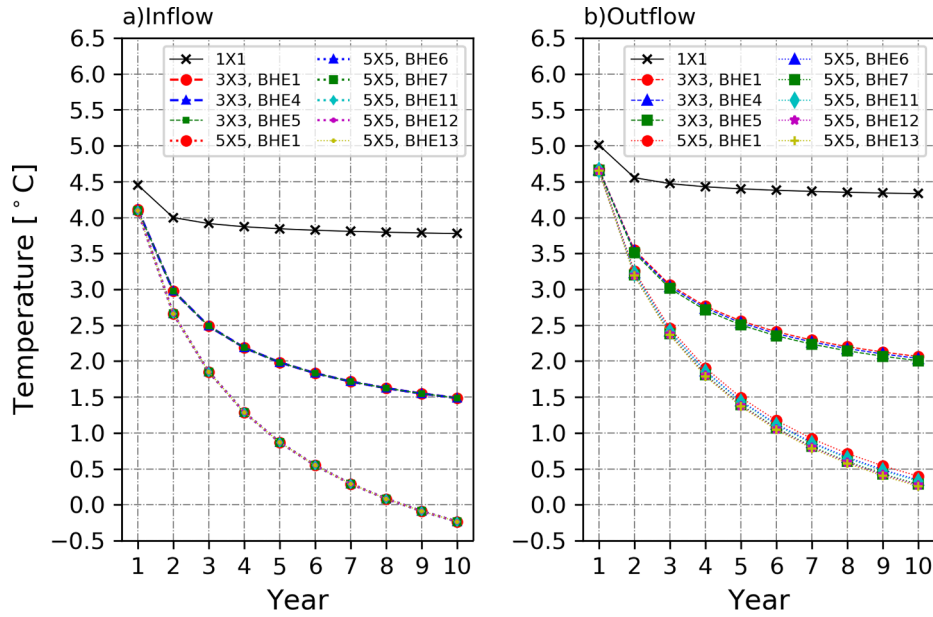


Fig. 10. Evolution of BHE inflow (a) and outflow (b) temperature in the end of January (peak heating load) over 10 years with different array arrangements.

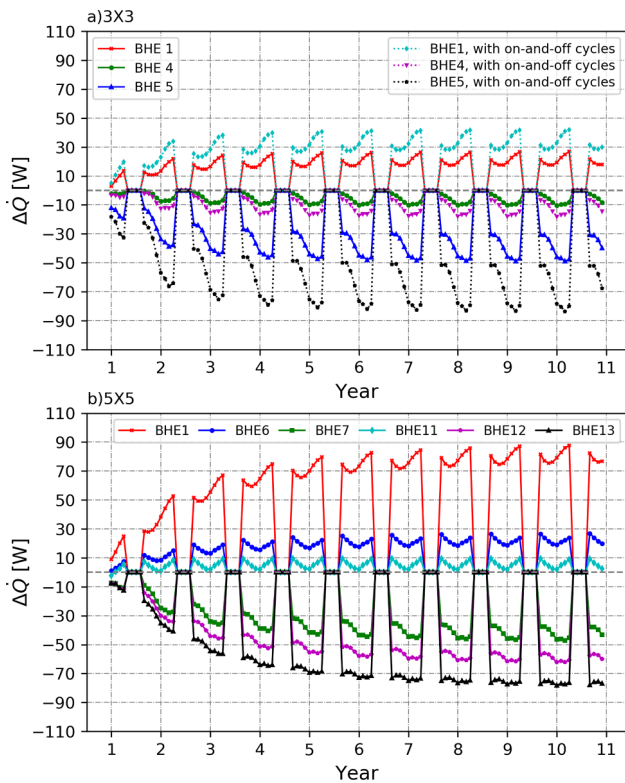


Fig. 11. (a) Evolution of the shifted heat extraction rate of BHE in 3×3 over 10 years; (b) Evolution of the shifted heat extraction rate of BHE in 5×5 over 10 years.

40% in the 3×3 case up to 12 to 105% in the 5×5 case. It means a more intensive shifting can be expected with increasing number of installed BHEs. This behaviour was also reported by Gultekin et al. [44] in their analytical formulation. In addition, according to Gultekin's research, the adjacent distance among the BHEs is also an important factor to affect the thermal interaction in the BHE array. In this work a distance of 6 m was assumed, which is the minimum value allowed by the German guideline. How the distance can be optimised to mitigate the shifting behaviour would be one of the critical issues for future

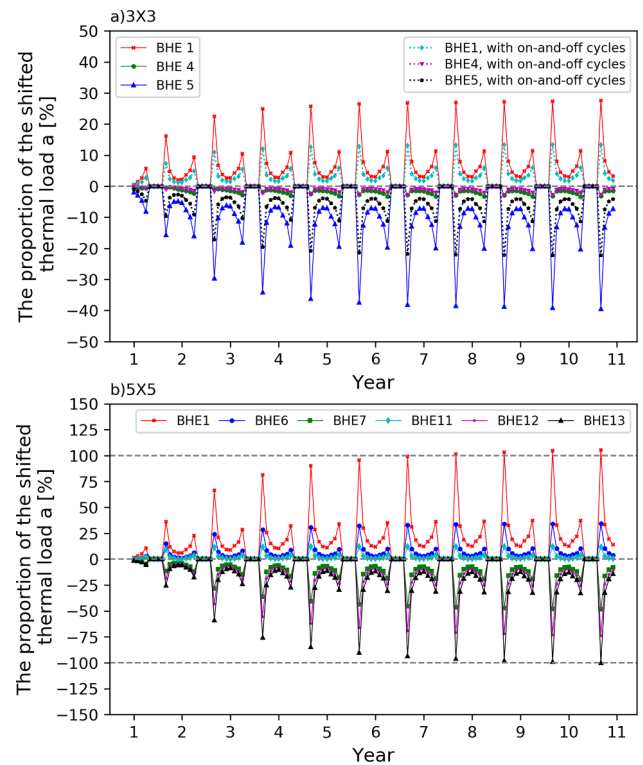


Fig. 12. (a) Evolution of the shifted heat extraction rate proportion of BHE in 3×3 over 10 years; (b) evolution of the shifted heat extraction rate proportion of BHE in 5×5 over 10 years.

investigation.

5.3. Seasonal and long-term behaviour

In Fig. 13, the shifted heat extraction rate of BHE was depicted over the 10th year, when the quasi-steady-state has been achieved. In both arrangements, with absolute amount of shifted thermal load ΔQ change very slightly over the heating month (17 W maximum in the 3×3 case, and 11 W maximum in the 5×5 case). However, the picture is considerable different when the percentage of shift was calculated. The

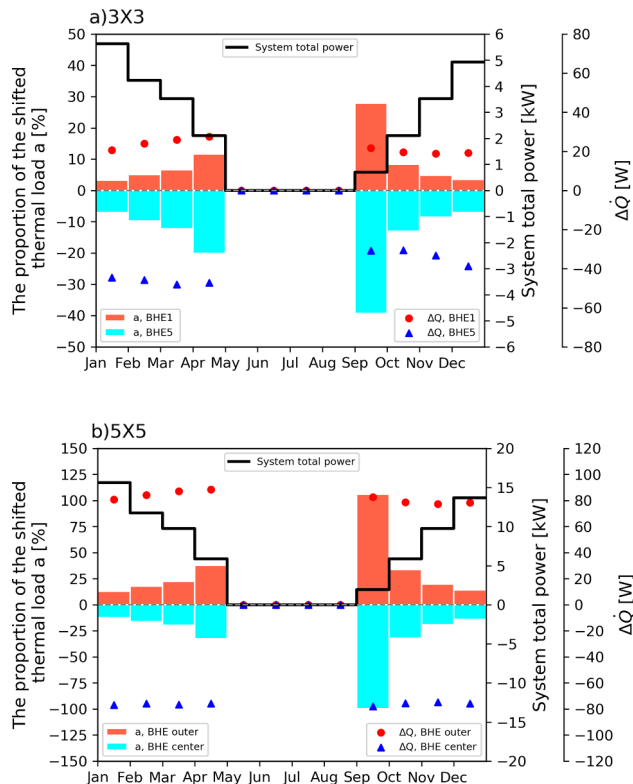


Fig. 13. Seasonal behaviour of shifted heat extraction rate on individual BHEs over a single year with (a) 3×3 and (b) 5×5 arrangements in the 10th year.

maximum percentage of shift a was observed to be 40% and 105% respectively in September, when the lowest heating demand was imposed. The minimum percentage of shift a is 3% and 12% in January, when the highest heating load was present. The result indicates the shifting behaviour has a minor impact on the system in the peak heating month, but it overall influence can be significant when the total thermal load is low. As shown in the Section 5.2, the evolution of the shifting heat extraction rate is strongly time dependent. It is further analysed here with respect to its seasonal and long-term behaviour.

5.3.1. Long term behaviour

As shown in Fig. 11, the heat extraction rates on BHEs located inside the array were depressed over time in both arrangements, while the rates on those at the outer part were elevated gradually. The maximal reduced rate was observed on the BHE at the center, with -50 W in the 3×3 and -80 W in the 5×5 arrangement. The maximum elevated rate was on the BHEs located at the edge, with $+27$ (3×3) and $+89$ W (5×5). It becomes evident that over the long-term operation of the BHEs array, the heat extraction rate at the centre of the BHEs array is shifting gradually towards the periphery. Such shifting behaviour has also been confirmed in the study conducted by You et al. [28] through an analytical approach. Over the 10 years' long operation, the time necessary to achieve the quasi-steady-state depends heavily on the size of the BHE array. It requires 3 years to achieve a stable amount of shifted thermal load in the 3×3 case, while this time increases to 6 years in the 5×5 case. Typically, the system with a larger thermal demand requires a longer time to reach equilibrium with the thermal recharge in the subsurface.

5.3.2. Seasonal behaviour

Besides the long-term behaviour discussed above, the shifting also demonstrates different patterns within a single year over different seasons. In Fig. 13, the amount of shifted thermal extraction rates were plotted over the 10th year, where the quasi-steady-state of the system

has already been reached. In both the 3×3 and 5×5 arrangements, the absolute amount of shifted heat extraction rate on each BHE remains quiet stable, although the total system thermal load changes intensively in each month. As a result, when the lowest total thermal load was imposed in September, the highest percentage of shifting was observed on BHEs located at the centre of the array. This phenomenon will enhance itself when the system size grows larger. For example in the 5×5 arrangements, a more than 100% reduction of the heat extraction rate was found on BHE #13 after 9 years of operation. At the same time, the heat extraction rate have been doubled on BHE #1, which is located at the edge. This suggests that BHE #13 is recharging the subsurface with the heat extracted from outer BHEs in this particular month, and the system load is solely supplied by those BHEs at the periphery of the field. It also suggests that the BHEs located at the outer part are more important to maintain the system working status during operation. It should be noticed that such seasonal behaviour is not unique and was also reported by other researchers in the literature. For example, Bayer et al. [15] observed similar pattern and developed an optimisation strategy based on it. They suggested that a given number of critical BHEs located at the centre should be disconnected from the array to improve system efficiency. With the newly extended numerical model, a more accurate prediction can be made on the inflow and outflow temperature on each BHE, with the recharge and thermal interference effect explicitly considered. Hence the design of optimisation strategy may also benefit from the numerical model from this work.

5.4. Heat extraction rate shifting behavior with daily switch on and off cycles

In reality, a GSHP system may not work continuously all the time. Being aware of this fact, a scenario with daily on-and-off thermal load was simulated with the 3×3 BHEs configuration for a period of 10 years. The heat pump was assumed to be operating for 8 h everyday, accompanied with a 16-h long recovery period. To maintain a fair comparison, the same amount of heat has to be extracted from the subsurface. The thermal load on the BHE array was then tripled in comparison to other scenarios (see the curve in the Fig. 7). With this configuration, a 37.54 W/m specific heat extraction rate on each BHE was reached in the peak month (January) every year. In the modelling result, The soil temperatures at 1 m distance from the centre BHE #5 at a depth of 27 m dropped by 5.2 °C after 10 years, which indicating the existence of the underground soil thermal imbalance. The dotted lines in Fig. 11 and Fig. 12 depict the evolution of shifted heat extraction rate in the on-and-off scenario. The trend of shifting largely remains the same. It suggests that the daily recovery cycle has only limited impact. Besides, due to the tripled peak thermal load, the minimum inflow and outflow temperature shows a much deeper draw-down in comparison to other scenarios. These values were found to be -8.5 °C and -6.8 °C respectively. This implies that the short-term (within the heating season) temperature evolution is more determined by the peak thermal load, while the long-term (over multiple years) development is largely controlled by the subsurface thermal recharge.

6. Discussion

6.1. Implication for super-position based analytical solution

As has been discussed in the introduction of this work, most super-positioned infinite line source models assume a constant heat extraction rate on each BHE and also do not consider the thermal interference as shown in this work. The soil temperature distribution computed by such approaches may lead to considerable deviation in comparison to the reality. It is thus meaningful to quantify such deviation by comparing results from the traditional analytical approach and the newly extended numerical model. For this purpose three configurations were designed based on the 25 BHEs scenario as in Section 4. The model was

calculated for 10 years with 3 different configurations. In the first case, the super-position method as described in Section 3 with Eq. (7) is applied to predict the soil temperature distribution. Then, OpenGeoSys numerical model was simulated both without (case 2) and with the pipe network (case 3). In case 2, each BHE was imposed with the same annual thermal extraction rate curve (black line illustrated in Fig. 7) over the heating season. In case 3, a total thermal load was calculated by summing up the heat extraction rate curves of each BHE and it was imposed on the pipe network. In this case, re-distribute of the total load is allowed among different BHE. The soil temperature distribution on the observation profile (A-A') was depicted at a depth of 27 m and compared in Fig. 14.

As shown in Fig. 14a, a clear deviation can be observed with respect to the soil temperature distribution predicted by the analytical and two numerical approaches. A maximum 2.5°C difference (cf. Fig. 14b) was obtained between the analytical against numerical result. The result from analytical approach consistently predicts lower soil temperatures. It confirms our hypothesis in the introduction that the seasonal ground surface temperature and bottom geothermal flux will contribute to the subsurface recharge (see also the results by Hein et al. [30]). It needs to be noticed that the peak seasonal average specific heat extraction rate on each BHE is assumed to be 12.5 W/m in this study, which is considerably lower than the usually applied load in field application (at around 20 to 35 W/m). It suggests that a larger deviation in soil temperature will be produced by the analytical approach. Compare to this effect, the soil temperature deviation caused by the shifted thermal load among BHEs is around $\pm 0.3^\circ\text{C}$ as demonstrated by the blue curve in Fig. 14b. This suggests the thermal interference and shifted thermal load does lead to a different soil temperature distribution. Yet, such deviation is rather negligible if compared to the one caused by the re-charging effect.

The above comparison leads to several implications for the applicability of the analytical and numerical approaches. For long-term and high thermal load (e.g. thermal storage) applications, ignorance of the subsurface recharge process will over-estimate the draw-down in soil temperature. In such kind of applications, analytical results based on infinite line source model and super-position principle may lead to deviation in the soil temperature distribution. Hence, the application of such analytical approach should be limited. However, if the specific heat extraction rate is relatively low, as the value of 12.5 W/m case demonstrated in this study, the soil temperature deviation is very limited ($<0.5^\circ\text{C}$) with or without considering the shifting of thermal load through pipelines.

6.2. Total thermal load on the BHE array

In recent years, there are increasing number of large BHE array systems installed in densely populated cities, with the intention to fully explore the potential of shallow geothermal resources. Bayer et al. [7] suggested in their work that the thermal interference between adjacent installations could be critical and affect the potential exploitation capacity of the system. As shown into our results in Sections 5.1, Bayer's concern is validated, as the soil temperature and the circulating fluid temperature decrease intensively with the increase of the total thermal demand. In extreme cases, this may lead to freezing in the vicinity of the BHE or the failure of the heat pump [22,45]. To avoid that, the German guideline VDI4640 [35] has imposed a lower limit of -5°C on the inflow temperature of each BHE. In this work, each BHE is set to have an identical length (50 m), and all the modelling scenarios were configured in a way that the average specific heat extraction rate on each BHE was configured with the same annual load curve (cf. Fig. 7). The total system load was increased in proportion to the number of BHEs connected in the array. In the simulated results, an important phenomenon that caught our attention is the decreasing inflow temperature along with the increasing size of BHE array, which can be viewed in the data listed in Table 2 (an additional case with 7×7 BHEs

were also added). Following the data, a minimal inflow temperature was at 4.4°C with a 12.5 W/m average specific heat extraction rate. When the size of array grows, the minimum value of inflow temperature in other scenarios decreases with the increasing number of BHEs. As the inflow temperature is constrained to be no less than -5°C according to the guideline, it suggests that the array size cannot be expanded arbitrarily.

Meanwhile, along with the increasing size of BHE array, its influencing size is also extended. For instance, in the last Section 6.1 a temperature influence range in the soil part extends to about 40 m (cf. Fig. 14) after the long-term operation. This suggests that heat from the neighbouring subsurface has been exploited already. With this result in mind, the size of the array and how much shallow geothermal energy can be exploited may well depends on how much temperature drop can be tolerated at the boundary of the next neighbour. This conflict can be more frequent in densely populated cities. Considering both constrains from the minimal inflow temperature and the limit on temperature change at the property boundary, the exploitable capacity of the shallow geothermal energy within a limited space should be estimated by the amount of thermal recharge, instead of by the specific heat extraction rate on each BHE. Based on our results, the specific heat extraction rate may have to be scaled down along with the increasing array size, in order to sustain the long-term operation. This is a very interesting topic that needs to be further investigated in the future.

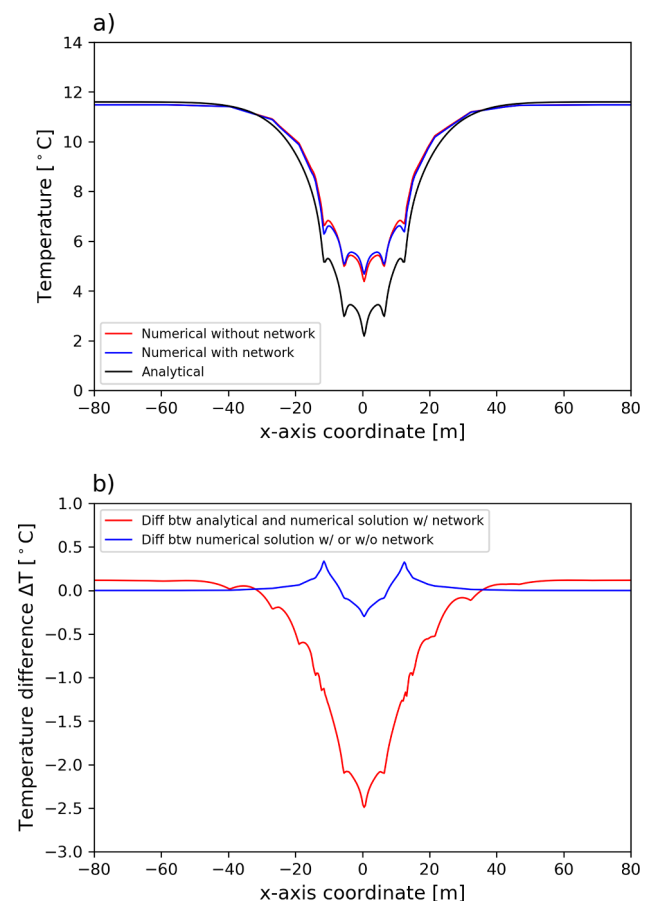


Fig. 14. (a) Soil temperature distribution over the profile (A-A') at a depth of 27 m after 10 years of BHE operation, predicted by analytical and two numerical approaches with or without the pipe network (b) Red line: Analytical solution minus the numerical solution with network; Blue line: Numerical solution without network minus the one with network. (For interpretation of the references to color in this figure legend, the reader is referred to the web version of this article.)

Table 2
Minimal inflow temperature of BHE in the modelled scenarios after 10 years operation.

BHE array	Number of BHEs in the array	Total BHE Length in [m]	System thermal load in [W]	Peak average specific heat extraction rate on each BHE in [W/m]	Minimal inflow temperature in [°C]
1 × 1	1	50	625	12.5	3.8
3 × 3	9	450	5625	12.5	1.5
	9	450	5625	37.54 (8-h on and 16-h off)	−8.5
5 × 5	25	1250	15625	12.5	−0.2
7 × 7	49	2450	30625	12.5	−1.5

6.3. Pipeline network design

Compared to the analytical approach from You et al. [28], the numerical model presented here has some advantages. Firstly, the seasonal ground surface temperature variation and the vertical geothermal gradient can be accurately quantified. Secondly, the numerical model is able to consider pipeline network with arbitrary connections. Within the pipeline network, the loss of hydraulic head due to friction is automatically computed based on the mass and energy conservation (see Section 2.2). Therefore the newly extended model could easily handle a complicated time-dependent hydraulic states within the entire closed-loop system according to different system operation strategy [46,47]. In addition, a temperature dependent heat pump efficiency curve and pressure-flow rate relationship of the hydraulic pump can also be added into TESPy as input parameters. With such information at hand, electricity consumption due to pump operation can be estimated as soon as the design of the system is available.

As showed in Section 3.2, the simulated heat extraction rate on individual BHE will deviate from the designed average value due to the cold thermal plume generated over the long-term operation. This process leads to the different outflow temperature based on the location of the BHE. However, because the BHEs are connected in a parallel way, circulating fluid with higher or lower temperatures will merge together and flows through the heat pump. Then in the next circulation, same inflow temperature will be provided to each BHE. With the parallel setup, the pipe network itself has an intrinsic feature of re-balancing the thermal load among different BHEs. With a higher load from the building, the BHE array responded with a uniform lower inflow and outflow temperature to draw more heat from the subsurface. In Fig. 10, this is demonstrated by the data points moving from the upper-left towards the lower-right corner. Yet, the distribution of load is not homogeneous among the BHEs. With those located at the edge in a better position of extracting heat from the surrounding soil, they also supply a large proportion of the heat.

It should be noticed that the presented pipeline network in this study has an intrinsic feature of re-balancing the thermal load among the BHEs, as it has a fully parallel structure. If the topology of the BHE array is different, the system may show an entirely different behaviour. For example, the connecting pipe may be routed to extract the shallow geothermal energy from BHEs at the periphery first, and using the BHEs in the centre only when the peak load is needed [46]. This opens new opportunities in future research to optimise the connectivity of BHEs in its designing phase. This is already under our investigation and will be presented in a separate manuscript.

7. Conclusion and outlook

In this work, a comprehensive numerical model was developed, with the shallow subsurface, the multiple BHEs and the pipe network explicitly quantified in a single modelling framework. Compared to other existing models, the thermal and hydraulic processes in the pipeline network was explicitly quantified to reproduce the shifting heat extraction rate caused by the thermal interference among multiple BHEs. It is found that over the long-term operation of a large BHE array,

the heat extraction rate in the centre was gradually shifted towards those located at the outer boundary. This phenomenon becomes significant with the increasing number of BHEs installed in the array. Over different seasons in a year, the most intensive shifting phenomenon was observed in the lowest thermal demand month. In comparison, the percentage of shifted load reaches its maximum in the month with the lowest thermal load.

As a result, the application of super-positioned infinite line source model with a constant heat flux is considered to be inaccurate for long-term and high thermal load applications. The numerical experiments in this work showed that such analytical approach will lead to an over-estimation in the reduction of soil temperature, as the subsurface re-charge process was ignored. In this study a relatively low specific heat extraction rate (maximum 12.5 W/m) was observed on each BHE. However, a maximum 2.5 °C soil temperature difference after 10 years was already been identified by comparing the analytical and our numerical result. It is also found that the soil temperature deviation between the models with or without considering the shifting of thermal load is very limited (<0.5 °C), when the specific heat extraction rate is relatively low as demonstrated in this study.

Currently, for simulating of GSHP system especially installed with a large number of BHEs in the array, the method described in this study still exists its shortcomings. A main shortcoming point to the slower computational time, since there are two computing processes (in OGS and in TESPy) within one timestep. In order to alleviate the long simulation time, our group are working on the parallelization of OGS-TESPy code, which may greatly accelerate the speed of simulation.

Acknowledgements

This study is supported by the National Natural Science Foundation of China (grant 41628203). Funding for the project was also provided by the German Federal Ministry of Economic Affairs and Energy (BMWi) under Grant No. 03ET6122B (“ANGUS II: Impacts of the use of the geological subsurface for thermal, electrical or material energy storage in the context of transition to renewable energy sources—Integration of subsurface storage technologies into the energy system transformation using the example of Schleswig-Holstein as a model area”) and is gratefully acknowledged. We would like to express our thanks also to our ANGUS II colleagues for the fruitful scientific collaboration and the project lead and management.

Appendix A. Supplementary material

Supplementary data associated with this article can be found, in the online version, at <https://doi.org/10.1016/j.applthermaleng.2019.114750>.

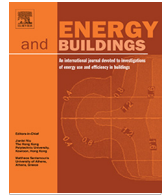
References

- [1] OECD/IEA, Heating without global warming, Tech. Rep., International Energy Agency, France, 2014.
- [2] IRENA, Geothermal Power: Technology Brief, Tech. Rep. September, International Renewable Energy Agency, Abu Dhabi, 2017, ISBN: 9789292600365.
- [3] J.W. Lund, T.L. Boyd, Geothermics Direct utilization of geothermal energy 2015

- worldwide review, *Geothermics* 60 (2016) 66–93, <https://doi.org/10.1016/j.geothermics.2015.11.004> ISSN 0375-6505.
- [4] T. Kurevija, D. Vulin, V. Krapec, Effect of borehole array geometry and thermal interferences on geothermal heat pump system, *Energy Convers. Manage.* 60 (2012) 134–142, <https://doi.org/10.1016/j.enconman.2012.02.012> ISSN 01968904.
- [5] K. Zhu, P. Blum, G. Ferguson, K.-D. Balke, P. Bayer, The geothermal potential of urban heat islands, *Environ. Res. Lett.* 5 (2010) 6, <https://doi.org/10.1088/1748-9326/5/4/044002>.
- [6] J.A. Rivera, P. Blum, P. Bayer, Increased ground temperatures in urban areas: estimation of the technical geothermal potential, *Renew. Energy* 103 (C) (2016) 388–400, <https://doi.org/10.1016/j.renene.2016.11.005> ISSN 0960-1481.
- [7] P. Bayer, G. Attard, P. Blum, K. Menberg, The geothermal potential of cities, *Renew. Sustain. Energy Rev.* 106 (February) (2019) 17–30, <https://doi.org/10.1016/j.rser.2019.02.019> ISSN 1364-0321.
- [8] P. Eskilson, *Thermal Analysis of Heat Extraction Boreholes* (Ph.D. thesis), University of Lund, Sweden, 1987.
- [9] M.A. Bernier, P. Pinel, R. Labib, R. Paillot, A multiple load aggregation algorithm for annual hourly simulations of GCHP systems, *HVAC&R Res.* 10 (4) (2004) 471–487, <https://doi.org/10.1080/10789669.2004.10391115>.
- [10] L. Lamarche, B. Beauchamp, A new contribution to the finite line-source model for geothermal boreholes, *Energy Build.* 39 (2007) 188–198, <https://doi.org/10.1016/j.enbuild.2006.06.003>.
- [11] S. Koochi-Fayegh, M.A. Rosen, Examination of thermal interaction of multiple vertical ground heat exchangers, *Appl. Energy* 97 (2012) 962–969, <https://doi.org/10.1016/j.apenergy.2012.02.018> ISSN 0306-2619.
- [12] S. Koochi-Fayegh, M.A. Rosen, An analytical approach to evaluating the effect of thermal interaction of geothermal heat exchangers on ground heat pump efficiency, *Energy Convers. Manage.* 78 (2014) 184–192, <https://doi.org/10.1016/j.enconman.2013.09.064> ISSN 01968904.
- [13] H. Qian, Y. Wang, Energy for Sustainable Development Modeling the interactions between the performance of ground source heat pumps and soil temperature variations, *Energy Sustain. Develop.* 23 (2014) 115–121, <https://doi.org/10.1016/j.esd.2014.08.004> ISSN 0973-0826.
- [14] J.A. Rivera, P. Blum, P. Bayer, Influence of spatially variable ground heat flux on closed-loop geothermal systems: line source model with nonhomogeneous Cauchy-type top boundary conditions, *Appl. Energy* 180 (2016) 572–585, <https://doi.org/10.1016/j.apenergy.2016.06.074> ISSN 0306-2619.
- [15] P. Bayer, M. de Paly, M. Beck, Strategic optimization of borehole heat exchanger field for seasonal geothermal heating and cooling, *Appl. Energy* 136 (2014) 445–453, <https://doi.org/10.1016/j.apenergy.2014.09.029> ISSN 03062619.
- [16] C. Zhang, Y. Wang, Y. Liu, X. Kong, Q. Wang, Computational methods for ground thermal response of multiple borehole heat exchangers: a review, *Renew. Energy* 127 (C) (2018) 461–473, <https://doi.org/10.1016/j.renene.2018.04.083> ISSN 0960-1481..
- [17] G. Hellström, *Ground Heat Storage: Thermal Analyses of Duct Storage Systems* (Ph.D. thesis), Lunds University, Sweden, 1991.
- [18] B. Morrone, G. Coppola, V. Raucchi, Energy and economic savings using geothermal heat pumps in different climates, *Energy Convers. Manage.* 88 (2014) 189–198, <https://doi.org/10.1016/j.enconman.2014.08.007> ISSN 0196-8904.
- [19] D. Pahud, A. Fromentin, PILESIM: a simulation tool for pile and borehole heat exchanger systems, *Bulletin d'Hydrologie* 17 (1999), <https://www.geothermal-energy.org/pdf/IGAstandard/EGC/1999/Pahud.pdf>.
- [20] C.K. Lee, H.N. Lam, A simplified model of energy pile for ground-source heat pump systems, *Energy* 55 (2013) 838–845, <https://doi.org/10.1016/j.energy.2013.03.077> ISSN 0360-5442.
- [21] P. Hein, K. Zhu, A. Bucher, O. Kolditz, Z. Pang, H. Shao, Quantification of exploitable shallow geothermal energy by using Borehole Heat Exchanger coupled Ground Source Heat Pump systems, *Energy Convers. Manage.* 127 (2016) 80–89, <https://doi.org/10.1016/j.enconman.2016.08.097> ISSN 01968904.
- [22] M. Saaly, P. Maghoul, M. Kavgi, D. Polyzois, Performance analysis of a proposed geothermal pile system for heating and cooling energy demand for a building in cold regions, *Sustain. Cities Soc.* 45 (August 2018) (2019) 669–682, <https://doi.org/10.1016/j.scs.2018.12.014> ISSN 2210-6707..
- [23] COMSOL, *Introduction to COMSOL Multiphysics*, 2018. <https://www.comsol.de/documentation>.
- [24] B. Hénault, P. Pasquier, M. Kummert, Financial optimization and design of hybrid ground-coupled heat pump systems, *Appl. Therm. Eng.* 93 (2016) 72–82, <https://doi.org/10.1016/j.applthermaleng.2015.09.088> ISSN 1359-4311.
- [25] S. Kavanaugh, K. Raffert, *Ground source heat pumps. Design of geothermal systems for commercial and institutional buildings*, ASHRAE, USA, 2014, ISBN: 9781936504855.
- [26] A. Gultekin, M. Aydin, A. Sisman, Effects of arrangement geometry and number of boreholes on thermal interaction coefficient of multi-borehole heat exchangers, *Appl. Energy* 237 (August 2018) (2019) 163–170, <https://doi.org/10.1016/j.apenergy.2019.01.027> ISSN 0306-2619..
- [27] H.J.L. Witte, A novel tool for assessing negative temperature interactions between neighbouring borehole heat exchanger systems, in: 14th International Conference on Energy Storage, Adana, Turkey, 2018.
- [28] T. You, X. Li, S. Cao, H. Yang, Soil thermal imbalance of ground source heat pump systems with spiral-coil energy pile groups under seepage conditions and various influential factors, *Energy Convers. Manage.* 178 (July) (2018) 123–136, <https://doi.org/10.1016/j.enconman.2018.10.027> ISSN 0196-8904.
- [29] J. Xi, Y. Li, M. Liu, R.Z. Wang, Study on the thermal effect of the ground heat exchanger of GSHP in the eastern China area, *Energy* 141 (2017) 56–65, <https://doi.org/10.1016/j.energy.2017.09.060>.
- [30] P. Hein, O. Kolditz, U.J. Görke, A. Bucher, H. Shao, A numerical study on the sustainability and efficiency of borehole heat exchanger coupled ground source heat pump systems, *Appl. Therm. Eng.* 100 (2016) 421–433, <https://doi.org/10.1016/j.applthermaleng.2016.02.039> ISSN 13594311.
- [31] C. Chen, H. Shao, D. Naumov, Y. Kong, K. Tu, O. Kolditz, Numerical investigation on the performance, sustainability, and efficiency of the deep borehole heat exchanger system for building heating, *Geotherm. Energy* 7 (1) (2019) 18, <https://doi.org/10.1186/s40517-019-0133-8> ISSN 2195-9706.
- [32] S. Miglani, K. Orehoung, J. Carmeliet, A methodology to calculate long-term shallow geothermal energy potential for an urban neighbourhood, *Energy Build.* 159 (2017) 462–473, <https://doi.org/10.1016/j.enbuild.2017.10.100> ISSN 0378-7788.
- [33] Energy Saving Trust, *Domestic Ground Source Heat Pumps: Design and installation of closed-loop systems – A guide for specifiers, their advisors and potential users*, The Energy Saving Trust Report CE82, London, 2007.
- [34] The Association of German Engineers, (Verein Deutscher Ingenieure), *Thermische Nutzung des Untergrunds Erdgekoppelte Waermepumpenanlagen; VDI 4640, Blatt, 2* Beuth Verlag GmbH, Berlin, 2001.
- [35] The Association of German Engineers, (Verein Deutscher Ingenieure), *Thermal use of the underground Ground source heat pump systems; VDI 4640, Blatt 2, Entwurf, VDI-Gesellschaft Energie Und Umwelt* (2015).
- [36] GB50366, *Technical code for ground-source heat pump system*, Ministry of Housing and Urban-Rural Development, PR China, 2009.
- [37] H.-J.G. Diersch, D. Bauer, W. Heidemann, W. Rühaak, P. Schätzl, Finite element modeling of borehole heat exchanger systems: Part 1, *Fundament. Comput. Geosci.* 37 (8) (2011) 1122–1135, <https://doi.org/10.1016/j.cageo.2010.08.003> ISSN 00983004.
- [38] F. Witte, *Thermal Engineering Systems in Python*, 2019, doi: <https://doi.org/10.5281/zenodo.2555866>, URL <https://doi.org/10.5281/zenodo.2555866>.
- [39] L. Böswirth, S. Bschorer, *Technische Strömungslehre*, Springer Fachmedien Wiesbaden, 2014, <https://doi.org/10.1007/978-3-658-05668-1>.
- [40] I.H. Bell, J. Wronski, S. Quoilin, V. Lemort, Pure and pseudo-pure fluid thermo-physical property evaluation and the open-source thermophysical property library CoolProp, *Industr. Eng. Chem. Res.* 53 (6) (2014) 2498–2508, <https://doi.org/10.1021/ie4033999>.
- [41] O. Kolditz, S. Bauer, L. Bilke, et al., OpenGeoSys: an open-source initiative for numerical simulation of thermo-hydro-mechanical/chemical (THM/C) processes in porous media, *Environ. Earth Sci.* 67 (2012) 589–599, <https://doi.org/10.1007/s12665-012-1546-x> ISSN 1866-6280.
- [42] L.A. Rossman, EPANET 2: users manual, Cincinnati US Environmental Protection Agency National Risk Management Research Laboratory 38 (September) (2000) 200, doi: <https://doi.org/10.1177/0306312708089715>. ISSN 03063127.
- [43] M. Richter, C. Huber, K. Reinhardt, H. Wachmann, A. Gerschel, Potential of heat supply for Saxon gardening companies utilizing geothermal energy as subject to site-specific geological conditions and different business organisations/ utilisation concepts (Möglichkeiten der Wärmeversorgung von sächsischen Gartenbaubetrieben mit Geothermie in Abhängigkeit von geologischen Standortfaktoren und verschiedenen Betriebsstrukturen/Nutzungskonzepten), 2015.
- [44] A. Gultekin, M. Aydin, A. Sisman, Thermal performance analysis of multiple borehole heat exchangers, *Energy Convers. Manage.* 122 (2016) 544–551, <https://doi.org/10.1016/j.enconman.2016.05.086> ISSN 01968904.
- [45] T. You, W. Wu, W. Shi, B. Wang, X. Li, An overview of the problems and solutions of soil thermal imbalance of ground-coupled heat pumps in cold regions An overview of the problems and solutions of soil thermal imbalance of ground-coupled heat pumps in cold regions, *Appl. Energy* 177 (September) (2016) 515–536, <https://doi.org/10.1016/j.apenergy.2016.05.115> ISSN 0306-2619.
- [46] H.M. Haq, E. Hiltunen, An inquiry of ground heat storage: Analysis of experimental measurements and optimization of system's performance, *Appl. Therm. Eng.* 148 (October 2018) (2019) 10–21, doi: <https://doi.org/10.1016/j.applthermaleng.2018.11.029>. ISSN 13594311.
- [47] K.W. Tordrup, S.E. Poulsen, H. Bjørn, An improved method for upscaling borehole thermal energy storage using inverse finite element modelling, *Renew. Energy* 105 (2017) 13–21, <https://doi.org/10.1016/j.renene.2016.12.011> ISSN 18790682.

B.2 Paper 2

S. Chen, W. Cai, F. Witte, X. Wang, F. Wang, O. Kolditz, H. Shao,(2020). Long-term thermal imbalance in large borehole heat exchangers array-A numerical study based on the Leicester project. Energy and Buildings, 231 (Jan 2021), 110518. DOI: 10.1016/j.enbuild.2020.110518.



Long-term thermal imbalance in large borehole heat exchangers array – A numerical study based on the Leicester project



Shuang Chen^{a,b}, Wanlong Cai^{a,c}, Francesco Witte^d, Xuerui Wang^e, Fenghao Wang^c, Olaf Kolditz^{a,b}, Haibing Shao^{a,*}

^a Helmholtz Centre for Environmental Research – UFZ, Permoserstraße 15, 04318 Leipzig, Germany

^b Faculty of Environmental Sciences, Dresden University of Technology, Germany

^c School of Human Settlements and Civil Engineering, Xi'an Jiaotong University, Xi'an, Shaanxi 710049, China

^d Flensburg University of Applied Sciences, 24943 Flensburg, Germany

^e Institute of Mechanics and Computational Mechanics, University Hannover, Germany

ARTICLE INFO

Article history:

Received 14 July 2020

Revised 2 September 2020

Accepted 26 September 2020

Available online 7 October 2020

Keywords:

Shallow geothermal energy utilisation

Building heating and cooling

Borehole Heat Exchanger (BHE) array

Ground source heat pump

OpenGeoSys (OGS)

Thermal Engineering System in Python

(TESPy)

ABSTRACT

When a Borehole Heat Exchanger (BHE) array is coupled with heat pump to provide cooling and heating to the buildings, thermal interaction between BHEs may occur in the subsurface. In the long term, imbalanced seasonal thermal load may lead to low or high temperature zones accumulating in the centre of the array. In this study, numerical models are configured according to a real BHE array project in Leicester, UK, and verified against monitoring data. Based on this reference model, a series of numerical experiments are conducted to investigate the response of circulation fluid temperature to different settings of imbalanced thermal load. It is found that over long-term operation, the sub array with a larger number of installed BHEs is shifting its thermal load towards the other branch with less BHEs installed. Within each sub array, the heat injection rate on the central BHEs is gradually shifted towards those located at the edge. A linear correlation is also found between the working fluid temperature increment and the amount of the accumulated heat injected into the subsurface.

© 2020 Elsevier B.V. All rights reserved.

1. Introduction

Geothermal heat, due to its wide availability, has been considered as a renewable and sustainable energy source for building cooling and heating [1,2]. Shallow geothermal exploitation is even favourable in urban areas, because the accelerated heat fluxes from the warm basement often lead to elevated temperatures in the subsurface [3,4]. In modern building projects, a common practice is to install dozens of Borehole Heat Exchangers (BHE) prior to the building construction and then connect them through a pipe network to form a BHE array. This array is later connected with heat pumps to extract or inject thermal energy out of or into the shallow subsurface [5,6]. A recent trend in the industry is to build large BHE arrays with hundreds or sometimes thousands of BHEs to meet the high demand from commercial buildings and residential neighbourhood [7].

Despite of minor differences, most countries follow the same design procedure for large BHE array as the guideline recom-

mended by the American Society of Heating, Refrigerating and Air-Conditioning Engineers (ASHRAE) [8]. It is based on the well known line source method originally developed by Carslaw and Jaeger [9] and later promoted by Ingersoll and Zobel [10]. First, the thermal load of the building is quantified. This load is divided into three successive pulses, i.e. the peak load, the monthly average load, and the annual average load (in kW). When the heating and cooling load is in equilibrium, the total length of all BHEs are then calculated based on the short-term peak load and the effective thermal resistance of the ground. In the second step, the total length is equally divided based on the depth of each BHE, so that the number of BHEs to be installed on site can be determined accordingly. If the heating and cooling load is not balanced, then the penalty temperature T_p and the total BHE length will be calculated in an iterative manner. Based on the ASHRAE procedure, several alternative methods have been developed in recent years, to improve the calculation of T_p in particular [11,12]. Ahmadfarid and Bernier [13] have presented a comprehensive review on the available BHE array designing procedures. In both the original ASHRAE guideline and all the extended procedures, the minimum borehole separation distance S is always defined as an empirical

* Corresponding author.

E-mail address: haibing.shao@ufz.de (H. Shao).

Nomenclature

Nomenclature

S	adjacent distance between BHEs (m)	ζ	Darcy friction factor as used in Eq. (1) (–)
T_p	penalty temperature (°C)	π	mathematical constant Pi (–)
p	hydraulic pressure of the circulating fluid (bar)	λ	thermal conductivity ($\text{W m}^{-1} \text{K}^{-1}$)
v	flow velocity in pipelines (ms^{-1})	η	dynamic viscosity of circulating fluid (Pa s)
Re	Reynolds number (–)	<i>in</i>	inlet pipe
k_s	roughness coefficient of the pipe (m)	<i>out</i>	outlet pipe
d	diameter of the pipe installed in the BHE (m)	<i>f</i>	fluid
l	length of the pipe (m)	<i>p</i>	pipe
\dot{m}	flow rate of the circulating fluid (kg s^{-1})	<i>ini</i>	initial time
T	temperature (°C)	<i>s</i>	solid or soil
c	specific heat capacity ($\text{J kg}^{-1} \text{K}^{-1}$)	<i>g</i>	grout
D	diameter of the BHE (m)	<i>i</i>	index of BHE as used in Eq. (4)
b	wall thickness of pipe installed in the BHE (m)	\int	integral operator
L	length of the BHE (m)	Δ	difference operator
Q	amount of heat (MWh)	Σ	summation operator
\dot{Q}	heat extraction rate on the BHE (watt)	BHE	borehole heat exchanger
t	time (–)	GSHP	ground source heat pump
V	volume of the BHE array (m^3)	1U	single U-shape pipe
ρ	density (kg m^{-3})	COP	coefficient of performance
		PSTL	proportion of the shifted thermal load (%)

parameter to reduce thermal interference between individual boreholes, and it is also used in the calculation of penalty temperature T_p (cf. Chapter 35.1 in [8]).

When looking into different countries, the regulation on this minimum distance S is not exactly the same. The ASHRAE guideline in United States fix the S value at 6m [8]. Switzerland requires a minimum distance of 5 m (cf. Miglani et al. [14]). In Germany, this value has been increased from 5 m to 6 m in the 2019 updated VDI guideline [15,16]. In China, a distance between 3 m to 6 m is recommended [17]. In Sweden, a much larger distance of 20 m is enforced (cf. Haehnlein et al. [18]). Due to the fact that different countries have varying climate conditions and initial soil temperatures, this minimum distance S value remains a parameter that is empirically determined. Another issue in the ASHRAE and other guidelines is that the specific heat extraction rate is assumed to distribute equally on each BHE and spread evenly along the entire borehole length. This assumption holds true under the ideal condition where no thermal interference exists among BHEs. However, during the long-term operation, thermal interaction is difficult to avoid and it often varies in space and also over time. Details about this shifted thermal load behaviour could be found in our previous work (Chen et al. [19]) through numerical simulation, or from the work of You et al. [20] through an analytical analysis. Furthermore, if the BHEs are connected in a sequential manner, it is not possible to have identical heat extraction rate on each borehole [21].

In most BHE array projects, the annual cooling and heating load is often not fully balanced. This means thermal plumes can form and accumulate in the subsurface, causing the working fluid temperature to gradually increase or decrease over time. In extreme cases, this may lead to freezing in the vicinity of the BHE or causing the failure of the heat pump [22–24]. Instead of the adjacent distance S and penalty temperature T_p , the size of a BHE array is more constrained by the outflow temperature of the circulation fluid. In cooling applications, this temperature normally should not exceed 35 °C, otherwise the heat pump will not be working efficiently. When operated in heating mode, the circulation temperature has to be kept above 0°C [13], in order to mechanically protect the heat pump and avoid ground freezing. As mentioned above, engineers who are designing the BHE array would like to have a calculation

procedure, in which the change of circulation fluid temperature can be accurately estimated. In order to do that, a scientific question has to be answered first, i.e. how will the circulation fluid temperature change in response to the imbalanced thermal load, when the thermal interaction in a BHE array can not be avoided?

One obstacle preventing the exploration of the above scientific question is the lack of monitoring data. In order to fully capture the system behaviour, both the annual amount of imbalanced heat imposed on the BHE array and the responding ground loop temperature have to be quantified. This means, sensors and flow meters have to be installed on the inlets and outlets of the building loop, the heat pumps, and also different branches of the ground loops. Continuous monitoring has to be conducted for several years, in order to catch the trend in circulation fluid temperature. Fortunately, Naicker et al. [25] has recently carried out such an intensive monitoring campaign and made the data available to the general public. Their BHE array project is located in Leicester, UK (hereafter as Leicester Project). The building thermal load, heat pump operation, and also ground loop temperatures have been monitored for over 3 years with minute-wise data readings. Detailed introduction of the project is available in Naicker's PhD thesis [26], as well as in his following publications [27,25]. Interested readers may also access the monitoring data set from the Research Data Archive at the University of Leeds [28].

In this study, we investigate the BHE array behaviour under imbalanced annual thermal load by conducting a series of numerical experiments based on the Leicester project monitoring data. In Section 2, the mathematical background of the numerical model is introduced. In Section 3, the numerical model is set up based on the Leicester project and validated against the monitored data set. Analysis on the modelling results reveals the thermal imbalance and thermal interaction among BHEs. In Section 4, a series of extended numerical experiments are designed and simulated, aiming to investigate the relationship between the circulation fluid temperature change and the amount of imbalanced thermal load. Since the form and accumulation of thermal plume is a critical issue for the long-term operation of a BHE array, the amount of stored thermal energy in the subsurface has been carefully analysed and quantified. Discussions (Section 5) are also given on the potential implications of our findings.

2. Method

As discussed in our previous work [19], most analytical approaches have difficulties in quantifying the thermal interaction in large BHE arrays. In comparison, numerical models offer more flexibility, by considering different boundary conditions, thermal recharge from the ground surface, groundwater flow and also the geothermal gradient effects [29–33]. For the large BHE array considered in this work, a pipeline network is always present, coupling the BHEs and the heat pump. The thermal behaviour on each BHE will be affected by this network over the long-term operation. Recently, we have presented the OpenGeoSys (OGS) model that takes the above-mentioned factors into account ([19]). In the Heat Transport BHE module of the OGS software, the variation of BHE outlet temperature and surrounding soil temperature field can be simulated by the dual-continuum approach. In the finite element mesh, the BHE is considered as line elements, while the surrounding soil is represented by prisms. The heat fluxes between BHE wall and the surrounding subsurface are quantified by the coupling term. Readers who are interested in this numerical scheme may refer to Al-Khoury et al. [34] and Diersch et al. [35,36] for more detailed explanation.

For the coupling of a pipeline network, the open-source simulator Thermal Engineering Systems in Python (TESPy) is introduced. Developed by Witte [37], TESPy is capable of simulating a pipe network with both the thermal and hydraulic balance equations. The nonlinear feature of the coupled equations require the Newton–Raphson iteration, in order to solve for pressure, mass flow and fluid enthalpy at each conjunction point. In OGS, the Python interface library pybind11 is embedded and used for the communication between OGS and TESPy. In this study, the OpenGeoSys version 6.2.2 and the TESPy version 0.2.0 is used accordingly. For more information on the coupling between OGS and TESPy, please refer to Chen et al. [19], and also the online documentation [38], in which detailed tutorials are available to the general public.

3. Modelling Leicester Project

3.1. Project description

In the Leicester Project [25], a large BHE array was installed. It is selected in this work as the reference to validate our numerical model. This system is configured to provide both heating and cooling to the Hugh Aston building with a total floor area of 16,467 m². The designed peak cooling capacity of this project is 360 kW through the Fan Coil Unit (FCU) and Air Handling Unit (AHU).

Table 1
Model parameters.

Parameter	Symbol	Value	Unit
Initial soil temperature	T_{ini}	11.7	°C
Soil thermal conductivity	λ_s	3.4	W.m ⁻¹ K ⁻¹
Soil heat capacity	$(\rho c)_s$	2576	kJm ³ K ⁻¹
Length of the BHE	L	100	m
Diameter of the BHE	D	0.125	m
Pipe inner diameter	d_p	0.026	m
Wall thickness of pipe	b_p	0.003	m
Wall thermal conductivity of pipe	λ_p	0.4	Wm ⁻¹ K ⁻¹
Grout thermal conductivity	λ_g	0.656	Wm ⁻¹ K ⁻¹
Grout heat capacity	$(\rho c)_g$	2700	kJm ³ K ⁻¹
Circulating fluid density	ρ_f	1020	kgm ⁻³
Circulating fluid heat capacity	$(\rho c)_f$	3962	kJm ³ K ⁻¹
Circulating fluid thermal conductivity	λ_f	0.485	Wm ⁻¹ K ⁻¹
Circulating fluid dynamic viscosity	η	0.0024	Pas
Length of the pipe for BHEs in the network	l	200	m
Diameter of the pipe for BHEs in the network	d_p	0.026	m
Pipe Roughness coefficient for pipes in the network	k_s	0.00001	m

The corresponding peak heating capacity is 330 kW through a underfloor heating system. The source side is equipped with 56 borehole heat exchangers, each of which has a depth of 100 m and a diameter of 125 mm. In the basement of the building, there are four water-to-water heat pumps which are all reversible for both cooling and heating application. A single variable speed circulation pump is installed for the ground loop, so that it is able to adjust the flow rate according to the operation condition of the heat pumps. Before construction, a thermal response test (TRT) was carried out on site and the result was evaluated based on the conventional line-source model. The geotechnical characteristics, including initial ground temperature, thermal conductivity and volumetric heat capacity of the subsurface were determined by the TRT. All detailed parameters and array layout could be found in Table 1 and Fig. 1, respectively.

3.2. Model setup

A comprehensive 3D numerical model (Fig. 1(a)), which comprises a BHE array, the surrounding subsurface, and a coupled pipeline network, is established according to the design of Leicester project described above [25]. The model domain is shown in the left part of Fig. 1(a). The subsurface domain around the BHE array has a size of 280 × 220 × 151 m³. In it, the soil part is discretized with prism elements, while the BHEs are represented by lines. In total, the mesh contains 69,275 nodes and 130,128 elements. The 56 BHEs are placed in the centre of the domain according to their real-world location. Each BHE has a single U-shape pipe (1U type) installed in it. The BHE top is set at a depth of 1 m from the surface. The arrangement of the array is illustrated in Fig. 1(b), which is in consistence with the original planning. Most of the BHEs have a distance of 5 m to its adjacent ones. However, BHE #11 is only 2 m away from its closest neighbour, exactly following its coordinates reported in Naicker et al. [25].

According to the ground loop configuration, a simplified closed-loop pipeline network is configured in the TESPy software (see the right part of Fig. 1(a)). Pre-defined components in the network are borehole heat exchangers (BHEs), water pump and heat pumps. Since in this study only the working condition on the ground side is investigated, the measured and reported ground loop thermal load in Leicester project is directly imposed as the thermal boundary condition in the BHE array model. The black lines in the network denote to the connection pipes between the components. And the arrows indicates the flow direction of the circulating fluid. After lifted by the water pump, the circulating fluid flows into the array with 56 parallelly connected BHEs. As shown in Fig. 1(b) the

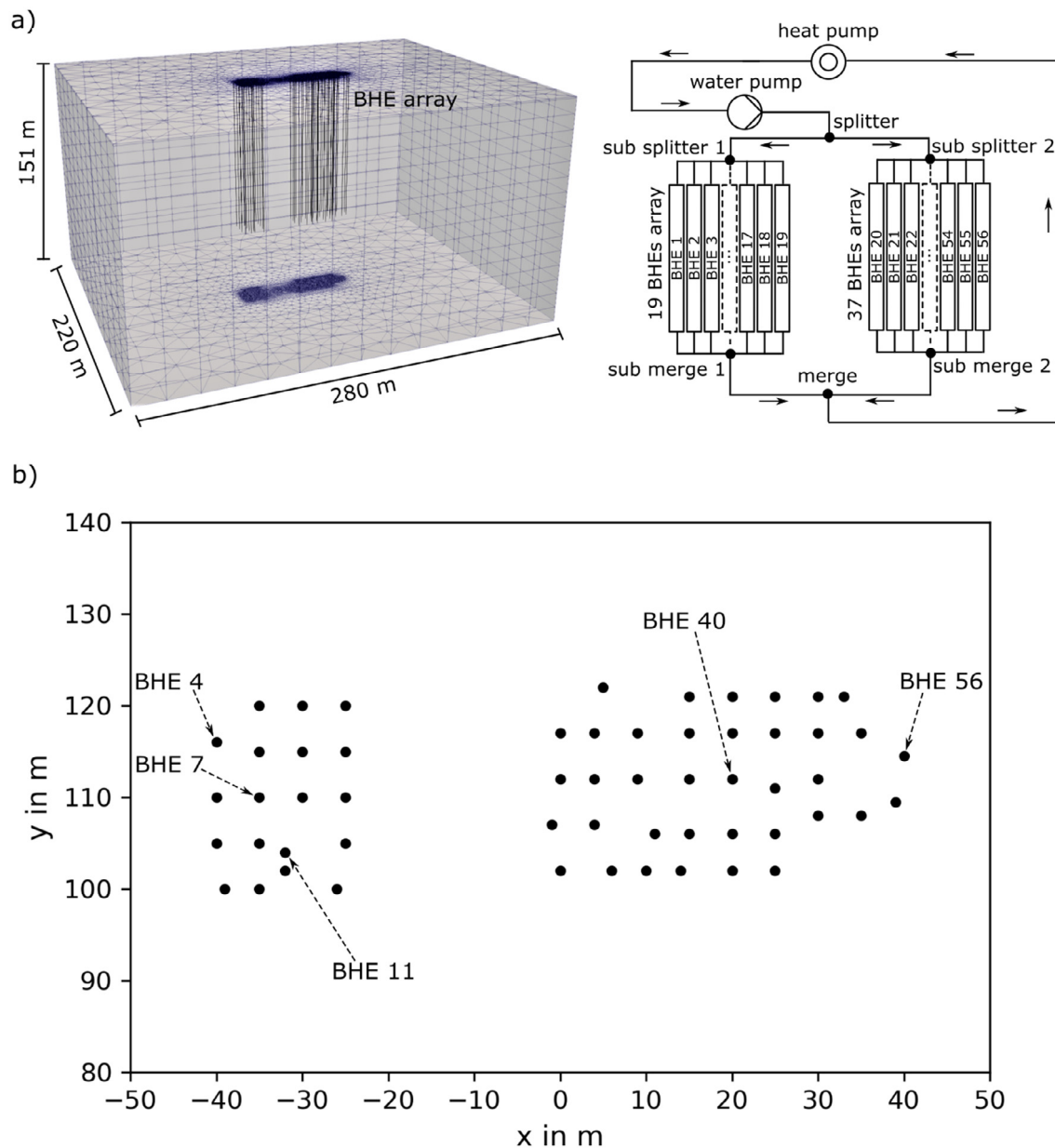


Fig. 1. (a) Left: 3D model domain representing the Leicester project in OGS; Right: 56 BHEs pipeline network model; (b) Arrangement of 56 BHE array.

entire array is divided into two parts, which is achieved by adding two sub-splitter and merge components in the network (see Fig. 1 (a) right). After circulating through each sub-array, the outflows are mixed at the merging point and then flow back to the heat pump, where the heat is either extracted to or injected based on the load profile from the building side. The physical configuration of each BHE pipe in the TESP network are assigned with the same parameters as those used in the OGS model. They are listed in Table 1 for reference.

Since there is no detailed information for the connection pipes on the ground side from the report of Leicester project, we have configured the model in a way that only the hydraulic and heat loss within the U-pipe in the BHEs are considered, while those loss along the connecting pipes are assumed to be negligible.

3.3. Initial and boundary conditions

Subsurface Part

Initially, the soil temperature is set to 11.7 °C in the whole model domain. A Dirichlet-type boundary condition is assigned on the surface of the domain with a ground surface temperature curve, which follows the corresponding measured daily mean air temperature in Naicker et al. [25]. The lowest air temperature reaches -5 °C in the winter and the peak temperature in summer is about 24 °C.

BHE Array Part

In TESP, the Darcy-Weisbach equation (Eq. (1)) is used to quantify the hydraulic head loss caused by the friction in the U-pipe within the BHE.

$$\begin{aligned}
 p_{in} - p_{out} &= \frac{\rho_f}{2} \cdot v^2 \cdot \frac{\zeta(Re, k_s, d_p) \cdot l}{d_p} \\
 &= \frac{8 \cdot \dot{m}^2 \cdot l \cdot \zeta(Re, k_s, d_p)}{\rho_f \cdot \pi^2 \cdot d_p^5}
 \end{aligned}
 \quad (1)$$

where the calculating flow velocity v is deduced through the pipe's dimensions, the fluid's density and mass flow rate \dot{m} in TESP. The fluid's density ρ depends on pressure and enthalpy. The Reynolds number Re is a function of pressure, enthalpy and flow rate.

At each time step, the measured inflow temperature and flow rate (Eq. (2)) are assigned as the boundary conditions for the simulation in TESP. In the Leicester project, the measured inflow temperature and flow rate are given by every minute. These measured values can not be directly imposed in the numerical model, as the time step size is fixed to be 1 h (see our description in the following section). To resolve this discrepancy, minute-wise monitoring data is aggregated. First, those noise readings, the values of which are way beyond a reasonable range, are removed. The date set, containing ca. 1.02 million entries altogether, are aggregated to an averaged value per hour. The average is achieved by calculating the weighted mean of the measured inflow temperature values,

$$T_{aver} = \frac{\sum_{i=1}^{60} T_i \cdot \dot{m}_i}{\sum_{i=1}^{60} \dot{m}_i}, \quad (2)$$

where T_i and \dot{m}_i are the measured inflow temperature and flow rate at each measurement interval ($\Delta T = 1$ min). At the same time, the average flow rate is calculated by the arithmetic mean of the measured values.

As mentioned in Section 3.2, since the time step size in this model is set to 1 h, the model is not capable of predicting short-term behaviour of the BHE array. However, despite of more than 130,128 mesh elements and a total of 17,237 time steps, it is possible to complete the two-year long validation simulation (cf. Section 3.4) within 129 h using a small workstation equipped with a 3.40 GHz CPU and 16 GB of memory.

3.4. Model validation

To validate the OGS-TESPy numerical model, the two years long operation phase of BHE array is simulated with the aforementioned configurations. The simulated outflow temperature, as well as the amount of exchanged heat, is compared with the corresponding

measurements and presented in Fig. 2. The exchanged amount of heat in each month is estimated using the following equation,

$$Q = \int c_f \dot{m} (T_{in} - T_{out}) dt, \quad (3)$$

where c_f is the specific heat capacity of the circulating fluid. As mentioned in Section 3.1, although the measured inflow temperature has been aggregated in order to be used as the model input, the simulation predicted outflow temperature evolution still fits the monitored values very well. As stated in [25], a modest year-by-year increase in the outflow temperature is observed between the first and second year. This phenomena can also be seen in our modelling results. Moreover, both the calculated and measured amount of heat have a consistent tendency in the temporary evolution, which corresponds well to the evolution of the outflow temperature. The slight discrepancies between the measured and computed amount of heat in some months, e.g. in the 15-th, 16-th, 20-th and 21-st month, are most likely caused by the averaging of the measured inflow temperature values. Quantitatively speaking, the accumulated amount of heat injected in the simulation (using the processed data) is about 3.2% higher than in the original data measured data.

3.5. Analysis of the model predictions

3.5.1. Subsurface thermal imbalance

Through the two-year long operation of Leicester project, the subsurface part was dominated by heat injection process, which can lead to thermal accumulation especially in the centre field of the BHE array. In Fig. 3, the computed soil temperature distribution after 2 years of operation is illustrated. Our suspicion is confirmed by the model prediction, as the elevated temperature in the centre area of the array can be clearly recognised. In Fig. 3 lower figure, the maximum temperature increment in the centre is about 2.6 °C. Obviously, the thermal accumulation in the right array is more intensive than that in the left array, as the former part has more BHEs installed than the latter one.

To investigate the temporal evolution of the soil temperature over time, five points (#P4, #P7, #P11, #P40 and #P56) (Fig. 3) are selected. They are located at a depth of $z = -51$ m, and 1 m away from their closest BHEs (BHE #4, #7, #11, #40 and #56 in Fig. 1(b) accordingly).

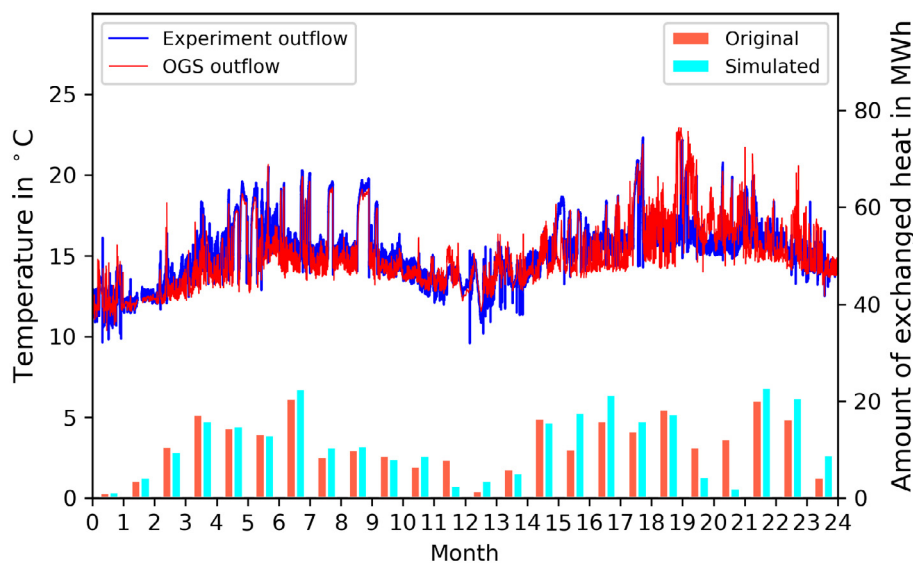


Fig. 2. Comparison of the numerical result for the evolution of the outflow temperature over 2 years with the original data.

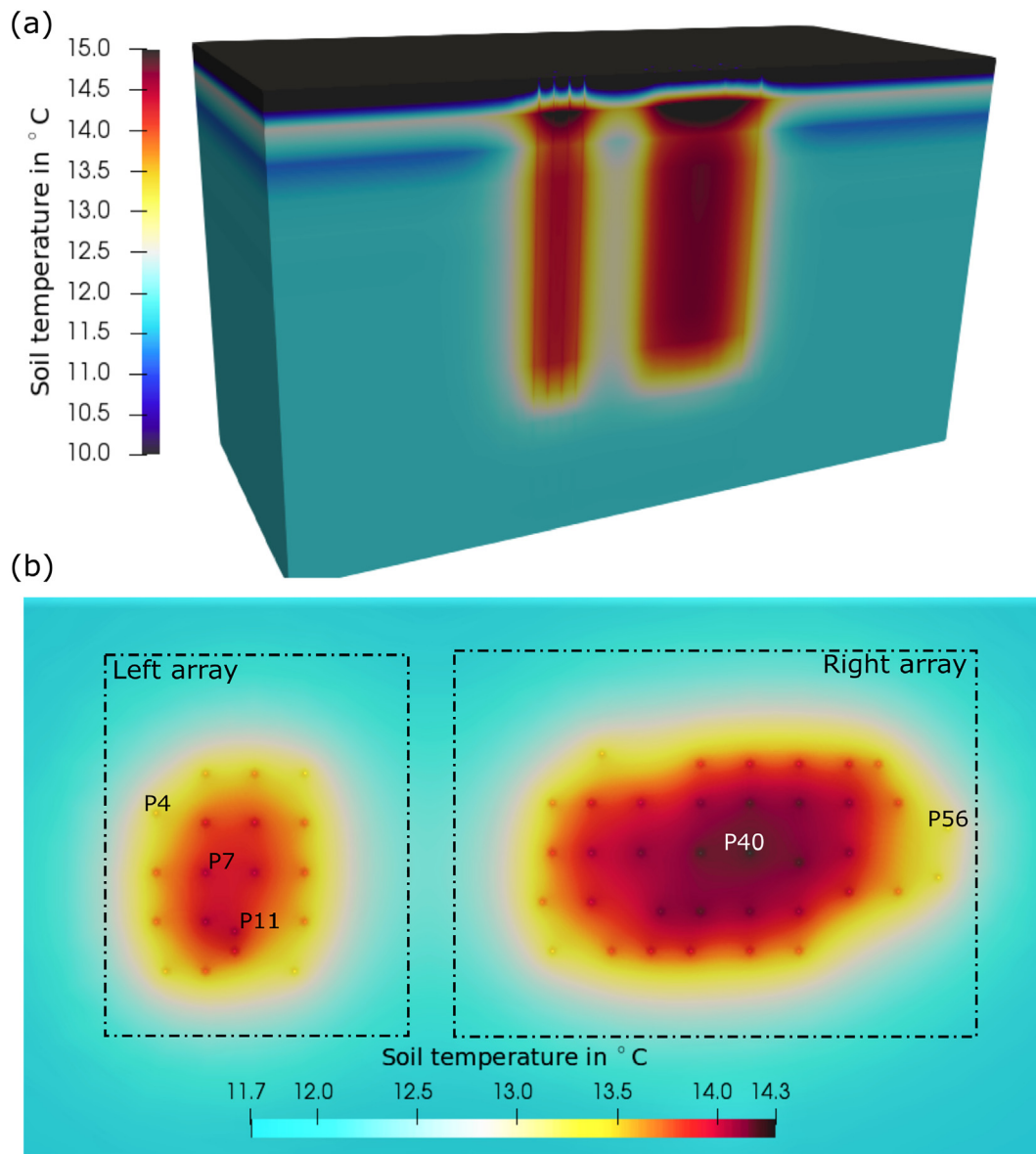


Fig. 3. (a): Vertical cross-section of the 3D soil temperature distribution in the middle of the array after 2 years; (b): Horizontal view of temperature distribution at a depth of -51 m.

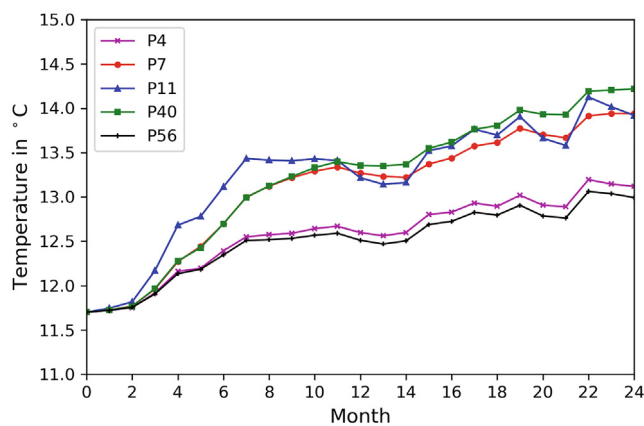


Fig. 4. Evolution of the soil temperature on the selected points in the end of each month over 2 years.

Fig. 4 illustrates the soil temperature at all five points at the end of each month over 2 years' operation. Compared to the temperature evolution at points #P4 and #P56, the temperature increase at #P7 and #P40 is more intensive. This indicates that the thermal accumulation effects are concentrated in the centre of each array, where #P7 and #P40 are located. After 2 years' operation, a 1 °C temperature difference is predicted between #P4 and #P7 in the left array, while a greater difference of 1.3 °C is found between #P40 and #P56 in the right array. Meanwhile, #P40, which is located in the centre of the right sub-array, is predicted to have a slightly higher temperature by 0.3 °C than that at #P7, which locates in the left sub-array. This strong variation at #P40 could have resulted from the influences of BHEs from both sub-arrays sides. It can be seen from the upper part of Fig. 3 that thermal accumulation does happen between the left and right arrays. Overall, the modelling result indicates that the array with more BHEs could produce more intensive imbalance in the underground. Among the five points, the strongest temperature variation is found at #P11. It

increases more intensively during the first 6 months since it is affected by two nearby BHEs at the same time. To sum up, the soil temperature is not solely affected by the nearby BHEs. Further, the accumulative thermal process in a BHE array could have strong influence on the temperature distribution as well in the long term.

3.5.2. Load shifting behaviour

As stated in our previous work (Chen et al. [19]), the interactions among the BHEs during long-term system operation can lead to load shifting in the BHE field. The monitoring data obtained from Leicester project provides an excellent opportunity for us to further investigate the trend of load shifting under realistic conditions. The heat injection rate at four represent BHEs, i.e. BHE #4, #7, #40 and #56 is quantified based on the simulated inflow and outflow temperature on each BHE. In Fig. 5, the percentage of the shifted thermal injection rate (hereafter as PSTL) on BHE is calculated by

$$PSTL_i = \frac{\dot{Q}_i - \dot{Q}_{mean}}{\dot{Q}_{mean}} \times 100, \quad (4)$$

where i refers to the index of the BHE. \dot{Q}_i and \dot{Q}_{mean} are the heat injection rate at i -th BHE and the mean heat injection rate, respectively.

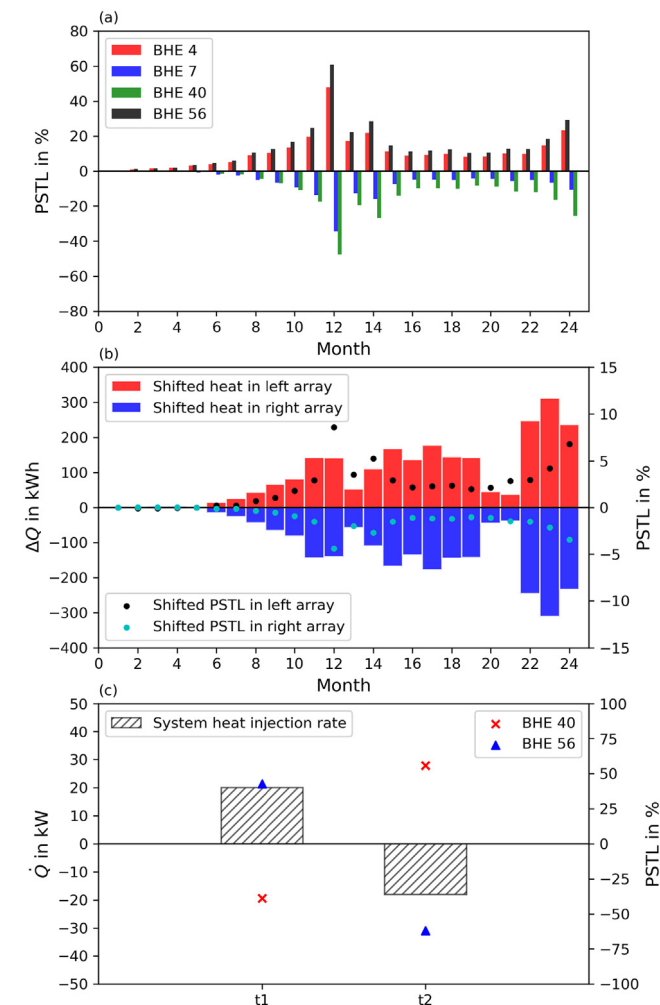


Fig. 5. (a) Monthly averaged percentage of shifted thermal injection rate on the selected BHEs over the 2-year period; (b) Monthly total amount of shifted heat and the corresponding averaged percentage values in the left and right sub-array; (c) Percentage of shifted thermal injection rate on the selected BHEs at time $t_1 = 17,007$ hour and $t_2 = 17,011$ hour.

In Fig. 5(a), a general trend can be observed that the thermal load is gradually shifted away from the centre to the outer edge of the array. The heat injection rates on the centre BHEs (#7 and #40) are lower than the designed average value ($PSTL < 0$), while they become higher than the mean value ($PSTL > 0$) at the edge BHEs (#4 and #56). The reason behind is that the soil temperature in the centre part is generally higher than that in the outer area (cf. Fig. 3). Moreover, the thermal shifting is found to be stronger in the right sub-array (BHE #56 and #40) than in the left part, as more BHEs are installed in the right area. In Fig. 2(a), the most intensive shifting (PSTL value of 60.7%) is found in the 12-th month of the first year, where the system has the lowest thermal demand. This phenomena is consistent with the observations reported in our previous work [19].

In Fig. 5(b), the load shifting phenomenon between the left and right sub-array is further investigated. If there is no thermal interaction, each BHE should deliver same amount of heat, as they are connected in a parallel manner. Following this assumption, the rate of extracted heat from the left or right sub-array should be according to the corresponding number of installed BHEs, i.e. following a ratio of 19 : 37. Using this proportion as a reference, the amount of shifted heat ΔQ of the left or right sub-array can be quantified by first integrating the amount of extracted heat on each BHE, and then comparing it with the reference value. In Fig. 5(b), the monthly change of ΔQ and its corresponding percentage of deviation PSTL is depicted for each sub-array. It can be found that, after 4 months of heat injection, the heat extraction rate shifts gradually from the right towards the left array. The reason behind is the soil temperature difference in the left and right part during the system operation. As shown in Fig. 3(b), a higher soil temperature can be found in the right array after 2 years. This is mainly caused by the more number of BHEs on the right side. As the inflow temperature is kept consistent by the pipe network for all BHEs, the actual heat injection rate on each BHE is dependent on the temperature difference in comparison to the surrounding soil. By comparing the actual simulated value with the design reference, the shifting phenomenon is well observable. With regard to the shifted percentage, the maximum value is found to be about 8.6% in the left sub-array and it is observed in the 12-th month. This is in good agreement with the result shown in the Fig. 5(a). The amount of heat shifted away from the right array is fully transferred to the left part. Therefore, due to the fact the original designed load on the left is only about half (19 : 37) of that on the right, the percentage of elevated extraction rates on the left is about twice as much as that on the right side.

Fig. 5(c) shows the performance of two BHEs, i.e. BHE #40 and #56 at two selected moments. At time $t_1 = 17,007$ hour, the system is dominated by heat injection, while at $t_2 = 17,011$ hour heat extraction is the main process. BHE #40 is located at the centre of the right sub-array, while BHE #56 is at the edge. At t_1 , the heat injection rate of BHE #40 drops by about 39%, while it increases by about 43% on BHE #56. In the heat extraction dominated period (t_2), the corresponding values at BHE #40 and #56 are switched to +56% and -62%, respectively. It indicates that in the long-term operation of a BHE array, when both heating and cooling are applied, the thermal recharge of the subsurface can partially mitigate the shifting phenomenon.

4. Extended numerical experiment

4.1. Scenarios description

In the Leicester project reported by Naicker and Rees [25], the cooling-dominant system was designed with a 360 kW peak capacity. However, if one looks into the monitored data, it can be found

that the maximum heat injection rate imposed on the BHE array was only 73 kW, which accounts for only 20.3% of the peak designed capacity. Considering the energy consumption on the heat pump, this rate could be much lower with respect to the actual thermal load at the ground side during the system peak cooling capacity. Since there is no reported information for both the actual COP curve and the peak cooling capacity of the BHE array in the project, we assumed the (360 kW) peak cooling capacity of building as the peak cooling load on the BHE array at the ground side. Therefore, it is interesting to see the long-term behaviour of the system, if the actual heat injection rate is gradually approaching the designed peak. In this context, five additional scenarios (numbered from #1 to #5) are numerically simulated with gradually increasing heat injection rates. We choose to lift the total amount of exchanged heat imposed on the array to 100%, 197%, 296%, 395% and 493% of the real observed value in the first year operation of the Leicester project. Under these conditions, the original designed peak capacity could be reached, while the characteristics of the load profile remains unchanged. From the second year forward, the annual system thermal load profile is specified to follow that of the first year and repeats itself until the end of 20-th year. All five scenarios are then simulated to reveal the long-term behaviour of the BHE array.

Since the simulation aims to investigate the long-term behaviour and does not focus on its short-term responses, a monthly averaged system thermal load is specified in each scenario. The original measured values are reported in every minute, thus a conversion calculation is performed. By executing two steps, the resulting load profile specified in scenario #1 (The red line in Fig. 6(b)) is generated. The minute-wise extracted (heating mode, in negative MWh values) or injected (cooling mode, in positive MWh) heat is integrated separately over each month using the equation (Eq. (3)). Summing the absolute values of heat exchanged in these two modes into the total amount of heat exchanged ($Q_{exchanged} = Q_{cooling} + |Q_{heating}|$) in each month. Subsequently the monthly averaged system thermal load $\dot{Q}_{average}$ is obtained dividing

by the duration of the month t_m (Eq. (5)). The positive and negative of this averaged value are then defined as the cooling and heating loads in that month, respectively. The duration of the cooling or heating period in each month could be calculated using Eq. (6), where $Q_{cooling}$, $Q_{heating}$, and $Q_{exchanged}$ are the amount of the injected heat, extracted heat and total exchanged heat of the system in one month, respectively.

$$\dot{Q}_{average} = \frac{Q_{exchanged}}{t_m} \quad (5)$$

$$t_{cooling/heating} = \frac{|Q_{cooling/heating}|}{Q_{exchanged}} \cdot t_m, \quad (6)$$

According to Ahmadfard and Bernier [13], the monthly total flow rate could be set to 0.25 Ls^{-1} per kW of the thermal load (Fig. 6(b)). By observing the data reported by Naicker et al. [25], the minimal and maximal flow rates of the system were between 2 Ls^{-1} and 30 Ls^{-1} , respectively. In our numerical model, the circulation flow rate is then set to be linearly dependent on the absolute value of system thermal load, while being kept within the same minimum and maximum range. On the upper boundary of the model domain, an averaged monthly air temperature curve is imposed as Dirichlet boundary condition, based on the data reported in the first year operation [25] (cf. Fig. 6(a), black line). Following the designed logic described above, the annual system thermal load and flow rate in scenario #2 to #5 are adjusted proportionally, i.e. 197%, 296%, 395%, 493% based on scenario #1. As a consequence, the monthly exchanged heat in each scenario is also lifted proportionally, as illustrated in Fig. 6(a). In scenario #5, the peak system thermal load is set to be 173.6 kW, which is still only ca. half of the original design. All other settings of scenario #2 to #5 remain the same as those presented in Section 3.

4.2. Results and analysis

Fig. 7(a) illustrates the simulated temporal evolution of the outflow temperature in all five scenarios. To ensure a sustainable performance of the BHE array, the temperature of circulation fluid at the inlet of the heat pump should usually be kept below $35 \text{ }^\circ\text{C}$ in the cooling mode [13]. This $35 \text{ }^\circ\text{C}$ threshold is indicated with a dotted line in this figure. Since the system is dominated by heat injection, a gradual but steady increasing trend in the outflow temperature is observed in all five scenarios, although with different magnitudes. Among the five scenarios, the lowest temperature of $16.3 \text{ }^\circ\text{C}$ is observed after 20 years in scenario #1, where the amount of exchanged heat is minimum. The most intensive increase happens in scenario #5, where the thermal load is the highest. After 20 years' operation, the highest outflow temperature in scenario #5 reached $34.5 \text{ }^\circ\text{C}$, which is already approaching the $35 \text{ }^\circ\text{C}$ threshold. This suggests that the BHE array can be sustainably utilised for 20 years, but not much longer, if the actual imposed thermal load is close to the designed maximum heat capacity as reported in [25]. However, in our model the peak cooling load at the ground site is assumed to be identical as the reported designed peak load from the building side. When considering the energy consumption on the heat pump, a higher peak cooling load at the ground site could be expected. Therefore under real working condition, the designed peak cooling load at building site may cause an elevated outflow temperature from the BHE array to exceed $35 \text{ }^\circ\text{C}$.

In Fig. 7(a), with the alternating cooling and heating load imposed, the outflow temperature shows a monthly fluctuation pattern. In scenario #1, with the lowest heat extraction rate (6.3 Wm^{-1} on each BHE), the temperature fluctuation is found to be the weakest with a magnitude of about $1.5 \text{ }^\circ\text{C}$. The strongest

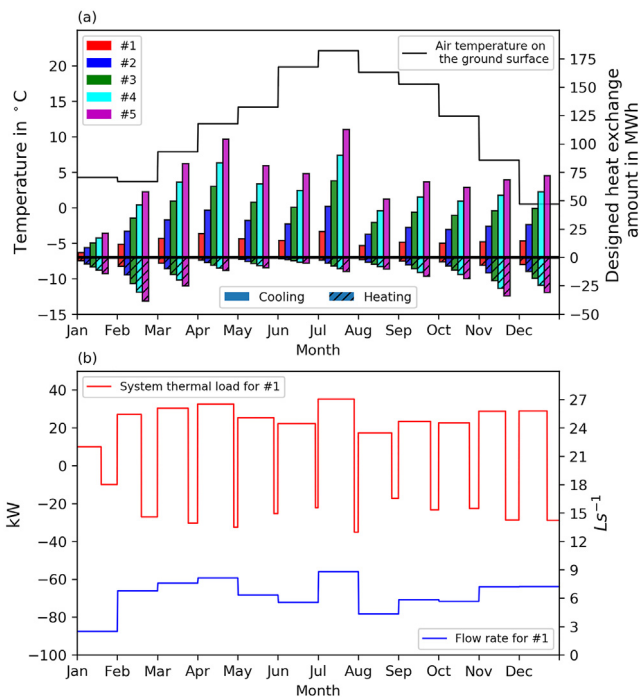


Fig. 6. (a) Designed monthly heat exchange amount in the 5 scenarios and the annual air temperature on the ground surface. (b) Profile curve of system thermal load and flow rate specified in scenario #1.

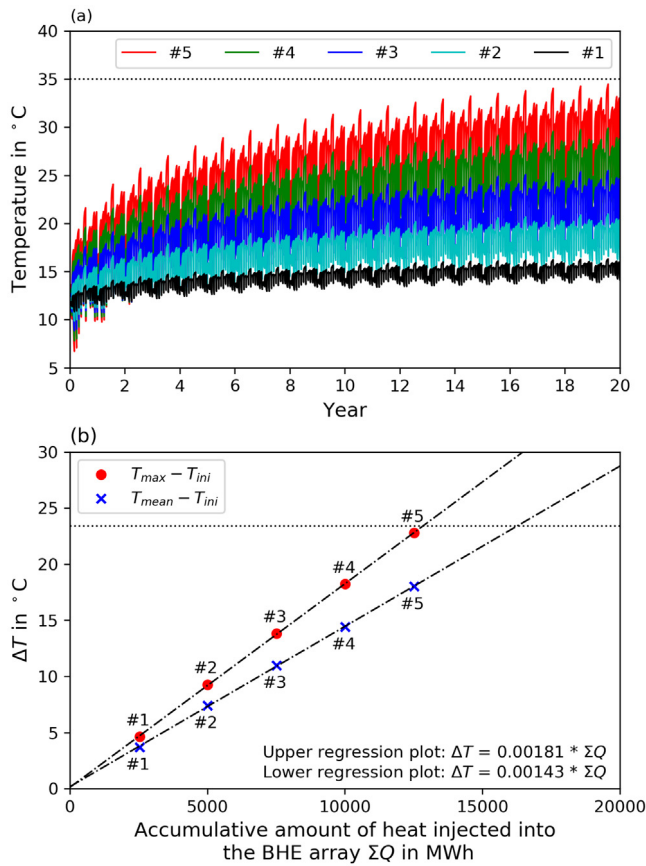


Fig. 7. (a) Temperature evolution of the working fluid flowing out from the BHE array in the 5 scenarios over 20 years; (b) Regression plot for the correlation between the maximum and mean outflow temperature against the total amount of accumulated heat injected into the BHE array at the end of the 20-th year.

fluctuation is observed in scenario #5, with the highest heat exchange rate in all 5 scenarios (31 Wm^{-1}). The deviation between the annual highest and lowest outflow temperature accounts for $11.5 \text{ }^\circ\text{C}$. As aforementioned, the imposed system thermal load is averaged on a monthly basis, hence a much stronger fluctuation in the fluid temperature could be expected in real operations, especially when a high peak cooling load is imposed.

The maximum rise in outflow temperature from all five scenarios are evaluated and presented in Fig. 7(b). Assuming the subsurface is thermally not disturbed, i.e. there is no additional heat injected or extracted, then the outflow temperature from the BHE array should equal to the initial soil temperature. This reflects the physical meaning of the origin point in Fig. 7(b). From scenario #1 to #5, the amount of additional heat is gradually increased. As a result, the increment in outflow temperature is also rising accordingly. In Fig. 7(b), both the maximum (red dots) and mean (blue crosses) temperature increments follow strict linear relationships with the amount of accumulated heat injected into the subsurface through the BHE array. Meanwhile, it is also noticed that the two slopes are distinctly different. This suggest that even with the same amount of accumulated heat, the outflow temperature can also be fluctuating due to the peak load imposed on the array. Based on the simulated data, the correlation between ΔT and ΣQ can be fitted perfectly with two linear regression lines with R-squared values of 99.989% (maximum ΔT) and 99.982% (mean

ΔT). Both temperature trends hint us that when other factors, such as the distance between the boreholes and the soil heat capacity is considered, it is possible to develop a simplified formula to estimate the change of system outflow temperature in response to the total amount of imbalanced heat accumulated over the years. Moreover, once the linear relationship is identified, the acceptable amount of accumulative imbalanced heat for a particular BHE array can be inversely estimated by giving a threshold value of the working fluid temperature.

4.3. Temporal change of stored heat

In the previous part, it is clearly demonstrated that the elevated soil and circulation fluid temperature, caused by the annually imbalanced thermal load, are the controlling factors whether a BHE array can be sustainably operated in the long-term. Since the elevated soil temperature reflects the amount of heat accumulated in the subsurface, it is important to know how much heat is stored in the subsurface, and also its percentage in comparison to the amount of heat transferred to the building. The amount of stored heat in the subsurface can be quantified by integrating the amount of sensible heat in each element of the soil compartment in one time step, and then comparing that total value with the one at the beginning of the simulation.

Fig. 8(a) illustrates the evolution of the annual amount of stored heat in scenario #3 and its percentage with respect to the total amount of system imbalanced heat. The stored heat increases gradually over the years, from 360 MWh in the first year up to 5043 MWh in the 20-th year. Meanwhile, its percentage drops from nearly 100% at the beginning and stabilises at ca. 70% in the end. This suggests that there is an increasing proportion of imbalanced heat dissipating to the atmosphere through the ground surface. This trend is consistent as the behaviour found in our previous work [30,19], where a heating-only scenario was anal-

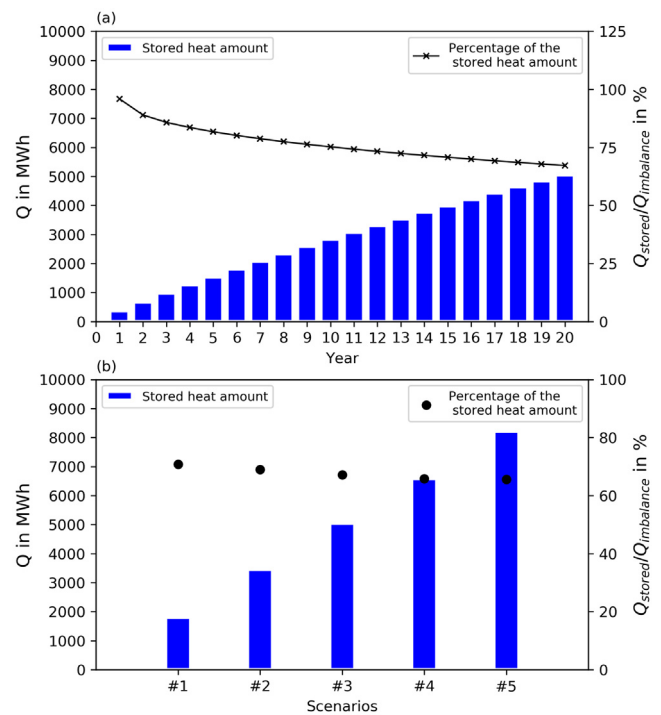


Fig. 8. (a) Evolution of the amount of stored heat in the entire domain over 20 years, based on simulated result of scenario #3; (b) Total amount of stored heat and their proportion from scenarios #1 to #5.

used. There the thermal recharge through the ground surface has a cumulative influence on the soil temperature distribution in and around the BHE array. More specifically, the area with elevated soil temperature will extend itself over the long-term heat injection, thus enhancing the thermal gradient from the subsurface towards the ground surface. Therefore, the amount and proportion of thermal discharge are also elevated over time. Despite of the elevated thermal discharge, analysis on the scenario #3 result reveals that there is still 67.2% of the total imbalanced heat stored in the subsurface after 20 years. When the amount of imbalanced heat increases from 2534 MWh to 12512 MWh from scenario #1 to #5, the amount of stored heat is also increasing accordingly (see the blue bars in Fig. 8(b)). However, due to the elevated thermal discharge mentioned above, its percentage slightly drops from 70.8% down to 65.6%. Based on the above analysis, one can conclude that over the long-term operation of a BHE array, the majority of the annual imbalanced heat will be stored in the subsurface, and its percentage is less dependent on the amount of heat injected.

4.4. Spatial distribution of stored heat

To further investigate the spatial distribution of the stored heat in the subsurface, we have created two controlled spaces. Each contains a BHE sub-array inside. The boundary of the space is drawn with a 2.5 m distance from the BHE located at the peripheries of the array (see that dark grey area marked in Fig. 9(a)). This setup results in a space of 50000 m³ for the left sub-array and 158000 m³ for the right part. With both parts considered together, the specific stored heat (kWh m⁻³) is quantified by normalising the total amount of stored heat over the volume. These specific heat values for 5 different scenarios are depicted in Fig. 9(b). These values have been also compared against the total amount of imbalance heat, and the resulting percentages are presented in the same figure.

In the five scenarios, the specific stored heat values increase along with the elevated amount of imbalance heat. In scenario #5, a maximal specific stored heat of 20.0 kWh m⁻³ is achieved. According to the findings in Section 4.2, the temperature of the outflow fluid is already approaching the 35 °C threshold in this case. One can conclude that with the current system design, 20.0 kWh m⁻³ can be considered as the upper-limit in the capacity of storing imbalanced heat in the subsurface. When normalising this value by the total amount of imbalanced heat, its ratio remains at around 25%. Combined with the analysis in the previous section, it can be concluded that heat actually dissipates far way from the array location and the thermal plume spreads into a much larger area. For all the heat stored in the subsurface, around 37% is stored in the array area, while the rest goes to the surrounding subsurface.

Nevertheless, if the distance among adjacent BHEs is enlarged, the above specific heat values and ratios may change as well. Here, a preliminary relationship can be illustrated between the amount of stored heat and the respective adjacent distance S . In scenario #5, a 7 m instead of 5 m BHE distance is specified. After 20 years' operation, a maximum outflow temperature of 30.5 °C is being predicted, which is lower than the 34.5 °C value when the model is specified with 5 m distance. The reason behind this is the decreasing of the specific stored heat value in the BHE array. As shown in Fig. 9(c), the value decreases from 20.0 kWh m⁻³ to 12.9 kWh m⁻³ when S is enlarged to 7 m. Meanwhile, 32.2% of system total amount of imbalance heat is stored in the enlarged BHE array, which is higher than the 25% value calculated in the 5 m model. Therefore one can conclude that the adjacent distance has an important role in determining the long-term operation behaviour of a large BHE array. To be specific, the adjacent distance is as important as the length of BHE. Thus, the subsurface volume

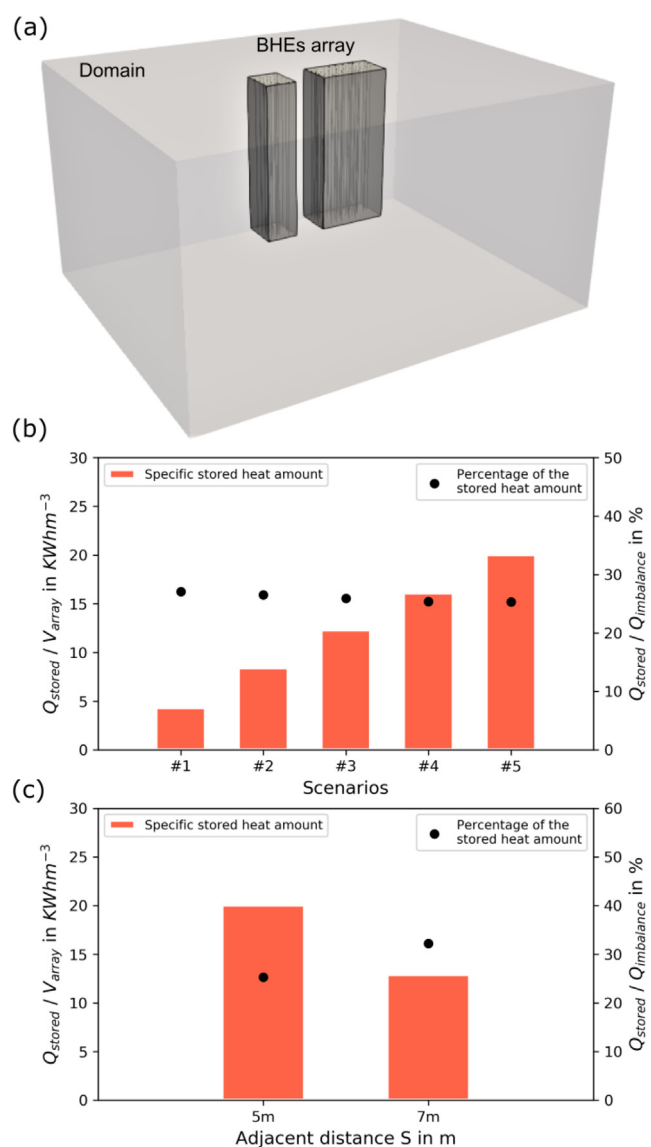


Fig. 9. (a) Selected subsurface volume (marked with dark grey); (b) Specific heat stored in the selected volume and its percentage of over the amount of total imbalanced heat after 20 years' operation in the 5 scenarios; (c) Specific heat stored in the selected volume and its percentage of over the amount of total imbalanced heat after 20 years' operation in scenario #5, in models specified with a 5 m and 7 m adjacent distance.

around the BHE array, which is determined by the adjacent distance as well as the length of the BHE, should be considered as one of the characteristic factors in the designing of the BHE array.

5. Discussions

5.1. Pipeline network design

As shown in Section 3.2, a simplified pipeline network model is built according to the ground loop design reported in the Leicester project. By adopting this coupled feature, the hydraulic states within the entire ground loop could be captured. In all scenarios stated in Section 4, the average hydraulic loss in the entire BHE array is below 1% compared to the amount of the system thermal load over the long-term operation. A transient maximum percentage with 2.2% can be found in scenario #5, due to the high flow rate

there. It should be noticed that all the connection pipes in the circulation loop are assumed to have no hydraulic loss in this study. When detailed information on the material and diameter of the pipes are available, it is more reasonable to consider the hydraulic losses when predicting the long-term behaviour of a large BHE array. In reality, both the form of BHE array and the system operation strategy varies greatly from each GSHP project [39,21]. Regarding this point, the present numerical model shows its advantage, because it is capable to consider pipeline network with arbitrary connections. In the TESP network, the hydraulic states for each pipe is automatically computed based on the mass and energy conservation. In addition, a temperature dependent heat pump COP curve can also be specified in TESP as one of the input parameters. With such information at hand, a multiple BHE array system based on the amount of energy consumption at building site can be predicted by our model in a more accurate manner.

Besides, it should be noticed that the heat extraction rate shifting phenomenon shown in Fig. 5 is the effect of current pipe network design. With the parallel BHE array setup, all BHEs are receiving an identical inflow temperature and then deliver different thermal load performances due to the soil temperature imbalance in the array. It indicates that the pipe network itself has an intrinsic feature of re-balancing the thermal load among different BHEs. Therefore it is necessary to simulate a large BHE array system, with the coupled pipeline network explicitly considered. Only in this way, the system behaviour over the long-term operation can be correctly revealed.

5.2. Optimisation of the system operation

As shown in Fig. 5 and discussed in Section 3.5.2, thermal shifting phenomenon in a large BHE array system can be clearly observed over the long-term operation. When the shifting happens, BHEs located at the edge of each sub-array have larger heat injection rates than the mean designed value, while those BHEs at the centre have lower rate. It should be noticed that such seasonal shifting behaviour is not unique and has already been reported by several researchers. For example, our previous research [19] has investigated the shifting behaviour in detail. This phenomena has also been confirmed in the study conducted by You et al. [20] through an analytical approach. Bayer et al. [40] observed similar pattern and developed an optimisation strategy based on it. They suggested that a given number of BHEs located at the centre of the array should be disconnected from the pipe network in order to mitigate the thermal anomalies in the BHE array subsurface.

Besides, as stated in Section 3.5.2, when a heating phase is applied in between the cooling seasons, the thermal recharge of the subsurface can partially mitigate the shifting phenomenon. Based on our analysis in the previous section, the heat dissipation pattern can be further utilised to improve the array operation. More specifically, during the heating phase, only those BHEs located at the array centre should be applied, because the elevated soil temperature there allows them to deliver a higher specific heat extraction rate. Also, the cold plume created by heating application can be utilised later on by the BHEs at the peripheries. Such optimisation strategy requires a series of numerical simulations and is currently being investigated by our team.

5.3. Unconsidered factors

As this study is based on the monitoring data from the Leicester project, the amount of heat injected into the subsurface is more than that extracted. Most findings in this work should be considered as only effective for cooling application dominated BHE

arrays. However, in heating dominated systems, a similar but inverse trend can be expected. A similar correlation between the drop in fluid temperature and the accumulative amount of extracted heat can also be expected over the long term operation. There, the limiting factor could be the 0 °C temperature limit on the outflow circulation fluid, which is imposed by the heat pump [13]. By considering this limit, the acceptable total amount of extracted heat from the BHE array subsurface for a sustainable system operation can also be estimated.

It is well known that groundwater flow could enhance the capacity of a BHE array, by bringing in additional thermal recharge from the upstream subsurface. In this work, information on groundwater flow is not reported by Naicker et al. [25]. Although the OpenGeoSys code used here is capable of simulating the BHE array under groundwater flow conditions (see e.g. Meng et al. [41]), we assume that there is no groundwater present in the Leicester site. For the majority of shallow geothermal GSHP projects, our assumption is also conservative but safe. Therefore, the main findings and conclusions achieved in this work are applicable to most BHE array projects.

6. Conclusion and outlook

In this work, the long-term behaviour of a large BHE array located in Leicester, UK is investigated by conducting numerical simulations. The model is validated against monitoring data through two years of operation under real working conditions. It is found that heat starts to accumulate in the centre of the BHE array due to higher amount of cooling load imposed on the system. This results in the heat injection rate being gradually shifted from the BHEs in the centre towards those at the edges. At the mean time, the thermal load is also slowly transferred from the right-side array towards the left side.

In the Leicester project, the actual heat injection rate is only 20.3% of its peak designed value. Scenario simulation with gradually increasing heat injection rates reveals that the BHE array can be sustainably utilised for 20 years even under the designed peak thermal load, but likely not any longer. It is more interesting to find that the rise in outflow temperature follows a perfect linear dependency on the amount of accumulated heat injected into the BHE array. Moreover, it is found that around 37% of the total imbalance heat can be stored in the subsurface volume around the BHE arrays. When the circulation fluid temperature is approaching the 35 °C upper limit, a maximum of 20.0 kWh m⁻³ specific heat can be stored in the subsurface. Nevertheless, when the distance among the adjacent BHEs increases from 5 m to 7 m, the corresponding outflow temperature decreases from 34.5 °C to 30.5 °C, and the specific heat value also decreases to 12.9 kWh m⁻³. It indicates that the adjacent distance among BHEs has an important role to determine how much imbalanced heat a multiple BHE array can sustain.

As discussed in Section 5.2, based on the prediction of seasonal thermal shifting, the operation strategies could be optimised to achieve a higher specific heat extraction rate. More importantly, with the consideration of other factors such as the distance between the boreholes and the soil heat capacity, it is possible to develop a simplified formula to estimate the change of system outflow temperature in response to the total amount of imbalanced heat accumulated over the years. This relationship can help to prevent the system from being overloaded in the long-term operation. However, the exact relationship between the amount of imbalanced heat, the distance between adjacent BHEs, and the increment in circulation fluid temperature, needs to be further investigated in the future.

CRediT authorship contribution statement

Shuang Chen: Methodology, Software, Validation, Formal analysis, Investigation, Data curation, Writing - original draft, Visualization. **Wanlong Cai:** Software, Formal analysis, Data curation, Writing - original draft. **Francesco Witte:** Methodology, Writing - review & editing. **Xuerui Wang:** Formal analysis, Data curation, Writing - review & editing. **Fenghao Wang:** Resources, Project administration. **Olaf Kolditz:** Resources, Supervision, Project administration, Funding acquisition. **Haibing Shao:** Conceptualization, Methodology, Resources, Data curation, Writing - review & editing, Supervision, Funding acquisition.

Declaration of Competing Interest

The authors declare that they have no known competing financial interests or personal relationships that could have appeared to influence the work reported in this paper.

Acknowledgements

The research work is part of the new Helmholtz Research Program “Changing Earth–Sustaining our Future” Topic 8 “Geo-resources for the Energy Transition and a High-Tech Society” within the program-oriented research (POF IV). This study receives partial funding from the “ANGUS II” project (Grant No 03ET6122B) and the “EASyQuart” project (Grant No 03EGB0016C), which are provided by the German Federal Ministry of Economic Affairs and Energy (BMWi). Both funding is gratefully acknowledged.

Appendix A. Supplementary data

Supplementary data associated with this article can be found, in the online version, at <https://doi.org/10.1016/j.enbuild.2020.110518>.

References

- [1] P. Bayer, G. Attard, P. Blum, K. Menberg, The geothermal potential of cities, *Renewable and Sustainable Energy Reviews* 106 (2019) 17–30, <https://doi.org/10.1016/j.rser.2019.02.019>.
- [2] B. van der Zwaan, F. Dalla Longa, Integrated assessment projections for global geothermal energy use, *Geothermics* 82 (2019) 203–211, <https://doi.org/10.1016/j.geothermics.2019.06.008>.
- [3] K. Zhu, P. Blum, G. Ferguson, K.-D. Balke, P. Bayer, The geothermal potential of urban heat islands, *Environmental Research Letters* 5 (2010) 6, <https://doi.org/10.1088/1748-9326/5/4/044002>.
- [4] J.A. Rivera, P. Blum, P. Bayer, Increased ground temperatures in urban areas: estimation of the technical geothermal potential, *Renewable Energy* 103 (C) (2016) 388–400, <https://doi.org/10.1016/j.renene.2016.11.005>.
- [5] U. Lucia, M. Simonetti, G. Chiesa, G. Grisolia, Ground-source pump system for heating and cooling: review and thermodynamic approach, *Renewable and Sustainable Energy Reviews* 70 (2017) 867–874, <https://doi.org/10.1016/j.rser.2016.11.268>.
- [6] W. Cai, F. Wang, J. Liu, Z. Wang, Z. Ma, Experimental and numerical investigation of heat transfer performance and sustainability of deep borehole heat exchangers coupled with ground source heat pump systems, *Applied Thermal Engineering* (2018), <https://doi.org/10.1016/j.applthermaleng.2018.12.094>.
- [7] T. Kurevija, D. Vulin, V. Krapec, Effect of borehole array geometry and thermal interferences on geothermal heat pump system, *Energy Conversion and Management* 60 (2012) 134–142, <https://doi.org/10.1016/j.enconman.2012.02.012>.
- [8] ASHRAE, 2019 ASHRAE Handbook - Heating, Ventilating, and Air-Conditioning Applications (SI Edition), American Society of Heating, Refrigerating and Air-Conditioning Engineers, Atlanta, GA, 2019..
- [9] H. Carslaw, J. Jaeger, *Heat Conduction in Solids*, Clarendon Press, Oxford, 1947.
- [10] L. Ingersoll, A. Zobel, *Heat Conduction with Engineering and Geological Application*, second ed., McGraw-Hill, New York, 1954..
- [11] M. Fossa, The temperature penalty approach to the design of borehole heat exchangers for heat pump applications, *Energy and Buildings* 43 (2011) 1473–1479, <https://doi.org/10.1016/j.enbuild.2011.02.020>.
- [12] A. Capozza, M. De Carli, A. Zarrella, Design of borehole heat exchangers for ground-source heat pumps: a literature review, methodology comparison and analysis on the penalty temperature, *Energy and Buildings* 55 (2012) 369–379, <https://doi.org/10.1016/j.enbuild.2012.08.041>.
- [13] M. Ahmadvard, M. Bernier, A review of vertical ground heat exchanger sizing tools including an inter-model comparison, *Renewable and Sustainable Energy Reviews* 110 (2019) 247–265, <https://doi.org/10.1016/j.rser.2019.04.045>.
- [14] S. Miglani, K. Orehounig, J. Carmeliet, A methodology to calculate long-term shallow geothermal energy potential for an urban neighbourhood, *Energy & Buildings* 159 (2017) 462–473, <https://doi.org/10.1016/j.enbuild.2017.10.100>.
- [15] The Association of German Engineers (Verein Deutscher Ingenieure), *Thermische Nutzung des Untergrunds Erdgekoppelte Wärmepumpenanlagen*; VDI 4640, Blatt 2, Beuth Verlag GmbH, Berlin, 2001..
- [16] The Association of German Engineers (Verein Deutscher Ingenieure), *Thermal use of the underground – Ground source heat pump systems*; VDI 4640, Part 2, Beuth Verlag GmbH, Berlin, 2019..
- [17] GB50366, Technical code for ground-source heat pump system, Ministry of Housing and Urban-Rural Development, PR China, 2009..
- [18] S. Haehnlein, P. Bayer, P. Blum, International legal status of the use of shallow geothermal energy, *Renewable and Sustainable Energy Reviews* 14 (2010) 2611–2625, <https://doi.org/10.1016/j.rser.2010.07.069>.
- [19] S. Chen, F. Witte, O. Kolditz, H. Shao, Shifted thermal extraction rates in large Borehole Heat Exchanger array – a numerical experiment, *Applied Thermal Engineering* 167 (2020), <https://doi.org/10.1016/j.applthermaleng.2019.114750> 114750.
- [20] T. You, X. Li, S. Cao, H. Yang, Soil thermal imbalance of ground source heat pump systems with spiral-coil energy pile groups under seepage conditions and various influential factors, *Energy Conversion and Management* 178 (2018) 123–136, <https://doi.org/10.1016/j.enconman.2018.10.027>.
- [21] K.W. Tordrup, S.E. Poulsen, H. Bjørn, An improved method for upscaling borehole thermal energy storage using inverse finite element modelling, *Renewable Energy* 105 (2017) 13–21, <https://doi.org/10.1016/j.renene.2016.12.011>.
- [22] T. You, W. Wu, W. Shi, B. Wang, X. Li, An overview of the problems and solutions of soil thermal imbalance of ground-coupled heat pumps in cold regions, *Applied Energy* 177 (2016) 515–536, <https://doi.org/10.1016/j.apenergy.2016.05.115>.
- [23] W. Choi, R. Ooka, Y. Nam, Impact of long-term operation of ground-source heat pump on subsurface thermal state in urban areas, *Sustainable Cities and Society* 38 (2018) 429–439, <https://doi.org/10.1016/j.scs.2017.12.036>.
- [24] M. Saaly, P. Maghoul, M. Kavgić, D. Polyzois, Performance analysis of a proposed geothermal pile system for heating and cooling energy demand for a building in cold regions, *Sustainable Cities and Society* 45 (2019) 669–682, <https://doi.org/10.1016/j.scs.2018.12.014>.
- [25] S.S. Naicker, S.J. Rees, Long-term high frequency monitoring of a large borehole heat exchanger array, *Renewable Energy* 145 (2020) 1528–1542, <https://doi.org/10.1016/j.renene.2019.07.008>.
- [26] S.S. Naicker, Performance analysis of a large-scale ground source heat pump system, Ph.D. thesis, De Montfort University Leicester, 2015..
- [27] S.S. Naicker, S.J. Rees, Performance analysis of a large geothermal heating and cooling system, *Renewable Energy* 122 (2018) 429–442, <https://doi.org/10.1016/j.renene.2018.01.099>.
- [28] S.S. Naicker, S.J. Rees, Geothermal heat pump system operational data: high frequency monitoring of a large university building, University of Leeds, 2017, doi:10.5518/255..
- [29] S. Koohi-Fayegh, M.A. Rosen, Examination of thermal interaction of multiple vertical ground heat exchangers, *Applied Energy* 97 (2012) 962–969, <https://doi.org/10.1016/j.apenergy.2012.02.018>.
- [30] P. Hein, O. Kolditz, U.J. Görke, A. Bucher, H. Shao, A numerical study on the sustainability and efficiency of borehole heat exchanger coupled ground source heat pump systems, *Applied Thermal Engineering* 100 (2016) 421–433, <https://doi.org/10.1016/j.applthermaleng.2016.02.039>.
- [31] A. Nguyen, P. Pasquier, D. Marcotte, Geothermics Borehole thermal energy storage systems under the influence of groundwater flow and time-varying surface temperature, *Geothermics* 66 (2017) 110–118, <https://doi.org/10.1016/j.geothermics.2016.11.002>.
- [32] C. Chen, H. Shao, D. Naumov, Y. Kong, K. Tu, O. Kolditz, Numerical investigation on the performance, sustainability, and efficiency of the deep borehole heat exchanger system for building heating, *Geothermal Energy* 7 (2019) 18, <https://doi.org/10.1186/s40517-019-0133-8>.
- [33] S. Pan, Y. Kong, C. Chen, Z. Pang, J. Wang, Optimization of the utilization of deep borehole heat exchangers, *Geothermal Energy* 8 (2020) 6, <https://doi.org/10.1186/s40517-020-0161-4>.
- [34] R. Al-Khoury, T. Kölbl, R. Schramedei, Efficient numerical modeling of borehole heat exchangers, *Computers & Geosciences* 36 (2010) 1301–1315, <https://doi.org/10.1016/j.cageo.2009.12.010>.
- [35] H.-J. Diersch, D. Bauer, W. Heidemann, W. Rühaak, P. Schätzl, Finite element modeling of borehole heat exchanger systems: Part 1. fundamentals, *Computers & Geosciences* 37 (2011) 1122–1135, doi:10.1016/j.cageo.2010.08.003..
- [36] H.-J. Diersch, D. Bauer, W. Heidemann, W. Rühaak, P. Schätzl, Finite element modeling of borehole heat exchanger systems: Part 2. numerical simulation, *Computers & Geosciences* 37 (2011) 1136–1147, doi:10.1016/j.cageo.2010.08.002..

- [37] F. Witte, I. Tuschy, TESPpy: Thermal Engineering Systems in Python, *Journal of Open Source Software* 5 (2020) 2178, <https://doi.org/10.21105/joss.02178>.
- [38] L. Bilke, H. Shao, S. Chen, W. Cai, OpenGeoSys Tutorial, Website, 2020. <https://www.opengeosys.org/docs/userguide/basics/introduction/>.
- [39] H.M. Haq, E. Hiltunen, An inquiry of ground heat storage: analysis of experimental measurements and optimization of system's performance, *Applied Thermal Engineering* 148 (2019) 10–21, <https://doi.org/10.1016/j.applthermaleng.2018.11.029>.
- [40] P. Bayer, M. de Paly, M. Beck, Strategic optimization of borehole heat exchanger field for seasonal geothermal heating and cooling, *Applied Energy* 136 (2014) 445–453, <https://doi.org/10.1016/j.apenergy.2014.09.029>.
- [41] B. Meng, T. Vienken, O. Kolditz, H. Shao, Evaluating the thermal impacts and sustainability of intensive shallow geothermal utilization on a neighborhood scale: Lessons learned from a case study, *Energy Conversion and Management* 199 (2019), <https://doi.org/10.1016/j.enconman.2019.111913> 111913.

C

APPENDIX C

C.1 Python scripts

Python script for superposition principle based analytical solution to the temporal temperature change at an arbitrary location during the operation of a BHE array system following the concept of Bayer et al. [17].

```

1  '''
2  Python script for superposition principle based
3  analytical solution to the temporal temperature
4  change at an arbitrary location during the operation
5  of a BHE array system following the concept of
6  Bayer et al. (2014).
7
8  Bayer, P., de Paly, M., & Beck, M. (2014).
9  Strategic optimization of borehole heat exchanger field
10 for seasonal geothermal heating and cooling.
11 Applied Energy, 136, 445-453.
12 https://doi.org/10.1016/j.apenergy.2014.09.029
13
14 Author: Shuang Chen
15 Email: gechenshuang88@gmail.com
16 '''
17
18 import matplotlib.pyplot as plt
19 import numpy as np
20 from scipy import special as sp
21 import math
22 %% input parameters
23 # source term coordinates
24 po_x = np.array([-12,-12,-12,-12,-12,
25                 -6,-6,-6,-6,-6,
26                 0,0,0,0,0,
27                 6,6,6,6,6,
28                 12,12,12,12,12],dtype=float).reshape(-1,1)
29 po_y = np.array([162,156,150,144,138,
30                 162,156,150,144,138,
31                 162,156,150,144,138,
32                 162,156,150,144,138,
33                 162,156,150,144,138],dtype=float).reshape(-1,1)
34
35 po_dist_to_referencepo = np.zeros([25,1])
36 Temp_po_to_referencepo = np.zeros([25,1])
37
38 # specific heat exchange rate in Watt/metre in each month:
39 # 12.5,9.375,7.8125,4.6875,0,0,0,0,1.5625,4.6875,7.8125,10.9375
40 q1 = -12.5
41 q2 = -9.375
42 q3 = -7.8125
43 q4 = -4.6875
44 q5 = 0
45 q6 = 0
46 q7 = 0
47 q8 = 0
48 q9 = -1.5625
49 q10 = -4.6875
50 q11 = -7.8125
51 q12 = -10.9375
52
53 time_trans = 30*24*60*60 #time stepping val
54
55 #parameters
56 T0 = 11.98 # initial subsurface temperature in degreeC
57
58 poro = 10e-20 # porosity
59 lamda_f = 0.5984 # fluid thermal conductivity
60 density_f = 998.2032 # fluid density
61 cp_f = 4182.0 # fluid heat capacity
62 lamda_sp = 2.4 # solid thermal conductivity
63 density_sp = 1780 # solid density
64 cp_sp = 1120 # solid heat capacity
65
66 alpha_f = lamda_f/(density_f*cp_f) # thermal dispersion tensor
67 alpha_sp = lamda_sp/(density_sp*cp_sp) # thermal dispersion tensor
68
69 lamda_med = (1 - poro)*lamda_sp + poro*lamda_f # effective thermal conductivity
70 alpha_med = (1 - poro)*alpha_sp + poro*alpha_f # effective thermal dispersion tensor
71

```

```

72 # reference plot line A-A'section coordinates.
73 # A-A'section located 1 m away from the diagonal.
74 point_x = [-149,-148.402,-147.804,-147.206,-146.608,-146.01,-145.412,-144.814,
75           -144.216,-143.618,-143.02,-142.422,-141.824,-141.226,-140.628,-140.03,
76           -139.432,-138.834,-138.236,-137.638,-137.04,-136.442,-135.844,-135.246,
77           -134.648,-134.05,-133.452,-132.854,-132.256,-131.658,-131.06,-130.462,
78           -129.864,-129.266,-128.668,-128.07,-127.472,-126.874,-126.276,-125.678,
79           -125.08,-124.482,-123.884,-123.286,-122.688,-122.09,-121.492,-120.894,
80           -120.296,-119.698,-119.1,-118.502,-117.904,-117.306,-116.708,-116.11,
81           -115.512,-114.914,-114.316,-113.718,-113.12,-112.522,-111.924,-111.326,
82           -110.728,-110.13,-109.532,-108.934,-108.336,-107.738,-107.14,-106.542,
83           -105.944,-105.346,-104.748,-104.15,-103.552,-102.954,-102.356,-101.758,
84           -101.16,-100.562,-99.964,-99.366,-98.768,-98.17,-97.572,-96.974,-96.376,
85           -95.778,-95.18,-94.582,-93.984,-93.386,-92.788,-92.19,-91.592,-90.994,
86           -90.396,-89.798,-89.2,-88.602,-88.004,-87.406,-86.808,-86.21,-85.612,
87           -85.014,-84.416,-83.818,-83.22,-82.622,-82.024,-81.426,-80.828,-80.23,
88           -79.632,-79.034,-78.436,-77.838,-77.24,-76.642,-76.044,-75.446,-74.848,
89           -74.25,-73.652,-73.054,-72.456,-71.858,-71.26,-70.662,-70.064,-69.466,
90           -68.868,-68.27,-67.672,-67.074,-66.476,-65.878,-65.28,-64.682,-64.084,
91           -63.486,-62.888,-62.29,-61.692,-61.094,-60.496,-59.898,-59.3,-58.702,
92           -58.104,-57.506,-56.908,-56.31,-55.712,-55.114,-54.516,-53.918,-53.32,
93           -52.722,-52.124,-51.526,-50.928,-50.33,-49.732,-49.134,-48.536,-47.938,
94           -47.34,-46.742,-46.144,-45.546,-44.948,-44.35,-43.752,-43.154,-42.556,
95           -41.958,-41.36,-40.762,-40.164,-39.566,-38.968,-38.37,-37.772,-37.174,
96           -36.576,-35.978,-35.38,-34.782,-34.184,-33.586,-32.988,-32.39,-31.792,
97           -31.194,-30.596,-29.998,-29.4,-28.802,-28.204,-27.606,-27.008,-26.41,
98           -25.812,-25.214,-24.616,-24.018,-23.42,-22.822,-22.224,-21.626,-21.028,
99           -20.43,-19.832,-19.234,-18.636,-18.038,-17.44,-16.842,-16.244,-15.646,
100          -15.048,-14.45,-13.852,-13.254,-12.656,-12.058,-11.46,-10.862,-10.264,
101          -9.666,-9.068,-8.47,-7.872,-7.274,-6.676,-6.078,-5.48,-4.882,-4.284,
102          -3.686,-3.088,-2.49,-1.892,-1.294,-0.696,-0.098,0.5,1.098,1.696,2.294,
103          2.892,3.49,4.088,4.686,5.284,5.882,6.48,7.078,7.676,8.274,8.872,9.47,
104          10.068,10.666,11.264,11.862,12.46,13.058,13.656,14.254,14.852,15.45,
105          16.048,16.646,17.244,17.842,18.44,19.038,19.636,20.234,20.832,21.43,
106          22.028,22.626,23.224,23.822,24.42,25.018,25.616,26.214,26.812,27.41,
107          28.008,28.606,29.204,29.802,30.4,30.998,31.596,32.194,32.792,33.39,
108          33.988,34.586,35.184,35.782,36.38,36.978,37.576,38.174,38.772,39.37,
109          39.968,40.566,41.164,41.762,42.36,42.958,43.556,44.154,44.752,45.35,
110          45.948,46.546,47.144,47.742,48.34,48.938,49.536,50.134,50.732,51.33,
111          51.928,52.526,53.124,53.722,54.32,54.918,55.516,56.114,56.712,57.31,
112          57.908,58.506,59.104,59.702,60.3,60.898,61.496,62.094,62.692,63.29,
113          63.888,64.486,65.084,65.682,66.28,66.878,67.476,68.074,68.672,69.27,
114          69.868,70.466,71.064,71.662,72.26,72.858,73.456,74.054,74.652,75.25,
115          75.848,76.446,77.044,77.642,78.24,78.838,79.436,80.034,80.632,81.23,
116          81.828,82.426,83.024,83.622,84.22,84.818,85.416,86.014,86.612,87.21,
117          87.808,88.406,89.004,89.602,90.2,90.798,91.396,91.994,92.592,93.19,
118          93.788,94.386,94.984,95.582,96.18,96.778,97.376,97.974,98.572,99.17,
119          99.768,100.366,100.964,101.562,102.16,102.758,103.356,103.954,104.552,
120          105.15,105.748,106.346,106.944,107.542,108.14,108.738,109.336,109.934,
121          110.532,111.13,111.728,112.326,112.924,113.522,114.12,114.718,115.316,
122          115.914,116.512,117.11,117.708,118.306,118.904,119.502,120.1,120.698,
123          121.296,121.894,122.492,123.09,123.688,124.286,124.884,125.482,126.08,
124          126.678,127.276,127.874,128.472,129.07,129.668,130.266,130.864,131.462,
125          132.06,132.658,133.256,133.854,134.452,135.05,135.648,136.246,136.844,
126          137.442,138.04,138.638,139.236,139.834,140.432,141.03,141.628,142.226,
127          142.824,143.422,144.02,144.618,145.216,145.814,146.412,147.01,147.608,
128          148.206,148.804,149.402,150]
129 point_y = [0,0.598,1.196,1.794,2.392,2.99,3.588,4.186,4.784,5.382,5.98,6.578,
130           7.176,7.774,8.372,8.97,9.568,10.166,10.764,11.362,11.96,12.558,
131           13.156,13.754,14.352,14.95,15.548,16.146,16.744,17.342,17.94,
132           18.538,19.136,19.734,20.332,20.93,21.528,22.126,22.724,23.322,23.92,
133           24.518,25.116,25.714,26.312,26.91,27.508,28.106,28.704,29.302,29.9,
134           30.498,31.096,31.694,32.292,32.89,33.488,34.086,34.684,35.282,35.88,
135           36.478,37.076,37.674,38.272,38.87,39.468,40.066,40.664,41.262,41.86,
136           42.458,43.056,43.654,44.252,44.85,45.448,46.046,46.644,47.242,47.84,
137           48.438,49.036,49.634,50.232,50.83,51.428,52.026,52.624,53.222,53.82,
138           54.418,55.016,55.614,56.212,56.81,57.408,58.006,58.604,59.202,59.8,
139           60.398,60.996,61.594,62.192,62.79,63.388,63.986,64.584,65.182,65.78,
140           66.378,66.976,67.574,68.172,68.77,69.368,69.966,70.564,71.162,71.76,
141           72.358,72.956,73.554,74.152,74.75,75.348,75.946,76.544,77.142,77.74,
142           78.338,78.936,79.534,80.132,80.73,81.328,81.926,82.524,83.122,83.72,

```

```
143 84.318,84.916,85.514,86.112,86.71,87.308,87.906,88.504,89.102,89.7,
144 90.298,90.896,91.494,92.092,92.69,93.288,93.886,94.484,95.082,95.68,
145 96.278,96.876,97.474,98.072,98.67,99.268,99.866,100.464,101.062,
146 101.66,102.258,102.856,103.454,104.052,104.65,105.248,105.846,
147 106.444,107.042,107.64,108.238,108.836,109.434,110.032,110.63,
148 111.228,111.826,112.424,113.022,113.62,114.218,114.816,115.414,
149 116.012,116.61,117.208,117.806,118.404,119.002,119.6,120.198,
150 120.796,121.394,121.992,122.59,123.188,123.786,124.384,124.982,
151 125.58,126.178,126.776,127.374,127.972,128.57,129.168,129.766,
152 130.364,130.962,131.56,132.158,132.756,133.354,133.952,134.55,
153 135.148,135.746,136.344,136.942,137.54,138.138,138.736,139.334,
154 139.932,140.53,141.128,141.726,142.324,142.922,143.52,144.118,
155 144.716,145.314,145.912,146.51,147.108,147.706,148.304,148.902,
156 149.5,150.098,150.696,151.294,151.892,152.49,153.088,153.686,
157 154.284,154.882,155.48,156.078,156.676,157.274,157.872,158.47,
158 159.068,159.666,160.264,160.862,161.46,162.058,162.656,163.254,
159 163.852,164.45,165.048,165.646,166.244,166.842,167.44,168.038,
160 168.636,169.234,169.832,170.43,171.028,171.626,172.224,172.822,
161 173.42,174.018,174.616,175.214,175.812,176.41,177.008,177.606,
162 178.204,178.802,179.4,179.998,180.596,181.194,181.792,182.39,
163 182.988,183.586,184.184,184.782,185.38,185.978,186.576,187.174,
164 187.772,188.37,188.968,189.566,190.164,190.762,191.36,191.958,
165 192.556,193.154,193.752,194.35,194.948,195.546,196.144,196.742,
166 197.34,197.938,198.536,199.134,199.732,200.33,200.928,201.526,
167 202.124,202.722,203.32,203.918,204.516,205.114,205.712,206.31,
168 206.908,207.506,208.104,208.702,209.3,209.898,210.496,211.094,
169 211.692,212.29,212.888,213.486,214.084,214.682,215.28,215.878,
170 216.476,217.074,217.672,218.27,218.868,219.466,220.064,220.662,
171 221.26,221.858,222.456,223.054,223.652,224.25,224.848,225.446,
172 226.044,226.642,227.24,227.838,228.436,229.034,229.632,230.23,
173 230.828,231.426,232.024,232.622,233.22,233.818,234.416,235.014,
174 235.612,236.21,236.808,237.406,238.004,238.602,239.2,239.798,
175 240.396,240.994,241.592,242.19,242.788,243.386,243.984,244.582,
176 245.18,245.778,246.376,246.974,247.572,248.17,248.768,249.366,
177 249.964,250.562,251.16,251.758,252.356,252.954,253.552,254.15,
178 254.748,255.346,255.944,256.542,257.14,257.738,258.336,258.934,
179 259.532,260.13,260.728,261.326,261.924,262.522,263.12,263.718,
180 264.316,264.914,265.512,266.11,266.708,267.306,267.904,268.502,
181 269.1,269.698,270.296,270.894,271.492,272.09,272.688,273.286,
182 273.884,274.482,275.08,275.678,276.276,276.874,277.472,278.07,
183 278.668,279.266,279.864,280.462,281.06,281.658,282.256,282.854,
184 283.452,284.05,284.648,285.246,285.844,286.442,287.04,287.638,
185 288.236,288.834,289.432,290.03,290.628,291.226,291.824,292.422,
186 293.02,293.618,294.216,294.814,295.412,296.01,296.608,297.206,
187 297.804,298.402,299]
```

```
188
189 numbhe = 25 # BHE number in the array
190 num_refer_points = len(point_x)
191
192 # thermal load curve
193 qq = np.array([[q1,q2,q3,q4,q5,q6,q7,q8,q9,q10,q11,q12,
194               q1,q2,q3,q4,q5,q6,q7,q8,q9,q10,q11,q12,
195               q1,q2,q3,q4,q5,q6,q7,q8,q9,q10,q11,q12,
196               q1,q2,q3,q4,q5,q6,q7,q8,q9,q10,q11,q12,
197               q1,q2,q3,q4,q5,q6,q7,q8,q9,q10,q11,q12,
198               q1,q2,q3,q4,q5,q6,q7,q8,q9,q10,q11,q12,
199               q1,q2,q3,q4,q5,q6,q7,q8,q9,q10,q11,q12,
200               q1,q2,q3,q4,q5,q6,q7,q8,q9,q10,q11,q12,
201               q1,q2,q3,q4,q5,q6,q7,q8,q9,q10,q11,q12,
202               q1,q2,q3,q4,q5,q6,q7,q8,q9,q10,q11,q12])).reshape(1,-1)
203 qq_all = np.repeat(qq,num_refer_points,axis=0)
204
205 numtimesteps = 120
206
207 # analytical solver
208 numtemppoints = len(point_x)
209 T2=np.zeros([numtemppoints,numtimesteps])
210
211 coeff_all = np.zeros([numtemppoints,numtimesteps])
212
213 for currstep in range(0,numtimesteps):
```

```

214 Temp_po_to_referencepo= np.zeros([numtemppoints,numbhe])
215 po_dist_to_referencepo= np.zeros([numtemppoints,numbhe])
216 localcoeff_all= np.zeros([numtemppoints,1])
217 localcoeff= np.zeros([numtemppoints,numbhe])
218 localcoeff1= np.zeros([numtemppoints,numbhe])
219 for i in range(0,numbhe):
220     if(time_trans*(currstep+1)-time_trans*0>0):
221         for j in range(0,numtemppoints):
222             po_dist_to_referencepo[j,i] = abs(po_x[i] - point_x[j] )**2 + abs(
223                 po_y[i] - point_y[j] )**2
224             exp = po_dist_to_referencepo[j,i]/(4*alpha_med*time_trans*(currstep+1
225                 ))
226             n = sp.expl(exp)
227             localcoeff[j,i] = 1/(4*math.pi*lamda_med)*n
228         if(time_trans*(currstep+1)-time_trans*1>0):
229             for j in range(0,numtemppoints):
230                 po_dist_to_referencepo[j,i] = abs(po_x[i] - point_x[j] )**2 + abs(
231                     po_y[i] - point_y[j] )**2
232                 expl = po_dist_to_referencepo[j,i]/(4*alpha_med*time_trans*currstep)
233                 n1 = sp.expl(expl)
234                 localcoeff[j,i] = localcoeff[j,i] - 1/(4*math.pi*lamda_med)*n1
235
236     localcoeff_all= np.sum(localcoeff,axis=1).reshape(-1,1)
237     coeff_all[:,1:]=coeff_all[:, :numtimesteps-1]
238     coeff_all[:, :1]=localcoeff_all
239
240 for currstep in range(0,numtimesteps):
241     T2[:,currstep] = np.sum(coeff_all[:, :numtimesteps-1-currstep:]*qq_all[:, :currstep+
242         1],axis=1) + T0
243
244 T2_ini = np.zeros([num_refer_points,1]) + T0
245 T2 = np.concatenate((T2_ini,T2), axis=1)
246
247 T2_trans = T2
248
249 #%% plotting
250
251 png_num = 1
252 for i in range(png_num):
253     plt.figure()
254     plt.plot(point_x,T2[:,120],"r",label= 'Analytical')
255     plt.xlim([-150,150])
256     plt.ylim([0,15])
257     plt.ylabel('Temperature [ $^{\circ}$ C]')
258     plt.xlabel('x [m]')
259     plt.legend(loc='best',fontsize=8)
260     plt.title(f"Soil temperature distribution on A-A'section after 10 year",fontsize=
261         12)
262     plt.savefig('pngfile{}.png'.format(i), dpi = 300, transparent = False)

```